Universidad de Cantabria

E.T.S. Ingenieros de Caminos, Canales y Puertos

Dpto. de Ciencias y Técnicas del Agua y del Medio Ambiente

TESIS DOCTORAL

Enhancing surf zone hydrodynamics predictions through high-fidelity hybrid downscaling

---

Avances en la predicción de la hidrodinámica en la zona de rompientes mediante el uso de modelos híbridos

---

Autor: Manuel Zornoza Aguado

Supervisoras: Dra. Sonia Castanedo Bárcena
Dra. Beatriz Pérez Díaz

Geomatics and Ocean Engineering Group (GeoOcean)

Junio 2025

A mis cuatro abuelos

Ten siempre a Ítaca en tu mente.

Llegar allí es tu destino.

Mas no apresures nunca el viaje.

Mejor que dure muchos años

y atracar, viejo ya, en la isla,

enriquecido de cuanto ganaste en el camino

sin aguantar a que Ítaca te enriquezca.

Konstantinos Petrou Kavafis

And so castles made of sand, melts into the sea...

eventually

Jimi Hendrix

Acknowledgements

Lo que empezó como una decisión a priori arbitaria - inscribirme en el máster de Costas y Puertos por una clase en la Università di Roma Tre que me pareció interesante - desemboca aquí, con la escritura de esta tesis doctoral. El camino seguido no siempre ha sido marcado por decisiones de este tipo, pero sí considero que las personas que he conocido sin duda han facilitado el proceso. Esto es un agradecimiento a todas ellas.

Gracias a todo el grupo GeoOcean, por crear un entorno de trabajo que podría considerarse atípico visto desde fuera, pero que demuestra que las personas definen el trabajo y no viceversa. Gracias en especial a mis directoras de tesis, Sonia y Bea, por la infinita paciencia y la guía en este camino, *bajando al barro* cuando era necesario. También gracias a Fer por iniciar todo este *sarao* con aquella beca de colaboración y por esas ideas brillantes que ya le gustaría tener a la Inteligencia Artificial. Gracias a Laura por tantas horas de ayuda y por ser tiquismiquis con las figuras, al final siempre tienes razón y quedan mejor. A Ana, Alba, Nico, Isra, Sara, Andrea, Alba, Javitxu, Paula, Miri, Jared, Pablo, Kapi, Etienne, Jennifer; creo de verdad que he aprendido algo de cada uno de vosotros.

I would also like to thank all the people I met at the beautiful Santa Cruz during the fall quarter of 2023. Special mention to Curt Storlazzi, thank you very much for making my stay possible and make me feel as if I didn't leave Cantabria. Huge thanks to Sean Vitousek, for all the cool talks we had and for being such an incredible person. You are the proof that people define the jobs, and not viceversa. Thank you Anita for being so welcoming and including me in your daily life that easy. Alex, Eduardo, Andrew, Jay, Madison, Cedric, Julie, Dion and so many others, thank you all for the good times.

Gracias a quienes hayan compartido conmigo una rompiente en alguna playa, un pie de vía, un paseo, un sofá, un concierto, una tienda de campaña, una película, una montaña, una cerveza (o dos), un libro. Porque la vida es lo que se nos va mientras tratamos de ganárnosla.

Por último, me gustaría dar las gracias a toda mi familia, que me ha criado y que tienen gran parte de culpa de dónde estoy y cómo soy. Especialmente, a mi hermana, por ser un ejemplo de actitud y esfuerzo incondicionales (me tenías que haber dejado algo a mí), y a mis padres, por enseñarme que lo bonito es difícil y que la cultura no va de doctorados, si no de darle utilidad a lo inútil.

Contents

Abstract

Among global coastlines, beaches are dynamic and highly valued environments that provide vital ecosystem services but are increasingly exposed to anthropogenic pressure and climate-driven hazards. As the potential impacts are highly damaging to societies, environments and economies, holistic approaches are being implemented to adequately reduce coastal risks. To achieve this goal, Disaster Risk Reduction strategies are being developed, within which hazard characterization is a cornerstone of the process. Effective coastal management in beaches therefore requires a detailed understanding of nearshore processes, particularly the surf zone hydrodynamics and their interaction with seabed morphology. However, achieving this objective through dynamical simulations entails a substantial computational burden.

To address this challenge, metamodels and hybrid approaches in general are increasingly emerging as viable alternatives, offering computationally efficient solutions that substantially reduce the number of cases requiring full numerical simulation. Through data-mining techniques, these hybrid metamodels can be trained with plausible conditions, and when combined with dimensionality reduction methods, they enable accurate predictions without the need for extensive computational resources. In this thesis, a high-fidelity hybrid downscaling technique for surf zone hydrodynamics is described through the development of two metamodels.

Firstly, a hybrid methodology is presented for estimating wave-induced total water level (TWL) components in coastal areas, such as wave set-up (η_{setup}) and infragravity wave level component (η_{IG}), while explicitly accounting for surf zone hydrodynamics. The approach combines statistical techniques with the hydrodynamic model XBeach in

surfbeat mode, which solves the equations of wave transformation on wave groups scale, to efficiently generate high-resolution spatial fields of significant wave height (H_s), mean wave direction (θ_m), η_{setup} and η_{IG}. The methodology is numerically validated and applied at La Salvé beach (Cantabria, Spain), showing robust performance across diverse scenarios. To illustrate its potential as a coastal management tool, a TWL-driven coastal flooding hazard assessment is performed in the study site, and validated with records from past extreme storms. The results highlight the model's effectiveness in capturing localized hotspots of inundation and its potential as a decision-support tool for emergency planners, coastal engineers, and managers.

However, to fully resolve the physical processes involved in the interaction between coastal geomorphology and wave dynamics (refraction, diffraction, shoaling, nonlinear interactions, and wave breaking), a formulation that resolves the phase of individual waves must be used. Additionally, the morphodynamic variability of the beach is also a relevant parameter, as a reciprocal interaction exists: while bathymetric features influence wave propagation toward the coast, waves in turn modify the seabed through both longshore and cross-shore sediment transport.

Thus, a second hybrid, coupled metamodel is presented: HyWaThy. This metamodel advances beyond conventional wave downscaling approaches over static bathymetries by incorporating seabed variability and coupling it with the XBeach model in non-hydrostatic mode, which resolves key physical processes such as shoaling, refraction, diffraction, reflection, and wave breaking. Therefore, the representative cases are defined by both beach and sea states. Bathymetric variability is captured through Principal Component Analysis (PCA) applied to field-surveyed data, and wave parameters are obtained from offshore spectra and propagated with an additive model. Then, the nearshore domain is simulated with the phase-resolving XBeach model, forced with spatially varying spectral boundary conditions, generating a library of outputs corresponding to the representative scenarios. Once trained, the metamodel enables near-instantaneous reconstruction of spatial fields of nearshore H_s and θ_m. The model has been numerically validated and shows strong potential for forecasting, hindcasting, and coastal risk assessment applications.

Finally, to illustrate the wide range of potential applications of the HyWaThy metamodel, it has been employed to reconstruct an 85-year hourly time series of spatial

maps of H_s in La Salvé beach, a fundamental input for numerous coastal studies. This dataset has been used to derive key nearshore parameters, such as the depth of closure, and to analyze the extremes of the local wave climate and the influence of bathymetric variability on the spatial distribution of H_s. Additionally, the relationship between the wave climate at the study site and the most influential climate indices in the North Atlantic has been evaluated. The coupled metamodel has demonstrated robust performance at La Salvé beach, enabling the generation of 85 years of hourly nearshore conditions in a matter of minutes. While the current application focused on a specific site, the methodology is readily transferable to other coastal regions and its capabilities can be further enhanced through the integration of high-resolution, satellite-derived bathymetric data.

Resumen

A lo largo y ancho de las costas del mundo, las playas representan entornos dinámicos y de alto valor ecológico que proveen servicios ecosistémicos fundamentales, pero que están cada vez más expuestos a presiones antropogénicas y amenazas producidas por el cambio climático. Dado que los potenciales impactos pueden ser altamente perjudiciales para las sociedades, los ecosistemas y las economías, actualmente se están implementando enfoques holísticos orientados a reducir adecuadamente los riesgos costeros. Para alcanzar este objetivo, estrategias de Reducción del Riesgo de Desastres (DRR, por sus siglas en inglés) están siendo desarrolladas, dentro de las cuales la caracterización de la amenaza constituye un pilar fundamental del proceso. En este contexto, una adecuada gestión costera en playas requiere un conocimiento detallado de los procesos costeros, especialmente de la hidrodinámica en la zona de rompientes y su interacción con la morfología del fondo marino. Sin embargo, lograr este nivel de detalle mediante simulaciones dinámicas conlleva una carga computacional considerable.

Para hacer frente a este desafío, los metamodelos y los enfoques híbridos en general están emergiendo como alternativas viables, al ofrecer soluciones computacionalmente eficientes que reducen sustancialmente el número de casos que requieren simulación numérica completa. Mediante técnicas de análisis de datos, estos metamodelos híbridos pueden ser entrenados con condiciones plausibles y, combinados con métodos para reducir la dimensionalidad, permiten realizar predicciones precisas sin necesidad de grandes recursos computacionales. En esta tesis doctoral, se describe una técnica de downscaling híbrida de alta resolución para el estudio de la hidrodinámica de la zona

de rompientes mediante la implementación de dos metamodelos.

En primer lugar, se presenta una metodología híbrida para la estimación de los componentes del nivel total del agua (TWL, por sus siglas en inglés) inducido por oleaje en zonas costeras, tales como el set-up del oleaje (η_{setup}) y la componente de nivel producida por la onda infragravitatoria (η_{IG}), considerando explícitamente la hidrodinámica en la zona de rompientes. El enfoque combina técnicas estadísticas con el modelo hidrodinámico XBeach en modo *surfbeat*, que resuelve la transformación del oleaje a escala de grupo de ondas, generando de forma eficiente campos espaciales de alta resolución de altura de ola significante (H_s), dirección media del oleaje (θ_m), η_{setup} y η_{IG}. La metodología ha sido validada numéricamente y aplicada en la playa de La Salvé (Cantabria, España), mostrando eficiencia bajo distintos escenarios. Como una aplicación orientada a la gestión costera, se ha llevado a cabo una evaluación del riesgo de inundación costera inducida por el TWL, validada con registros de tormentas extremas del pasado. Los resultados ponen de manifiesto la eficacia del modelo para identificar zonas localizadas con alta susceptibilidad a la inundación, así como su utilidad como herramienta de apoyo a la toma de decisiones para entidades encargadas de la gestión de emergencias, ingenieros costeros y gestores del litoral.

Sin embargo, para resolver completamente los procesos físicos de la interacción de la geomorfología costera con el oleaje (refracción, difracción, asomeramiento, interacciones no lineales y rotura del oleaje), se debe emplear una formulación que resuelva la fase de la onda individual. Además, la variabilidad morfodinámica de la playa también representa un parámetro relevante, ya que existe una interacción recíproca: mientras las características batimétricas afectan la propagación del oleaje hacia la costa, las olas modifican a su vez el fondo marino mediante el transporte de sedimentos tanto longitudinal como transversal.

En este contexto, se presenta un segundo metamodelo acoplado e híbrido: HyWaThy. Este metamodelo es una alternativa a los enfoques convencionales de downscaling de oleaje sobre batimetrías estáticas al incorporar la variabilidad batimétrica y acoplarla con el modelo XBeach en modo *no hidrostático*, que resuelve procesos físicos clave como el asomeramiento, la refracción, la difracción, la reflexión y la rotura del oleaje. Por tanto, los casos representativos se definen tanto en función del estado de la playa como del estado del mar. La variabilidad batimétrica se caracteriza me-

diante Análisis de Componentes Principales (PCA) aplicado a datos batimétricos de campo, mientras que los parámetros de oleaje se obtienen a partir de espectros offshore y se propagan mediante un modelo aditivo. Posteriormente, el dominio costero se simula utilizando el modelo XBeach (resolviendo la fase de la onda), forzado con espectros direccionales variables espacialmente, generando una biblioteca de resultados correspondientes a los escenarios representativos previamente definidos. Una vez entrenado, el metamodelo permite reconstrucciones casi instantáneas de los campos espaciales de H_s y θ_m en el entorno costero. La validación numérica confirma la precisión del modelo y resalta su alto potencial para aplicaciones de predicción, reanálisis y evaluación de riesgos costeros.

Finalmente, como ejemplo ilustrativo del amplio abanico de aplicaciones del metamodelo HyWaThy, se ha empleado para reconstruir una serie horaria de 85 años de mapas espaciales de H_s en la playa de La Salvé, un dato básico y fundamental para numerosos estudios costeros. Este conjunto de datos ha sido utilizado para derivar parámetros clave de la zona litoral, como la profundidad de cierre, así como para analizar los extremos del clima marítimo local y evaluar la influencia de la variabilidad batimétrica sobre la distribución espacial de H_s. Asimismo, se ha evaluado la relación entre el clima de oleaje en la playa de estudio y los principales índices climáticos del Atlántico Norte. El metamodelo acoplado muestra un desempeño robusto en La Salvé, permitiendo generar 85 años de condiciones horarias cercanas a la costa en cuestión de minutos. Aunque la aplicación se ha centrado en un sitio específico, la metodología es fácilmente transferible a otras regiones costeras y su rendimiento puede mejorarse significativamente mediante la integración de batimetrías derivadadas de datos satelitales de alta resolución.

List of Acronyms

EWS Early Warning System

DDR Disaster Risk Reduction

LHS Latine Hypercube Sampling

MDA Maximum Dissimilarity Algorithm

PCA Principal Component Analysis

RBF Radial Basis Functions

PC Principal Component

EOF Empirical Orthogonal Function

RMSE Root Mean Square Error

XBSB XBeach model in *surfbeat* mode

XBNH XBeach model in *non-hydrostatic* mode

List of Tables

List of Figures

Chapter 1

Introduction

1.1 Motivation

Historically, coastal areas have served as focal points for human settlement and activity due to the wide range of ecosystem services they provide. Currently, more than one-third of the world's population lives within 100 km from the coast (Merkens et al., 2016; Reimann et al., 2023), in a growing trend (Maul & Duedall, 2019; Oppenheimer et al., 2022; Reimann et al., 2023). In these densely populated regions, coastal storms pose one of the most significant threats, as their inherent hazards (e.g. storm surge, coastal flooding, destructive winds) have significant impacts on environments, societies, and economies (Haigh et al., 2016; Masselink & Lazarus, 2019; IPCC, 2023). Additionally, with this increasing level of exposure (Dada et al., 2023), the influence of climate change response variables (e.g., sea level rise, ocean warming) on these extreme events is expected to exacerbate the impacts on coastal zones, as it translates into increased wave energy (Reguero et al., 2019) and more frequent and intense coastal erosion and flooding (Vitousek et al., 2017; Vousdoukas et al., 2018; Bramante et al., 2020; European Environment Agency, 2021). Consequently, coastal risk is projected to rise (Glavovic et al., 2022), making the understanding of natural hazards and the associated hydrodynamics essential for future management strategies

(one of the so-called "four pillars" of Early Warning Systems (EWS) design, WMO, 2022; UN, 2023; Turner et al., 2024).

Therefore, accurate modeling of nearshore processes is essential for local and regional scale studies of these damaging events (European Environment Agency, 2021), which generate huge losses around the world (Floods Directive, 2007; European Environment Agency, 2022; Pörtner & et al., 2022). Moreover, such modeling not only enhances our understanding of coastal risk, but also addresses a basic necessity for sustainable coastal development, coastal engineering projects, and mitigation of climate change impacts around the world (IPCC, 2023). In this context, Disaster Risk Reduction (DRR) strategies, which include challenges such as risk determination or the development of adaptation plans, have been identified as key tasks for present and future coastal management (IPCC, 2023). In this respect, as noted by Tintoré et al. (2009), the transformation of well-identified results into new methodologies and practical applications is essential to achieve proper coastal environment management. In recent years, several products have been developed for coastal protection, such as policies (e.g. the Sendai Framework for Disaster Risk Reduction 2015-2030 on a global scale, the Maritime Spatial Planning Directive on a European scale, and the Spanish Shoreline Climate Change Adaptation Strategy at a national level), data collection systems (e.g. Copernicus programme by the European Space Agency; Water Information System for Europe, WISE, by the European Environment Agency), ecosystem-based solutions (Vuik et al., 2016; Gracia et al., 2018; Moraes et al., 2022) or coastal hazard EWS (e.g. Harley et al., 2016; Gaztelumendi et al., 2016; Stokes et al., 2021; Garzon et al., 2023).

In order to develop methodologies that help to understand the intensity and spatial distributions of coastal hazards, accurately modeling surf zone hydrodynamics is essential, as coastal hazards often result from the combination of simultaneous oceanographic processes that occur at different temporal and spatial scales (Cagigal et al., 2020). One of the most widely utilized variables to aggregate this information is the total water level proxy (herafter TWL) (Haigh et al., 2014; Nederhoff et al., 2021; Caruso & Marani, 2022; Parker et al., 2023), which can serve for the development of several coastal risk assessment products (Gallien et al., 2015; Vousdoukas et al., 2016; Clemente et al., 2022). Additionally, surface ocean waves (usually represented by sig-

nificant wave height, hereafter H_s) play a major role in driving coastal and nearshore dynamics. Consequently, accurately characterizing waves across the continental shelf is essential for most of the coastal activities, such as coastal defence, port design, navigation, sediment transport studies or erosion and flooding assessments. Moreover, wave fields tend to exhibit greater spatial variability in coastal areas due to the intensified interactions with the seabed and local hydrodynamic currents (Varing et al., 2021).

In the present thesis, the conducted research focuses on the estimation of TWL, H_s and θ_m in sandy beaches. Amongst the different types of coastal landforms (e.g., rocky coasts, estuaries, sea cliffs, barrier islands), beaches are highly dynamic both temporally and spatially (Jackson & Short, 2020), and account for 31% of the ice free coasts of the world (Luijendijk et al., 2018). Their evolution plays a key role in coastal vulnerability (Mancini et al., 2021), as they offer essential services that support human well-being (Orlando et al., 2019), such as protection from extreme events (Jackson & Short, 2020; Agulles & Jordà, 2022; Toimil et al., 2024); water filtration and purification (Costanza et al., 2014) and biodiversity preservation (Schlacher et al., 2014; Barboza & Defeo, 2015; Alegría-Arzaburu et al., 2025; Christiaanse et al., 2025). Therefore, a deeper understanding of the hydrodynamic variability in these environments is needed, particularly how it responds to different climate forcings and to different morphodynamic states (Barnard et al., 2015), as this knowledge is a primary input for coastal management (Short & Jackson, 2013).

Sandy beaches are dynamic environments characterized by continuous bathymetric changes produced by waves, wave-induced currents, and wind (Jackson et al., 2011; Dodet et al., 2013; Castelle & Masselink, 2023). Simultaneously, these processes interact with the nearshore geomorphology, which modulates the propagation and dissipation of wave energy through mechanisms such as refraction, diffraction, shoaling, non-linear wave-wave interactions (triads) and eventually depth-induced breaking (Holthuijsen, 2007). Therefore, a two-way interaction exists: while bathymetric features affect wave propagation towards the coast, waves in turn modify the seabed through longshore and cross-shore sediment transport. Despite this reciprocal relationship, most numerical studies of nearshore hydrodynamics assume a static bathymetry, neglecting the influence of the seabed variability on wave dynamics. This simplification persists

largely due to the high computational cost of fully coupled hydro-morphodynamic simulations. Therefore, addressing the need to include the interaction between complex hydrodynamic and morphodynamic processes in nearshore modeling (Toimil et al., 2023) requires efficient approaches that account for seabed variability without imposing excessive computational demands.

1.2 State of the art

The available wave datasets generally offer spatial and temporal resolutions suitable for characterizing meteoceanographic conditions at a regional scale. However, in many practical applications, regional scale conditions are not accurately representative of specific local climate and extremes. These local characteristics are often strongly influenced by site-specific geomorphological features, which can lead to significant deviations from the regional climate. To obtain information on local meteoceanographic parameters, the outputs from global hindcast models are commonly used to force regional and local computations, a procedure also known as "downscaling".

This thesis focuses on the enhancement of surf zone hydrodynamics downscaling in sandy beaches. To achieve this goal, numerical models have been widely used and validated by the coastal community in recent years (Gomes et al., 2015; Ramakrishnan et al., 2018; Fernández-Montblanc et al., 2020; Ferreira et al., 2020; Garzón et al., 2022; amongst many others). When modeling nearshore processes, the 1-D approach (Rueda et al., 2019; Garzón et al., 2022) represents the most computationally efficient manner, but requires morphologically homogeneous shorelines or to carry out some assumptions (e.g. selection of representative beach profiles) that can worsen the outcomes in larger study areas. Additionally, some 2-D relevant processes are not modelled. Hence, 2-D modeling of nearshore hydromorphodynamics (Didier et al., 2019; Quataert et al., 2020; Toth et al., 2023) leads to more realistic results, as more spatio-temporal processes are considered. In this latter approach, dynamic downscaling with third-generation numerical models (e.g. SWAN, Booij et al., 1999) is commonly used as a wave transfer method, based on the direct computations of the local conditions using nested grids, by reproducing all the meteorological conditions and carefully modeling wave propagation up to the coast of all the sea states (Bellotti et al., 2021). Although

accurate, it is an excessively time-consuming and computationally demanding solution for the calculation of surf zone hydrodynamics, especially for the current needs for efficient downscaling techniques for the nearshore variables of interest (Wandres et al., 2020).

Typically, the improvement of nearshore wave resolution has relied on a downscaling methodology involving a system of nested domains, where each successive domain has a finer spatial resolution and a smaller spatial extent, with boundary conditions provided by the coarser outer mesh (Bingölbali et al., 2019; Romano-Moreno et al., 2022). More recent approaches use an unstructured grid with a varying mesh size. The primary advantage of unstructured grids in wave modeling lies in their ability to represent different spatial resolutions within a single computational domain, allowing enhanced detail in coastal areas without the need for multiple nested grids (Pallares et al., 2017). However, despite offering reduced computational costs compared to nested domain approaches, unstructured grids still entail considerable computational demand. Additionally, wave downscaling to nearshore areas often require to accurately represent varying physical processes (i.e. the implementation of different formulations) occurring at different parts and scales of the marine domain.

A potential way forward to downscale ocean dynamics at different spatiotemporal scales is the development and use of model-to-model interfaces: software wrappers that allow coupling of independent models (Payo et al., 2017). Recent works adapted this approach to model the spatial and temporal variability of nearshore hydrodynamics (Turner et al., 2024), with diverse purposes: combining numerical models and Bayesian networks to estimate wave-induced flooding (Garzon et al., 2023); developing a TWL warning system based on a non-hydrostatic wave model to predict overtopping (Merrifield et al., 2021); and coupling a very fast compound flooding model to several XBeach model domains to estimate hurricane-derived erosion and coastal flooding (Dongeren et al., 2023). Knowing this, and given the current needs for efficient downscaling techniques for the 2D nearshore hydrodynamics (Wandres et al., 2020), this work relies on the coupling of hybrid models (e.g. Rueda et al., 2019; Anderson et al., 2021; van Vloten et al., 2022; Ricondo et al., 2024a, 2024b; Zornoza-Aguado et al., 2024). These hybrid models, which combine statistical methods and numerical models, have been developed as computationally efficient alternatives to dynamical downscaling (Camus

et al., 2011a, 2011b), and are gaining wider adoption (Rodriguez et al., 2024), as they offer an effective approach for simulating multiple forcing combinations, bridging the gap between physical processes operating across various time and spatial scales (Marra et al., 2023; Storlazzi et al., 2024).

Depending on the nearshore variable to estimate, different assumptions are made. As this work uses unimodal wave spectra as forcing, peak wave period (T_p) is not calculated along the 2DH domain, as its variations can be considered minimum. The following subsections describe the most typical present approaches for calculating those variables.

1.2.1 Total Water Level modeling

Regarding TWL, it is usually calculated as the linear summation of mean sea level, astronomical tide, nontidal residuals, and storm wave-induced water level variations (Serafin & Ruggiero, 2014; Serafin et al., 2017):

$$TWL = \eta_{MSL} + \eta_{AT} + \eta_{NTR} + \eta_{waves} \tag{1.1}$$

where η_{MSL} is the mean sea level (MSL) relative to some datum (e.g. Mean Sea Level at Alicante in 1870-1880, Spain), η_{AT} is the deterministic astronomical tide, η_{NTR} is the nontidal residual and η_{waves} is the wave-induced level component. If sea level rise (SLR) was considered, it would be included as a part of η_{MSL}. η_{AT} can be computed with the harmonic constituents. η_{NTR} represents any elevation change in the water level over and below the deterministic tide, including low-frequency variations in the water level (e.g. seasonality or monthly mean sea level anomalies) and/or high-frequency components (e.g. storm surge) (Serafin et al., 2017). The η_{waves} component is the wave runup, a combination of the maximum set-up at the shoreline and the swash, which is the time-varying oscillations of the set-up including both incident (0.04-0.2 Hz) and infragravity waves (IG waves; 0.004-0.04 Hz). Regarding long-term components such as SLR, although their prediction and understanding is significantly relevant, what at present causes extreme flooding and erosion along coastlines is the concurrence of storm-induced waves over high water levels (Sallenger, 2000; Serafin

& Ruggiero, 2014). Therefore, several studies focus on the short-term scale, thus disregarding SLR and other long-term components as a component of TWL (Gallien, 2016; Vousdoukas et al., 2016; Nazari et al., 2022).

1.2.2 Significant wave height modeling

Despite the well-established two-way interaction between waves and bathymetry, as described in Section 1.1, the majority of numerical studies on nearshore hydrodynamics continue to rely on the assumption of a static seabed. This simplification overlooks the role of bathymetric variability in modulating wave propagation, energy dissipation, and transformation processes such as refraction, shoaling, and breaking. Both, nested and unstructured mesh approaches, commonly adopt this assumption, primarily due to the considerable computational resources required for fully coupled hydro-morphodynamic simulations, and the scarcity of high-resolution, spatially extensive, and temporally consistent bathymetric data (Cohn et al., 2021). Existing bathymetric datasets are often fragmented, site-specific, and concentrated in economically strategic areas in the coastal stretch (Wölfl et al., 2019). As a result, the broader implementation of bathymetric variability in operational or long-term simulations remains limited, despite its recognized importance for accurately characterizing nearshore processes (P. B. Smit et al., 2015; Cohn et al., 2021; Afentoulis et al., 2022).

1.3 Objectives

The primary objective of this thesis focuses on the study and development of innovative tools and methodologies that can aid the downscaling of nearshore hydrodynamics accounting for the seabed variability, using hybrid approaches and statistical techniques that significantly reduce computational time and resource demands. The development of such tools is particularly valuable for generating rapid, high-resolution nearshore hydrodynamics spatial maps, which are essential for diverse coastal actions, such as construction of structures, creation of forecasting systems, policy-making or implementation of ecosystem-based solutions.

Thus, the three specific aims adressed throughout the subsequent chapters are:

- Objective 1: To estimate waves and wave-induced TWL components in coastal areas, while explicitly accounting for surf zone hydrodynamics. The methodology should be computationally efficient and capable of delivering high-resolution outputs.

- Objective 2: To assess the effects of seabed variability on nearshore wave propagation by incorporating it into the modeling framework, which must account for all relevant physical processes occurring within the surf zone.

- Objective 3: To reproduce fast estimates of high-resolution maps of nearshore hydrodynamics, needed in diverse coastal applications. The methodology should be cost-efficient, taking advantage of statistical techniques and pre-run simulations.

1.4 Organization of the thesis

This thesis is structured in 5 chapters, with Chapter 2 being the basis of a paper published in *Coastal, Estuarine and Shelf Science* journal and Chapter 3 being under peer-review in *Coastal Engineering* journal at the time of submission. The PhD candidate is the lead author of all the work presented herein.

The structure of the present thesis is as follows. Chapter 1 "Introduction" presents the motivation and objectives of the thesis, as well as a general overview of the current state of knowledge in the field. Chapter 2 "An efficient metamodel to downscale TWL in open beaches" describes a hybrid methodology to downscale oceanic variables, such as significant wave height, mean wave direction and TWL components (wave set-up and infragravity wave level component) in coastal areas, taking into account the surf zone hydrodynamics involved. Chapter 3 "HyWaThy: Hybrid modeling of nearshore Waves with varying baThymetries" enhances the previously described metamodel by including seabed variability in the nearshore zone. Besides, it couples an additive model with a high-fidelity hydrodynamic model, being able to generate high-resolution spatial maps of nearshore oceanic variables, taking into account the influence of seabed variation. Chapter 4 "High-resolution nearshore wave climate" illustrates the wide

applicability of the HyWaThy metamodel by reconstructing 85-year hourly time series of spatial maps of H_s and using it as input for various coastal analysis (e.g. estimating the depth of closure, analyzing the extremes of the local wave climate or evaluating its relationship with the dominant climate indices in the North Atlantic). Finally, Chapter 5 "Summary and future research" summarizes the main findings of the thesis and outlines future research directions that could build upon the present work.

Chapter 2

An efficient metamodel to downscale total water level in open beaches

2.1 Introduction

One of the most widely utilized variables to understand the intensity and spatial distributions of coastal hazards is the TWL proxy (Haigh et al., 2014; Nederhoff et al., 2021; Caruso & Marani, 2022; Parker et al., 2023). Generally, it is calculated as the linear summation of mean sea level, astronomical tide, nontidal residuals, and storm wave-induced water level variations (see Eq. 1.1, from Serafin and Ruggiero, 2014; Serafin et al., 2017). In this equation, the η_{waves} component is the wave runup, a combination of the maximum set-up at the shoreline and the swash, which is the time-varying oscillations of the set-up including both incident (0.04-0.2 Hz) and infragravity waves (IG waves; 0.004-0.04 Hz). Considering its significant importance in open beaches, the study of its components has major relevance for coastal management tools. By unbundling η_{waves}, the individual wave-induced water level components can

be studied separately, thereby enabling a wide range of analyses and a better understanding of the overall coastal hazard. Wave set-up can notably contribute to the damaging potential of TWL (Hoeke et al., 2013), as it can represent as much as 30% of the TWL during a storm (R. G. Dean & Bender, 2006), whereas IG wave level component in swash can increase non-linearities depending on water depth and bottom friction (Toth et al., 2023), which can significantly contribute to wave set-up and run-up (Cheriton et al., 2016). On dissipative beaches, IG waves usually dominate the dynamics, due to the saturation of the short-wave incident-band in the surf zone and IG-band dominance at the seaward edge of the swash zone (Bertin et al., 2018; Roelvink et al., 2018). On steeper beaches (i.e. reflective), additional terms could be incorporated to fully represent the swash. Thereby, in this Chapter TWL will be herein defined as:

$$SWL = \eta_{MSL} + \eta_{AT} + \eta_{NTR} \tag{2.1}$$

$$TWL = SWL + \eta_{setup} + \eta_{IG} \tag{2.2}$$

where SWL is the still water level (i.e. the average water surface elevation at any instant, including MSL, tides and nontidal residuals (Eq. 1.1; Serafin et al., 2017; Parker et al., 2023), η_{setup} is the wave set-up and η_{IG} is the IG wave level component.

In this Chapter, a hybrid metamodel that aims to accurately and efficiently downscale the coastal hydrodynamics needed to estimate the TWL wave-related components, η_{setup} and η_{IG}, is presented. The separate analysis of these components allows a better understanding of coastal processes, that enhances the development of coastal management products, such as inundation risk assessment tools or forecast systems. To illustrate the functioning of the present methodology, the study site selected is La Salvé beach, in the North coast of Spain.

The Chapter is structured as follows. Section 2.2 introduces the study area and the datasets used. Section 2.3 describes the metamodel in detail, from the sampling and selection process to the numerical simulation and validation. Section 2.4 focuses on the application of the metamodel for three historical events. Finally, Section 2.5

summarizes the contents and presents the main conclusions.

2.2 Study area and data

This section describes the study area and the different datasets used in the presented metamodel. Section 2.2.1 introduces the geographical features of the study area, as well as the wave climate and its relationship with the local environment. Sections 2.2.2 and 2.2.3 describe the field (topobathymetry and sediment characterization) and oceanographic open data (waves and tides) used as input.

2.2.1 Study area

La Salvé beach is located on the northern coast of the Iberian Peninsula, bathed by the Cantabrian Sea. As shown in Fig. 2.1a, it is a 4.25 km-long urban sand spit that protrudes into Santoña Estuary, on which the city of Laredo is based. At its northern end, the Asón river meets the Santoña Bay sheltered by Mount Buciero, a cape pointing East that reaches almost 400 m over the local mean sea level. On its southern part, there is a fishing port and marina protected by a curved mound breakwater with a superstructure of more than 700 m in length.

Offshore waves come predominantly from the NW sector, with average periods of around 10 seconds and significant wave heights from 1 to 2 m, reaching 4 to 5 m during severe winter storms (Medina et al., 1995; Garrote et al., 2018; data available from https://www.puertos.es/es-es/oceanografia/Paginas/portus.aspx). La Salvé is a mesotidal dissipative beach, with semidiurnal and fortnightly tide cycles. The mean tidal range is around 3 m, rising to 5 m during spring tides (Medina et al., 1995; Garrote et al., 2018; data available from https://www.puertos.es/es-es/oceanografia/Paginas/portus.aspx). The medium grain size (D_{50}) alongshore has no significant variation, with a representative value of 0.23 mm (according to field data, see Section 2.2.2 and Fig. 2.1c).

The short-term sedimentary dynamic equilibrium between the river and the waves conforms a shoal located on the north side of the spit (Fig. 2.1b). This underwater

sand accumulation strongly refracts incident waves, concentrating wave energy above it and thus increasing wave heights. Therefore, in the mid-north part, a narrowing of the beach face can be noticed, mainly because of the erosion produced by the surf generated by greater wave heights breaking nearshore. In addition, a historical anticlockwise rotation of the spit has been pointed out (Garrote et al., 2018), as well as a lack of sediment (yet not recovered) since the 2013/2014 severe winter storms that impacted the Atlantic European coasts (Masselink et al., 2016; Garrote et al., 2018).

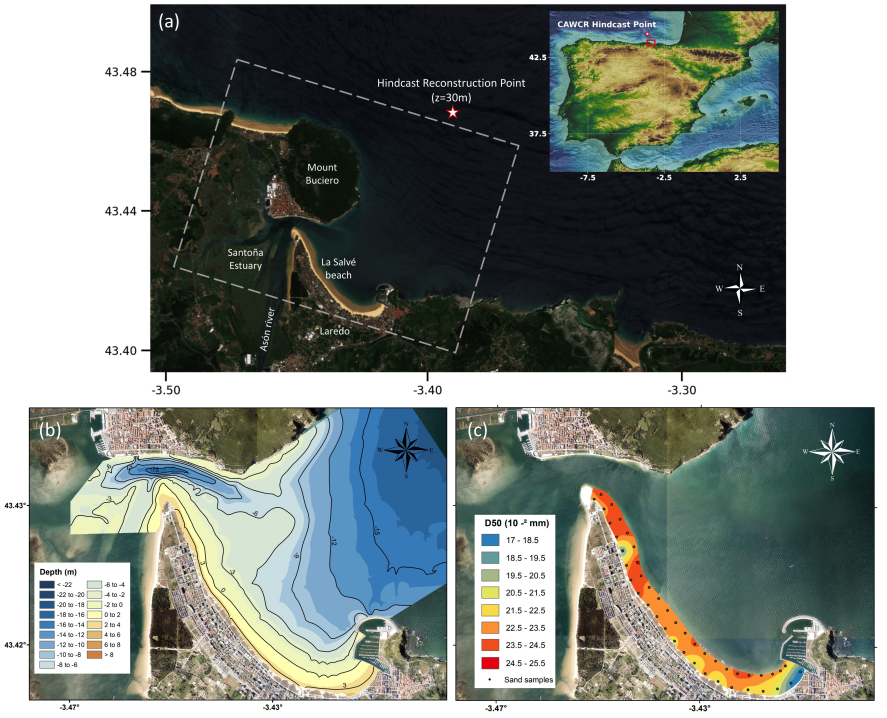

Figure 2.1: (a) Study area, with locations of interest: on the upper right subplot, study area location within the Iberian Peninsula (red rectangle) and CAWCR hindcast point (red point); on the main map, reconstruction point at z = 30m (red star), numerical domain layout (grey rectangle) and significant geographical elements. (b) Raw topobathymetry data of the study site used in this work, obtained in April 2015. (c) Grain size (D50) spatial distribution at La Salvé beach, samples from March 2021.

2.2.2 Field data

A semi-annual beach survey program was operational from 2012 to 2021 at La Salvé beach by the Civil Engineering Studies and Experimentation Center (CEDEX, by its Spanish acronym), whose domain goes from the dune crest to 25m depths. Land points were surveyed using a Real-Time Kinematic (RTK) system, with sample points measured alongshore in 90 profiles. Regarding the bathymetry, measurements were taken on profiles every 300 m with a single-beam echosounder on a vessel. These topobathymetric data were resampled to a 5 m horizontal resolution Digital Elevation Model (DEM) (Fig. 2.1b).

The topobathymetric data allows to obtain the beach face slope, a parameter closely interrelated with grain size (Bujan et al., 2019), which also provides valuable information on temporal beach morphodynamics (Jackson & Short, 2020). Beach sediment samples were taken by CEDEX, annually from 2012 to 2016, and Geomatics and Ocean Engineering Group (GeoOcean, Universidad de Cantabria), in March 2021 (Fig. 2.1c), covering the whole beach. The latter indicated that the average grain size (D_{50}) in La Salvé beach was around 0.23 mm, which concurred with the former. Based on the widely used classification proposed by Wright and Short (1984) where each morphodynamical beach state is related to specific incident waves and sediment size using the dimensionless fall velocity parameter (R. Dean, 1973; Dalrymple & Thompson, 1976), La Salvé beach is classified as a dissipative beach. This being said, some areas are seasonally or permanently affected by local phenomena (e.g. wave energy concentration, river mouth morphodynamics, sheltered zones from energetic swells), and present a longitudinal bar state. As minor variations in the morphodynamic state of La Salvé beach were observed in this analysis, a representative winter bathymetry from April 2015 was taken as input data for this study (Fig. 2.1b).

2.2.3 Oceanographic data

Oceanic data were retrieved from open-source global databases. Offshore partitioned wave parameters came from the Centre for Australian Weather and Climate Research (CAWCR) wave hindcast 1979-2022 generated by the Bureau of Meteorology

and CSIRO (Durrant et al., 2014; Smith et al., 2020; data available from https://data.csiro.au/collection/csiro:39819). It is a monthly updated database with a global resolution of 0.4^{o}, generated with the numerical model WAVEWATCH III (Tolman, 1991), forced with hourly surface winds from the Climate Forecast System Reanalysis (CFSR) developed by the National Center for Environmental Prediction (NCEP). Hourly sea level data (astronomical tide and surge due to pressure and wind) were obtained from the tide gauge located in Santander, 30 km west of the study area (State Ports, Spanish Government; https://www.puertos.es/es-es/oceanografia/Paginas/portus.aspx). Satellite data from the Integrated Marine Observing System (Integrated Marine Observing System (IMOS), 2019) were retrieved for hindcast correction, and hourly data from a deep-water buoy (Bilbao-Vizcaya buoy from State Ports, Spanish Government; https://www.puertos.es/es-es/oceanografia/Paginas/portus.aspx) were used for the hindcast validation. Using the aforementioned data, the HyWaves hybrid methodology (Ricondo et al., 2023) was applied to propagate the offshore hindcast close to the numerical domain limit. Thus, an accurate long-term series of sea state parameters was efficiently obtained in the study area (see Section 2.3.1 for further details).

2.3 Metamodel

The general methodology of the proposed metamodel is shown in Fig. 2.2. Section 2.3.1 will focus on the synthetic generation and the selection of cases, Section 2.3.2 will describe the numerical modeling, and Sections 2.3.3 and 2.3.4 will show the analysis and reconstruction of the results, respectively. Subsequently, in Section 2.3.5, a k-fold cross-validation is applied to estimate the skill of the metamodel.

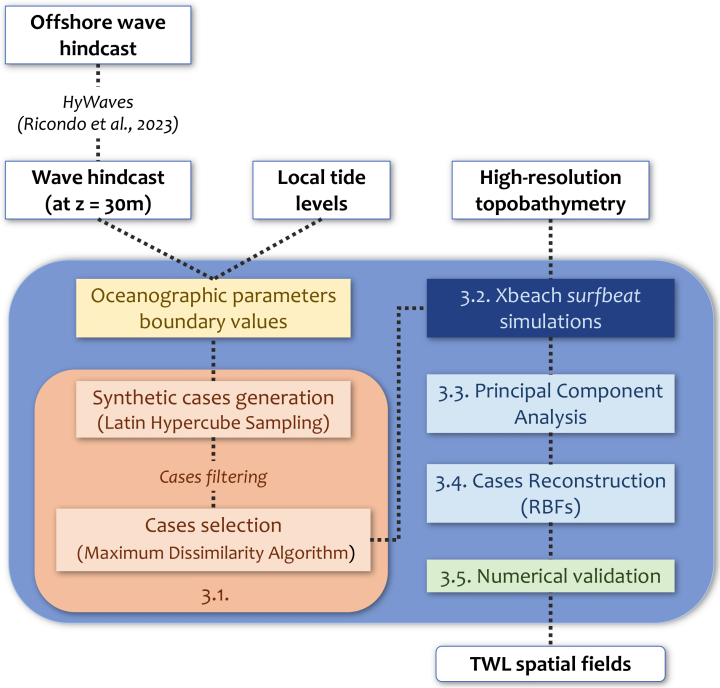

Figure 2.2: Flow chart of the proposed metamodel.

2.3.1 Sampling and selection

The starting step in the metamodel (shown in Fig. 2.2 in the upper left corner) is based on HyWaves, a hybrid model described in Ricondo et al. (2023). First of all, offshore wave partitions (significant wave height, peak wave period, mean wave direction and wave spreading - hereafter H_s, T_p, θ_m, and σ - for seas and swells) are retrieved from CAWCR hindcast dataset. Then, relying on the assumption of linear wave theory, a selection of representative wave partitions is numerically propagated and used in the interpolation and reconstruction of the different wave systems in a point at 30 m depth (in Fig. 2.1a, indicated as a red star). As linearity in the wave processes is assumed, this point must be far enough from the shoreline to assume that nonlinear interactions are negligible. It will also be taken as representative for the

entire contour of the numerical domain, whose limits go from intermediate to shallow waters (see Section 2.3.2).

Having the reconstructed series of sea state parameters, synthetic conditions are generated. For doing so, a range of scalar values is defined for each variable (see Table 2.1), given the local geometry and the limits defined by the series themselves. The selected variables are H_s, wave steepness (H_s/L_0, being L_0 the offshore wavelength), θ_m, σ, and SWL (referred to the same vertical datum as the topobathymetry (Mean Sea Level at Alicante, Spain)). H_s/L_0 restricts the spurious results, avoiding the creation of physically incongruent cases (e.g., huge wave heights with minimum periods). Considering that L_0 is defined by T_p, combining its definition with wave steepness formula allows to infer T_p taking into account its physical relationship with H_s. Considering that most of the North-East Atlantic sea states are predominantly unimodal (Espejo et al., 2014), in this case T_p serves as a parameter defining the majority of wave components of the spectrum. In case the metamodel were to be applied in a study site characterized by mixed seas, T_m or T_{m02} would be more pertinent.

Variable	**Boundary values**
H_s	[1, 12] m
H_s/L_0	[0.005, 0.05] m/m
θ_m	[310, 70] º
σ	[10, 50] º
SWL	[-2.0, 2.8] m

Table 2.1: Upper and lower boundary values used for each variable.

Once each variable has its limits defined, the Latin Hypercube Sampling method (hereafter LHS; McKay et al., 1979) is applied to generate a set of synthetic cases. This sampling method is a type of stratified Monte Carlo technique, which demands less computational effort and time consumption than Monte Carlo simulations. Each variable is divided into a user-defined number of ranges and must be independent or transformable into it. LHS operates in a manner that produces a sample size M from the n variables by dividing their correspondent ranges into M non-overlapping, equally probable intervals. From each interval, a value is picked attending to the probability density that defines it. This procedure is carried out M times for each variable, thus having n sets (one per variable) of M values (one per interval). These M values of

a variable are paired with the M values of another variable randomly, and so forth, until reaching the n^{th} variable. In this way, a set of $n \times M$ tuples are constructed, the Latin Hypercube sample. Thereby, the randomness of this sample is ensured as there are $(M!)^{n-1}$ possible combinations for given values of M and n.

The starting samples generated for the study area are $M = 12000$ hourly sea states. However, T_p output values inferred from H_s/L_0 are filtered to ensure that they are under the threshold of wind-generated "short waves", typically 0.04 Hz ($T_p \leq 25s$). In addition, to ensure that the selection is focused on energetic sea states (which are of particular relevance for coastal management), the 2% exceedence value of runup peaks ($R_{2\%}$) is calculated using the formulation proposed by Stockdon et al. (2006), excluding from the samples those whose ($R_{2\%}$) value is below 0.5 m. For each combination of H_0, L_0, and beach face slope (averaged from the available topobathymetries, $\beta_f = 0.017$), it is found that $\xi_0 < 0.3$ (ξ_0 being the Iribarren number (Battjes, 1974)) for all the cases, thus allowing the use of the Stockdon et al. (2006) formulation for extremely dissipative conditions. This formulation is suitable for application in this study site, but it is important to acknowledge that for different study sites (such as rocky or artificial coasts, or beaches with longshore varying foreshore slopes), the formulation may have limitations (see Stockdon et al., 2006; Plant and Stockdon, 2015). Therefore, alternative approaches should be considered (e.g. EurOtop, 2018 to estimate $R_{2\%}$).

The first 10000 tuples that fulfil both conditions constitute the synthetic dataset based on the local hindcast data used in this methodology, denoted as $M_i = \{H_{S,i}, T_{P,i}, \theta_{m,i}, \sigma_i, SWL_i\}; i = 1, ..., 10000$. It is important to highlight that LHS allows the determination of the limit values, thus enabling the creation of a tailor-made dataset of wave parameters based on real hindcast data. Furthermore, this technique offers the flexibility to modify these limits, so future projections can be incorporated to the dataset, such as SLR or larger wave heights.

To optimize computational resources while maintaining the accuracy of the variables reconstruction, a selection of 500 cases inside the design space (depicted in the scatter plots in Fig. 2.3, where the axes are defined by the ranges of the variables within M_i) is performed using the Maximum-Dissimilarity Algorithm (MDA). This algorithm, first described by Kennard and Stone (1969), is used to select a representative subset of the most dissimilar N sea states given a dataset of M sea states. This

selection algorithm is applied to the LHS dataset, thereby reducing the number of simulations required. Consequently, the resulting subset, denoted as $N_j = \{H_{S,j}, T_{P,j}, \theta_{m,j}, \sigma_j, SWL_j\}; j = 1, ..., 500$. The MDA algorithm ensures the selection of extreme events by iteratively exploring the most dissimilar data inside the multidimensional space (Camus et al., 2011a), exploring its edges first, where combinations of extreme wave parameters are located.

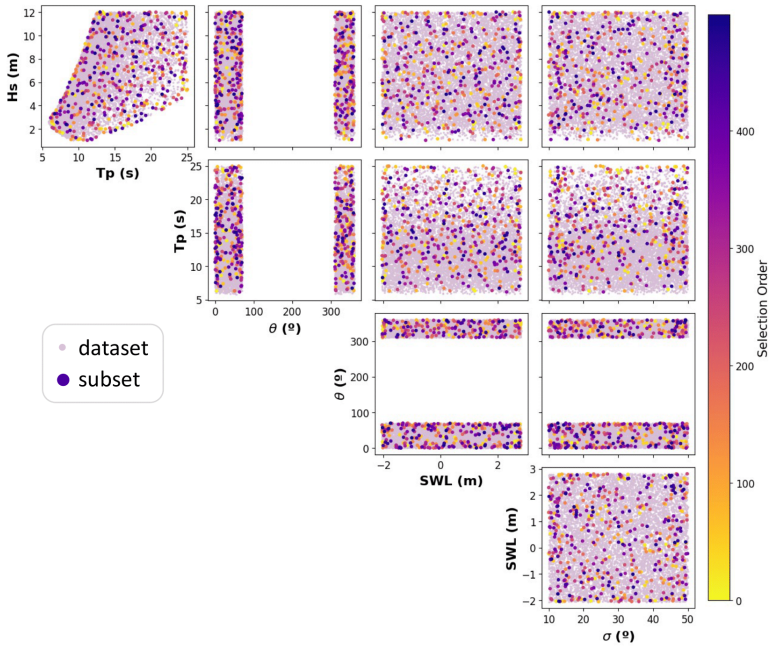

Figure 2.3: Multidimensional distribution of the LHS synthetically generated dataset and the MDA-selected cases.

2.3.2 XBeach configuration

The hydro-morphodynamic model XBeach in *surfbeat* mode (henceforth XBSB, Roelvink et al., 2009; Roelvink et al., 2010) is used to perform surf zone hydrodynamic simulations. Each set of offshore wave parameters within N_j subset is used to force the simulations. A non-regular rectangular grid is adopted, featuring a 10-metre resolution

in Santoña Bay and a coarser resolution in deep waters and lateral boundaries. The grid is orientated 17ºN, and the extend is defined so that Santoña Bay is far enough from the boundaries to minimize discretization errors (see Fig. 2.1a). The lateral boundary conditions are defined using the *Neumann* option inside the model. This condition is appropriate for quasi-stationary situations, where the offshore boundary conditions can be assumed uniform.

By means of the HISWA equations (HIndcasting Shallow WAter WAves, described in Holthuijsen et al., 1989), XBSB, a coupled wave and circulation model, solves the time-dependent horizontal equations of wave transformation (swash hydrodynamics) on wave groups scale, as well as the horizontal equations of conservation of mass and momentum (for mean surface and IG elevation). XBSB forces IG wave motions with the radiation stress gradients produced in the water column by short-wave height envelope variations, thus modeling the dynamics involved in IG wave generation, propagation and nonlinear dissipation (and their corresponding runup and rundown). XBSB also takes into account diverse nearshore phenomena, such as shoaling, dissipation due to bottom friction, refraction, wave breaking, wave blocking and wind generation, along with the influence of currents on them.

Along with the domain definition and the hydrodynamics formulation, a set of parameters and forcings are also settled down for numerical simulations. A constant Chèzy bed friction coefficient of $55m^{1/2}/s$ is used, representative of beach bottoms, as there is no data available in the study site. The dimensionless friction coefficient c_f associated with long period (IG) waves can be calculated from that Chèzy value, resulting in $c_f = 0.003$. In this work, a constant short-wave friction (f_w) of 0.03 is used, as dissipation factors for waves are one or two order of magnitude larger than drag coefficients for the mean current (Nielsen, 1992; Henderson & Bowen, 2002). Wave and water level boundary condition parameters are given as two equal sea states defined by two hourly JOint North Sea WAve Project (JONSWAP) spectra ($H_s, T_p, \theta_m, \gamma = 3.3, \sigma$ and SWL), in order to dismiss the first hour of simulation as it represents the model warm-up. It is considered that using a constant value of$\gamma = 3.3$, widely applied in engineering works, is deemed appropriate to describe the local wave climate, given the optimal values of γ in the northern coast of Spain (Mazzaretto et al., 2022). The outputs are the 1-h mean spatial distributions of η_{setup} and η_{IG} alongshore (the

latter inferred as $\eta_{IG} = A_{S_{IG}} = 2\sqrt{m_{0_{IG}}} = 2\sqrt{\sigma_n^2}$; being $A_{S_{IG}}$ the amplitude of the significant IG wave height and σ_n^2 the free surface variance), and the 1-h mean H_{rms} obtained as a 2-D spatial distribution along La Salvé beach (transformable into H_s following the relation $H_s = 1.416 H_{rms}$), with spatial resolution of 10 m.

The XBSB simulations were run on a CentOS7 cluster (x86-64) with up to 8 nodes, each with 48 cores (2.10 GHz Intel Xeon Gold 5318Y), up to 128 GB of RAM. The full 500 cases of N_j subset took approximately 4 days to run (∼17 hours per case, with parallelization of 102 cases).

2.3.3 Principal Component Analysis

XBSB outputs from N_j subset (spatial fields of mean H_s, η_{setup} and η_{IG}), are studied by means of Principal Component Analysis (PCA). PCA is a statistical technique widely used in coastal studies (e.g. Camus et al., 2014b; Lemos et al., 2021; Montaño et al., 2021b) that consists of a re-projection of the original data on a new space, reducing the multidimensionality of the data while explaining the maximum variance of the sample data. The eigenvectors of the data covariance matrix (Empirical Orthogonal Functions, EOFs) define the vectors of the new space, while the Principal Components (PCs) are the projections of the original data over the new vectors. EOFs are usually sorted increasingly according to the variance they explain (Explained Variance, EV), so the aim is to capture a reduced number of PCs that explain a desired variance, to efficiently reconstruct any combination of $\{H_s, T_p, \theta_m, \sigma, SWL\}$.

The EOFs obtained through PCA for the spatial fields of H_s, η_{setup} and η_{IG} show the dominant spatial patterns for each variable, whereas each N_j subset case has a correspondent component weight. The combination of the component weight (PC) with the EOF values represent the variance over the mean values. Thus, by visually combining the spatial patterns (EOFs) with the component weights (PCs), a fast performance verification can be done, identifying whether the results are consistent or not. The number of EOFs-PCs selected is enough to capture all the relevant spatial patterns in the coastal stretch within the study site, without compromising the performance of the metamodel. This section will consist of three parts: the first one will evaluate the results of PCA performance for H_s, whereas the second one will do

likewise with η_{setup} and the third one with η_{IG}.

Regarding H_s, the 2-D domain has been delimited to the lowest tide level of the MDA dataset, to avoid capturing the breaking waves patterns that affect the intertidal zone. PCA is carried out for H_s and for θ_m (analyzing its components separately along the x- and y-axes, i.e. the axes defined by the cardinal points, where positive values align with the North and East directions). The results of the first 3 PCs and EOFs of H_s, along with the mean H_s spatial distribution for the N_j subset, are shown in Fig. 2.4. Some interesting patterns that suggest a relationship between certain PCs and physical phenomena can be noticed. The first 2 EOFs-PCs (Fig. 2.4b and Fig. 2.4c) represent the relationship between H_s, T_p and SWL with spatial distributions of H_s: the larger the forcing of H_s and T_p, the larger the refraction of the waves is, which in addition has larger values of H_s in the eastern part of the bay (Fig. 2.4b). Fig. 2.4c shows the interdependence between H_s and SWL. It can be seen that larger waves break before reaching the shoal during high tides (larger values of SWL), and as SWL decreases, so does the breaking wave height in the shoal. Smaller waves mostly break after the shoal, independently of the tide. Besides, the third PC (Fig. 2.4d) emphasizes the influence of θ_m and σ in H_s values in certain zones: NE swells intensify nearshore H_s in the center and northern end of the beach, whereas NW swells with great H_s values have a particular impact on the southern end and the shoal. Besides, for N swells, low values of σ imply H_s amplifications near the Port; but, with larger values, H_s is amplified in the rest of the beach, as it overcomes the shelter of Mount Buciero. For this parameter, the first 9 PCs explain the 99.95% of the H_s data variance, significantly reducing data dimensionality.

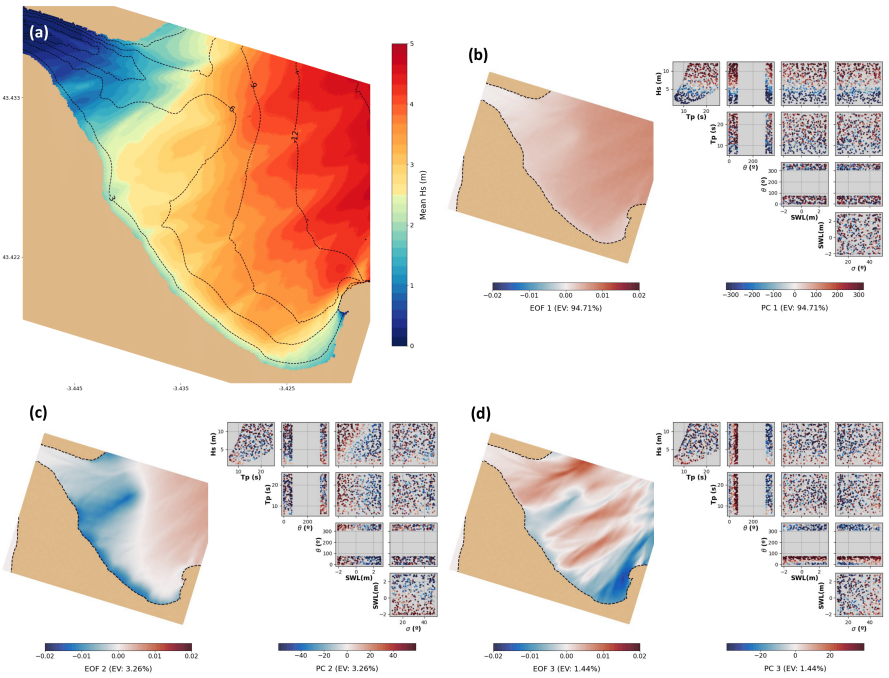

Figure 2.4: (a) Mean H_s spatial field of the 500 MDA-selected cases. (b), (c), and (d) represent the EOFs and scatter plots of the MDA subset wave parameters, colored according to the correspondent component weight, for H_s.

On the other hand, PCA of η_{setup} and η_{IG} is performed. In this case, each variable is calculated at the equivalent topographic contour of the correspondent SWL), but is shown on the zero contour for visualization purposes. The first three EOFs-PCs of the PCA of η_{setup} are shown in Fig. 2.5, as well as the mean η_{setup} distribution for the N_j subset. In the first EOF-PC (Fig. 2.5b), it can be seen how larger H_s-T_p values induce larger η_{setup} alongshore. The second EOF-PC of η_{setup} (Fig. 2.5c) shows the influence of θ_m and σ in this variable along the beach: waves coming from the NE sector generate larger η_{setup} in the northern end of the spit, whereas those coming from the NW sector do likewise in the southern end. Similarly to H_s third EOF-PC (Fig. 2.4d), N swells with low σ increase η_{setup} near the Port, but can affect the rest of the beach if σ is larger (Fig. 2.5c). Fig. 2.5d indicates that high tides

(large values of SWL) increase η_{setup} in the north-central part of the beach, and lower values of SWL) do the same in the northern part in a significant manner. However, as La Salvé beach has a strong dissipative beach profile, with absence of underwater morphological features such as sandbars, SWL) does not relate to alongshore spatial patterns in η_{setup}. For η_{setup}, first 8 PCs explained the 99.5% of the variance.

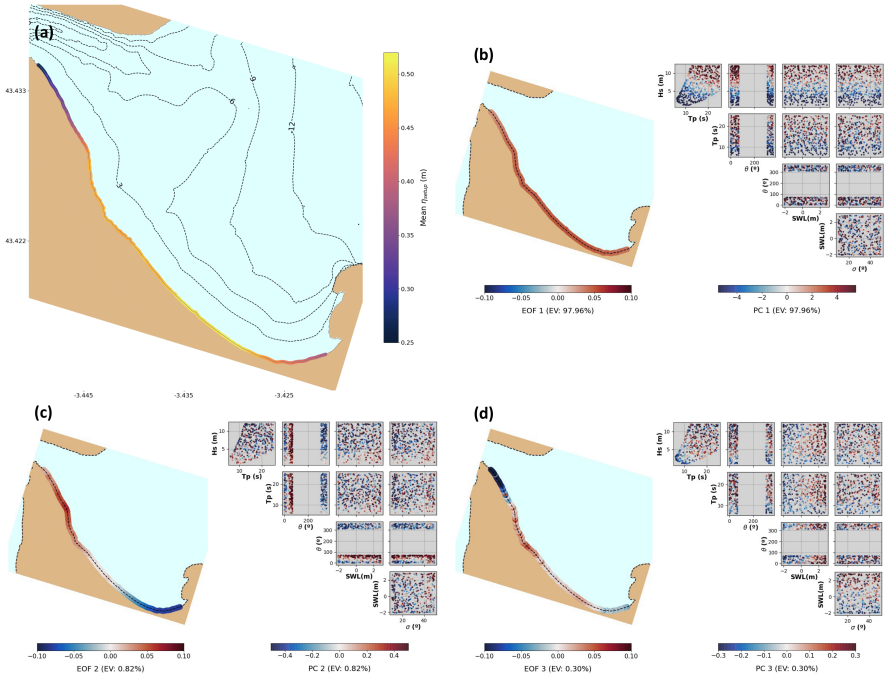

Figure 2.5: (a) Mean η_{setup} spatial field of the 500 MDA-selected cases. (b), (c), and (d) represent the EOFs and scatter plots of the MDA subset wave parameters, colored according to the correspondent component weight, for η_{setup}.

Regarding η_{IG}, the first EOF-PC (Fig. 2.6b), indicates a pattern similar to that of the first EOF-PC of η_{setup} (Fig. 2.5b), but with a higher dependence on T_p, rather than H_s. In the second EOF-PC (Fig. 2.6c), the influence of SWL can be noticed: extreme values (low and high tides) specially increase η_{IG} in the southern end, while mid to high tide affect to the northern end of the beach for waves with larger H_s-T_p. This notably raises η_{IG} in the north-central part of the beach and the rivermouth,

as these waves break far in the shoal and release more IG waves. In addition, an increase of η_{IG} in the southern end of the beach during energetic wave events, as well as an intensification with low-frequency waves in the northern end of the beach, can be pointed out. In Fig. 2.6d, it is highlighted the behaviour of η_{IG} along the beach during energetic wave events, where high tides especially affect the central part of the beach and low tides do the same in the southern and northern ends. For η_{IG}, the 99.5% of the variance was explained with the first 7 components.

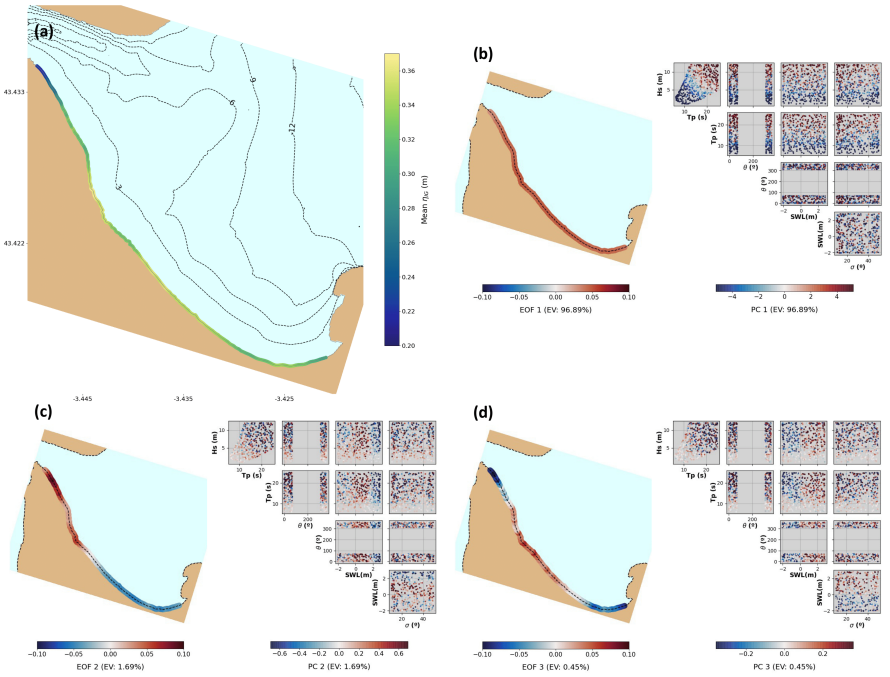

Figure 2.6: (a) Mean η_{setup} spatial field of the 500 MDA-selected cases. (b), (c), and (d) represent the EOFs and scatter plots of the MDA subset wave parameters, colored according to the correspondent component weight, for η_{setup}.

2.3.4 Reconstruction

Once the PCA is performed, reconstructions are conducted with the number of PCs that explain more than 99% of the variance for each variable. Once they are

identified, a reconstruction of the whole LHS dataset is performed using Radial Basis Functions (RBFs; see Franke, 1982), a non-linear interpolation technique based on a weighted sum of radially symmetric basic functions. These functions (Gaussian, linear, cubic...) are fitted to the data points, allowing the reconstruction of the 10000 sea states within the M_i dataset as if they had all been propagated nearshore. Given its accuracy and computational cost, this technique is often used to interpolate large sets of scattered data in high-dimensional spaces, as occurs with MDA-selected cases (Camus et al., 2011b).

Each sea state at deep water is defined as $D_i = \{H_{S,i}, T_{P,i}, \theta_{m,i}, \sigma_i, SWL_i\}; i = 1, ..., N$ whereas each propagated sea state is expressed as $P_j = \{H_{S,j}, T_{P,j}, \theta_{m,j}, \sigma_j, SWL_j\}; j = 1, ..., M$. The approximation function is of the form:

$$RBF(D_i) = p(D_i) + \sum_{j=1}^{M} a_j \Phi(||D_i - P_j||) \tag{2.3}$$

where $p(D_i) = b_0 + b_1 H_{S,i} + b_2 T_{P,i} + b_3 \theta_{m,i} + b_4 \sigma_i + b_5 SWL_i$, $||\bullet||$ is the Euclidean norm, and Φ is a Gaussian function with a shape parameter c that defines the form of the distributions. Coefficients $a_j = [a_1, \ldots, a_M]$ and $b = [b_0, \ldots, b_5]$ result from the interpolation condition:

$$RBF(P_j) = f_j(P_j);\ j = 1, ..., M \tag{2.4}$$

Numerical validation against XBSB simulations is performed using two energetic sea states as representative of the local wave climate (Fig. 2.7a and Fig. 2.7b). Each sea state is defined by the offshore wave parameters: $SS_1 = \{H_{S,1} = 3.5m, T_{P,1} = 15s, \theta_{m,1} = 335°, \sigma_1 = 40°, SWL_1 = 0.5m\}$ and $SS_1 = \{H_{S,2} = 8m, T_{P,2} = 20s, \theta_{m,2} = 315°, \sigma_2 = 30°, SWL_2 = 2m\}$. These wave parameters subsets represent an average winter storm and an extreme winter storm, respectively. Tide levels are arbitrarily selected within the range of observed tides at the study site.

As noticed in Fig. 2.7, the two simulated sea states are reconstructed within a few seconds in an appropriate way, with spatial fields showing minimum errors for the three

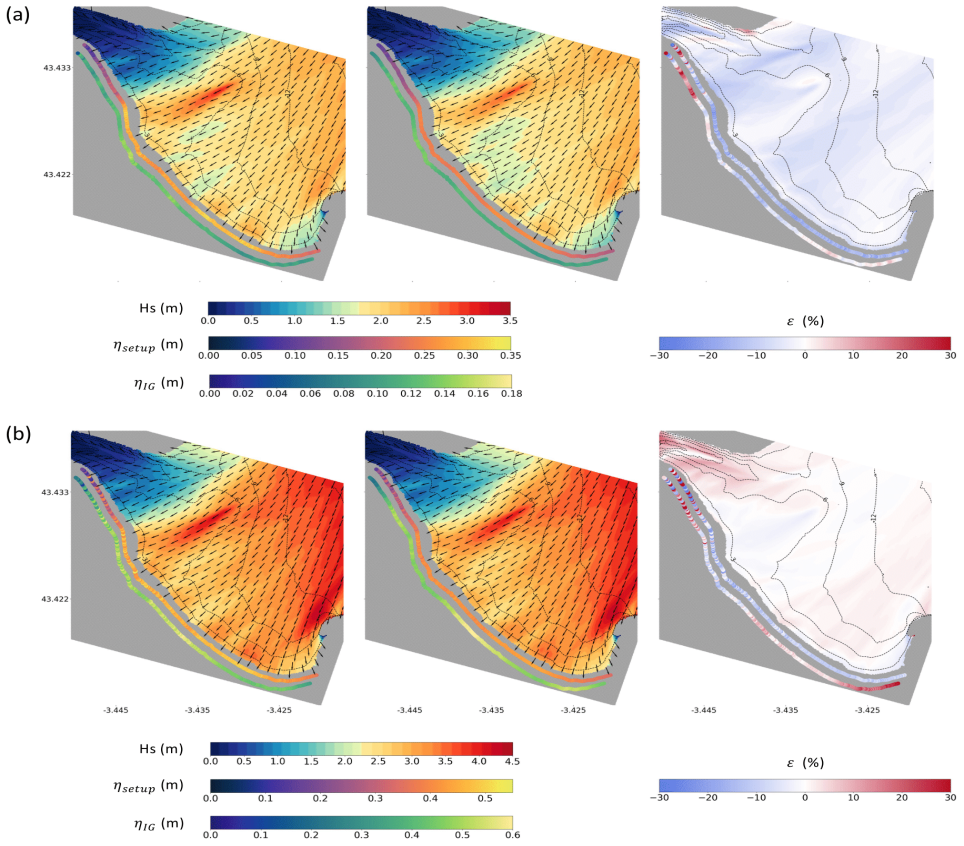

Figure 2.7: Numerical validation of the metamodel. For (a) average winter storm, and (b) extreme winter storm: comparison between XBSB outputs (first column) and their reconstruction (second column), and their relative errors (third column). 2D colormaps indicate H_s spatial distributions, lines along the coast represent the values of η_{setup} (seaside) and η_{IG} (landside) and black arrows indicate wave direction.

variables. The mean wave direction θ_m is reconstructed following the same procedure for its components x- and y-. Variations over the dynamically modelled values are less than 10% for H_s, around 10% for η_{setup}, and around 5% for η_{IG}. For SS_1, only 1% of the points reach values of relative error (ϵ) of $\pm 30\%$ for both η_{setup} and η_{IG}. For SS_2, 5% of the points reach an ϵ of $\pm 30\%$ for both variables. Additionally, spatial patterns are also precisely modelled, as can be noticed in the smooth colour gradients in the relative error maps. The relative errors in these two synthetic events show a very low error in the central part of the beach, where the shoal is located. The importance of this zone in the study site is major: due to its configuration, wave energy concentration is notable throughout the year. Therefore, coastal assets are likely to be affected by winter storms on a frequent basis. Regarding the southern part of the beach, the most exposed to the average wave climate, the three variables show good performance, defining the metamodel as a reliable tool for EWS and forecast systems.

PCA and RBF results were obtained in less than 3 minutes for each variable. Each variable was reconstructed for the 10000 cases in around 2 minutes on a 2.9 GHz Intel Core i7-10700 using up to 16 CPU cores and 32 GB of RAM.

2.3.5 Numerical validation

A k-fold cross-validation is carried out to test the skill of the metamodel to predict H_s, η_{setup} and η_{IG}. This procedure randomly rearranges and divides the dataset into k groups (for this application, $k = 5$). Each group is designated as the test set, while the remaining groups constitute the training dataset, upon which the RBF technique is fit to evaluate the test data. The disparity between the predicted and modelled values is quantified using the Root Mean Square Error (RMSE) for each group. For a better understanding of the validation, predicted and modelled values of H_s, η_{setup} and η_{IG} are normalized with the offshore significant wave height H_{S_0} of each case. The average of the normalized RMSEs is shown in Fig. 2.8, where the normalized variables are denoted as H_s^*, η_{setup}^* and η_{IG}^*. Generally, the metamodel shows a good performance for all three variables: H_s^* spatial field error is below 3%, while η_{setup}^* and η_{IG}^* spatial field errors are below 1%. Considering the orders of magnitude of the relationships between H_s, η_{setup} and η_{IG} and H_{S_0}, the results show low and homogeneous errors

in the study area. Therefore, these errors, inherent to the methodology itself, can be assumed, giving as a result a metamodel that produces fast and reliable TWL components spatial distributions.

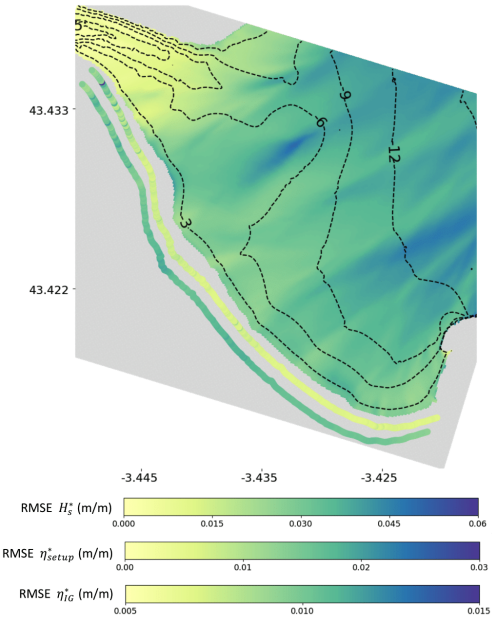

Figure 2.8: Average of the normalized RMSEs of the k-fold cross-validation. The 2D colormap indicates H_s^* RMSE spatial distribution, lines along the coast represent the values of η_{setup}^* RMSE (seaside) and η_{IG}^* RMSE (landside).

2.4 Application

The fast and accurate performance of the metamodel emphasizes its suitability for risk assessment tools. Under a changing climate, it is critical to have access to information regarding coastal hazards to take mitigation, adaptation or protection measures. In this scenario, fast and reliable forecast systems, as well as coastal hazard assessments, play an important role in decision-makers strategies. As this metamodel should be mostly used for extreme events management tools (e.g. EWSs, extreme TWL forecasts), a first filter for those events with an estimated wave runup below 0.5

meters following Stockdon et al. (2006) formulation is carried out. In Section 2.4.1, two historical energetic winter storms have been selected to emulate the use of the metamodel as a forecast system, and a qualitative validation against observed impacts is carried out. In Section 2.4.2, a TWL-driven coastal flooding hazard characterization is applied for those same events, as an example of a useful final product delivered by the use of the metamodel.

2.4.1 Reconstruction of historical events

To showcase the application of the metamodel to past or future real events, two historical winter storms from March 3rd 2014 and January 17th 2018 are selected and water levels are reconstructed (Fig. 2.9a and Fig. 2.9b). The former is defined by the wave parameters $W_1 = \{H_{S,1} = 8.14m, T_{P,1} = 19.1s, \theta_{m,1} = 330.2°, \sigma_1 = 40°, SWL_1 = 2.67m\}$; whereas the latter is defined by the wave parameters $W_2 = \{H_{S,2} = 6.13m, T_{P,2} = 17.55s, \theta_{m,2} = 332.7°, \sigma_2 = 30°, SWL_2 = 1.83m\}$ (buoy and tide gauge data available from State Ports, Spanish Government; https://www.puertos.es/es-es/oceanografia/Paginas/portus.aspx). The former, a compound event where strong spring tides and a high energetic sea state overlapped, caused major damages in the north of the spit, where low-lying infrastructures were unprotected from the overtopping rates that took place (Fig. 2.10b). Additionally, other more sheltered areas were also impacted by the large TWL and waves, destroying several parts of the seafront (Fig. 2.10c). Regarding the latter, W_2, although energetic, it was not as destructive as W_1. The combination of a lower SWL with a less energetic sea state caused less economic losses. Collisions with the previously mentioned low-lying structures also took place (Fig. 2.10e), but the absence of exposed buildings, as they were demolished after 2014 event, softened the effects of this storm. Fig. 2.10f shows protection measures taken by Laredo's Council: artificial dunes and a channel were built so a stream could flow seawards, therefore avoiding upstream floodings caused by the sand blocking the stream.

Both events are effortlessly reconstructed and prove the high performance of the metamodel in reconstructing nearshore variables. The spatial patterns of H_s, η_{setup} and η_{IG} and their intensity are consistent, pointing out the zones where substantial

damages were noticed (in Fig. 2.10a and Fig. 2.10d, the zones circled in black). The approach presented in this section could also be applied to forecast the three variables along the coast, thus allowing coastal managers and engineers to be prepared for and mitigate the impacts of future events on nearshore communities.

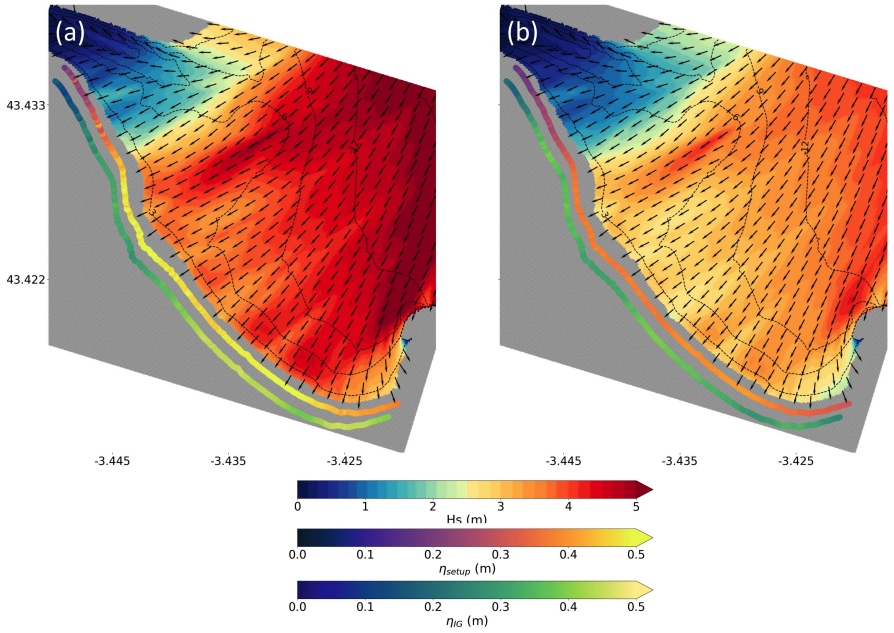

Figure 2.9: Reconstruction of mean H_s, η_{setup} and η_{ig} spatial fields of the events of (a) March 2014 and (b) January 2018.

2.4.2 Total Water Level hazard characterization

As an application of TWL as a proxy for coastal hazard, a determination of an impact rank scale (simplified from the 'Storm Impact Scale', presented by Sallenger (2000)) in La Salvé beach-dune system was performed (upper right corner of Fig. 2.10a and Fig. 2.10d). This approach has been previously used in several papers to characterize the impacts of storms at open beaches worldwide (e.g., Stockdon et al., 2007; Castelle et al., 2015; Leaman et al., 2021). In this study, the beach morphology was defined by the topobathymetry and introduced as a static feature, considering only

the hydrodynamic conditions of the storms (as done in other storm ranking methods described in Lemke and Miller (2020)). Two thresholds were established at the dune toe and crest, determining three hazard levels: safety, with TWL below the dune toe height; collision hazard, with TWL between dune toe and crest height; and overtopping hazard, with TWL above dune crest height. La Salvé beach was discretized in transects every 70 m, within which the dune toe and crest were identified, as well as the metamodel outputs on the MSL-equivalent topographic contour. Each transect was related to a storm impact level by comparing TWL (obtained as a linear summation of SWL, η_{setup} and η_{IG}), and the dune morphology, thus yielding a TWL-driven coastal flooding hazard spatial distribution. As noticed in Fig. 2.10a and Fig. 2.10d, representing W_1 and W_2 winter storm hazards, the northern end and central zone of the beach were exposed to larger hazards than the rest of the beach. These results match historical evidence: these zones are usually affected by greater coastal hazards due to the effect of the shoal on waves and the beach face configuration. For instance, the 2014 extreme winter storm (W_1, described in Masselink et al. (2016) and Garrote et al. (2018)) caused major damages, with destructive overtopping and collision events in the northern end of the beach (Fig. 2.10b). As for the winter storm of 2018 (W_2), although energetic, it was not as much destructive as the former, mainly due to the concurrence of a lower SWL with the high-energetic sea state. As can be noticed in Fig. 2.10e, the main hazard in this event was the collision with the dunes and low-lying structures, which is well represented in Fig. 2.10d.

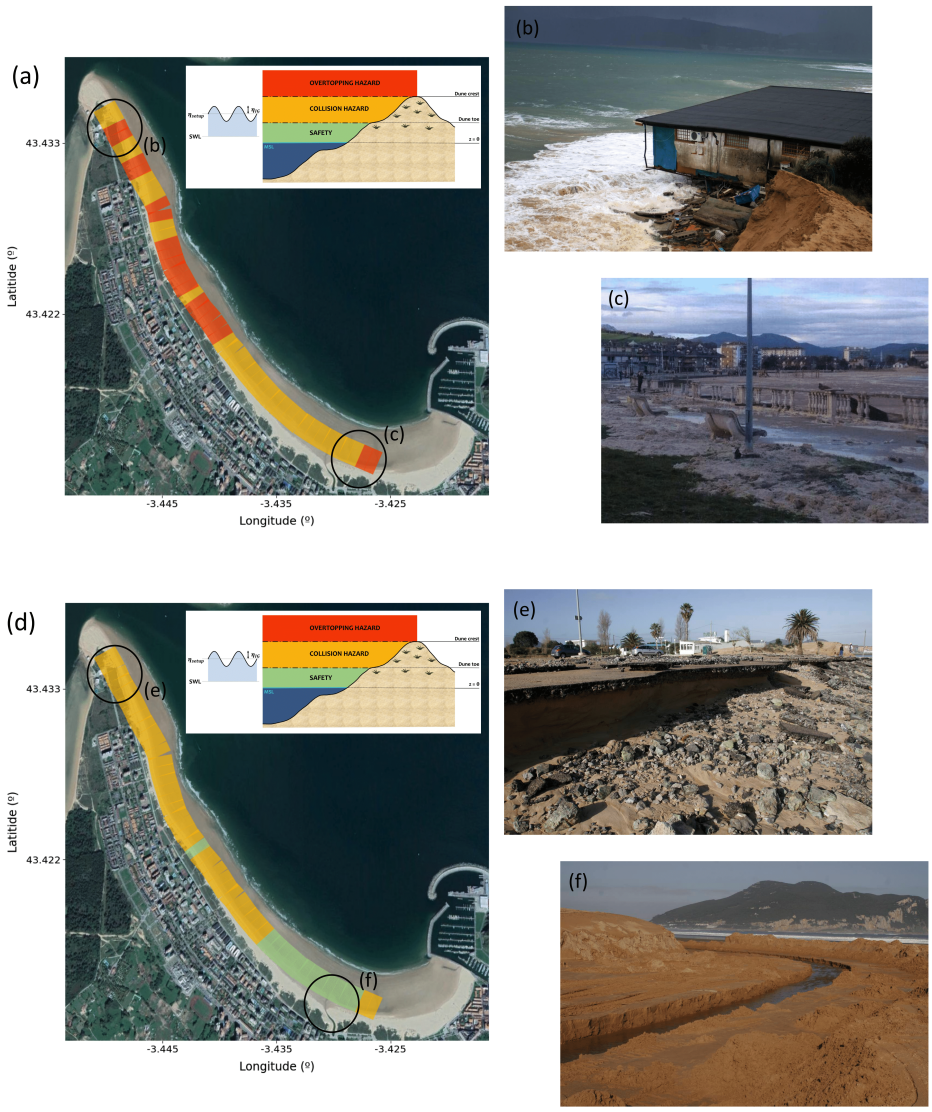

Figure 2.10: (a.1) Storm impact for 2014 winter storm and (b.1) 2018 winter storm (W_1 and W_2, see section 4.1) at La Salvé beach. The hazard is estimated using a vertical hazard scale simplified from Sallenger (2000), showed in the upper right corner of (a.1) and (b.1) along with a sketch of TWL hazard. Marked as black circles, zones where the adjacent photos were taken (a.2, a.3, b.2 and b.3) (Ph. Local press, "El Diario Montañés" (a.2, b.2 and b.3) and "El Faradio" (a.3)).

2.5 Summary and conclusions

An innovative metamodel has been introduced for characterizing surf zone wave dynamics. Once trained with series of offshore wave parameters and topobathymetry data, it generates high-resolution nearshore H_s and TWL components (η_{setup} and η_{IG}) within few seconds, while preserving the underlying physics. This hybrid methodology, built upon the combination of statistical and numerical methods, can be considered as an alternative for the high computational effort of dynamical downscaling, especially in scenarios where rapid results are required (e.g. EWS). The use of this innovative methodology allows to reconstruct H_s, η_{setup} and η_{IG} in a seamless manner, based on a library of just 500 pre-run cases. These synthetic cases are generated using MDA applied to the LHS dataset obtained from the local offshore hindcast. Furthermore, the use of LHS allows the generation of customized dataset, in which future or past projections can be included. Then, the selected cases are run by the hydromorphodynamic model XBeach in *surfbeat*mode, and its outputs are post-processed by means of PCA, notably reducing data dimensionality for the RBF reconstruction. A k-fold cross-validation has been performed to test the skill of the metamodel, showing a robust performance.

Regarding the modeling, XBSB allows the determination of TWL components of interest in open beaches where IG energy dominates. For different geographical settings, or if the focus is on other physical processes, alternative formulations and/or numerical models can be employed. As for the design space explored by the LHS and the MDA, it is noted that additional variables could enhance the representation of the local wave climate for different study sites. For example, given the importance of γ in certain coastal areas, the presented framework allows its inclusion as a variable within the design space. Generalizing the metamodel for different values of γ is feasible and could be done in future efforts. Beach state variability is also a parameter for further discussion, as it optimizes the number of representative topobathymetries of the whole beach spatiotemporal variation. A different approach must be used in more dynamic beaches, where having at least a winter- and a summer-representative bathymetry could enable better representation of nearshore processes.

With this methodology, TWL is downscaled in open beaches efficiently. The pro-

posed metamodel has great potential in coastal management applications and can be used as a guideline for policymakers to activate proper DRR measures based on downscaled models. Once trained locally, the computational complexity of this model is minimal. Further, the combination of its quickness and minimal deviation when compared to dynamical downscaling makes this methodology an useful tool to be considered for future EWS.

Chapter 3

HyWaThy: Hybrid modeling of nearshore Waves with varying baThymetries

3.1 Introduction

The aim of the present Chapter is to broaden the hybrid metamodel described in Chapter 2 for estimating nearshore hydrodynamics in La Salvé beach (Spain) under different bathymetric states. In order to fulfill this task, an additive hybrid method (Binwaves, Cagigal et al., 2024) for propagating wave spectra to nearshore waters is coupled to a metamodel using XBeach model in *non-hydrostatic* mode (henceforth referred to as XBNH; P. Smit et al., 2013; Roelvink et al., 2018; de Ridder et al., 2021). Unlike the *surfbeat* mode, XBNH fully resolves individual wave motions, making it more accurate for modeling nearshore processes such as runup, shoaling, refraction, and diffraction over complex bathymetries (P. Smit et al., 2010; Zijlema et al., 2011). Its non-hydrostatic, phase-resolving formulation enables explicit simulation of infragravity waves as low-frequency components generated by wave group modulation and

wave-induced currents, including undertow, longshore currents, and rip currents (McCall et al., 2010). Additionally, XBNH does not rely on empirical breaking models, allowing for more precise predictions of wave runup, swash, and overtopping (Lashley et al., 2018; Quataert et al., 2020; de Beer et al., 2021). Moreover, the integration of XBNH within a metamodeling framework represents a novel advancement in nearshore hydrodynamic modeling.

To take into account bathymetric changes, the PCA technique is used to explore the variability in seabed morphology. As stated by Miller and Dean (2007a), since PCA is purely a statistical technique for identifying patterns within a dataset, the results do not necessarily have an implicit physical interpretation. However, previous research has shown that given background knowledge of the environmental conditions at a site, physical interpretations of the results are often possible (e.g. Klovan, 1966; Winant et al., 1975; Aubrey, 1978; Liu and Zarillo, 1989; Losada et al., 1990; Liang and Seymour, 1991; Losada et al., 1993; Medina et al., 1994; Li and Pan, 2024). However, in most of these works, PCA has been performed to obtain oscillations in cross- and alongshore beach profiles. Therefore, this research also explores the suitability of PCA for characterizing two-dimensional seabed variability and its relationship with wave climate, with the aim of integrating such information into future hydrodynamic forecasting systems.

The Chapter is structured as follows. A description of the study site and the data used is provided in Section 3.2. Section 3.3 presents the coupled metamodel. This section includes the generation of synthetic sea and beach states (Section 3.3.1), the coupling of two metamodels to propagate the selected cases from offshore to coastal areas (Section 3.3.2 and 3.3.3), the nearshore hydrodynamics reconstruction (Section 3.3.4) and the numerical validation of the method (Section 3.3.5). The discussion of results is covered in Section 3.4 and the conclusions in Section 3.5.

3.2 Study area and data

3.2.1 Study area

The study area is described in detail in Section 2.2.1; therefore, only a brief summary is provided here. Some key aspects such as La Salvé beach hydrodynamics and some relevant geomorphological elements are highlighted in this section as they are essential for interpreting the present study. For further details, readers are referred to the aforementioned Section.

La Salvé beach is a sand spit enclosing the Santoña Estuary. It is a mesotidal dissipative beach, located in the northern coast of the Iberian Peninsula, where offshore waves predominantly come from the NW sector. The average wave period is around 10 seconds, with significant wave heights that go from 1 to 2 m, reaching 4 to 5 m during extreme winter storms . Tides are semidiurnal, with fortnightly tide cycles and a mean tidal range of around 3 m, rising to 5 m during spring tides (data available from https://www.puertos.es/es-es/oceanografia/Paginas/portus.aspx). In the northern end of the sand spit, the Asón river meets the sea with a mean flow of 21,85 m^3/s (https://www.chcantabrico.es/las-cuencas-cantabricas/marco-fisico/hidrologia/rios/ason).

Morphodynamically, the most active element in La Salvé beach is the ebb-tidal delta or shoal. It is located in the mid-northern part of the spit (Fig. 3.1), generated by the short-term sedimentary dynamic equilibrium between the Asón river, the astronomical tide and the incident waves. This underwater sand formation acts as a refraction element for incident waves, concentrating wave energy above it and thus increasing wave heights. As a result, a narrowing of the beach face in front of the shoal can be noticed, mainly due to erosion caused by the more intense surf generated by larger wave heights breaking nearshore. The interaction of breaking waves, tide levels and river discharges shape this element throughout different time scales, while most of the beach maintains a dissipative state.

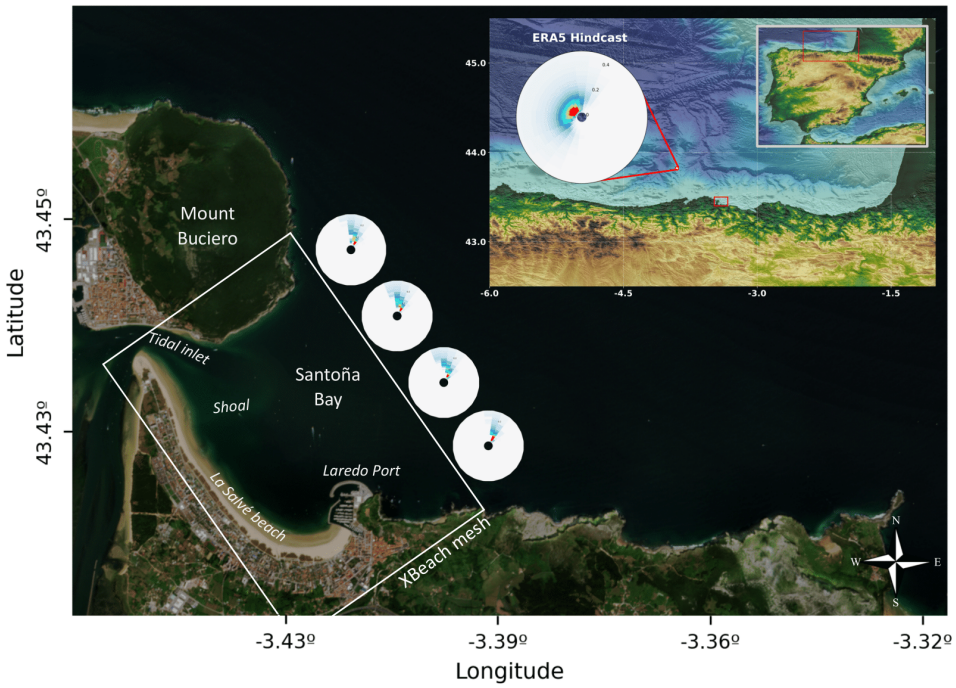

Figure 3.1: Study area, with geographical features of interest pointed out. The upper-right subplot shows the study area's location within the Gulf of Biscay, in the northern Iberian Peninsula, along with the location of the offshore spectral hindcast. The depicted spectra represent an extreme sea state observed in March 2014. On the main map, the propagations of the offshore spectrum and their locations are displayed with polar plots, as well as the numerical domain layout for the nearshore modeling (grey rectangle). For better visualization, only frequencies below 0.3 Hz are plotted in the propagated spectra.

3.2.2 Field data

The field data consists of a dataset of ten topobathymetries of the Santoña Bay and La Salvé beach (Fig. 3.2a), obtained from a semi-annual beach survey program conducted from 2012 to 2021 by the Civil Engineering Studies and Experimentation Center (CEDEX, by its Spanish acronym). The data cover an area extending from

the dune crests to approximately the 25 m isobath, and were resampled into a 5 m horizontal resolution Digital Elevation Model (DEM).

According to the widely used classification by Wright and Short (1984), which relates the dimensionless fall velocity parameter (R. Dean, 1973; Dalrymple & Thompson, 1976) to the different morphodynamic beach states, La Salvé beach, with an average grain size of 0.23mm (see Section 2.2.2 and Fig. 2.1c), is categorized as a dissipative beach over the observed time span. However, certain areas experience local phenomena, such as wave energy concentration, tidal inlet dynamics, and sheltered zones from energetic swells. These factors cause some regions to seasonally or permanently exhibit a longshore bar state.

3.2.3 Open data

Oceanic data were retrieved from open-source global databases. Hourly sea level data (mainly, astronomical tide and surge due to pressure and wind) were obtained from the tide gauge located in Santander, 30 km west of the study area (State Ports, Spanish Government; https://www.puertos.es/es-es/oceanografia/Paginas/portus.aspx). Offshore wave spectra hindcast 1980-2024 came from the ERA5 reanalysis (Hersbach et al., 2020), developed by the European Centre for Medium-Range Weather Forecasts (ECMWF, data available in https://cds.climate.copernicus.eu/datasets/reanalysis-era5-complete?tab=overview). It represents a monthly updated database of global wave spectra, providing hourly waves with a resolution of 0.5^{o}, forced with hourly wind fields and surface pressure data derived from the ERA5 atmospheric reanalysis (data available in https://cds.climate.copernicus.eu/datasets/reanalysis-era5-complete?tab=overview, Fig. 3.2b shows the aggregated parameters).

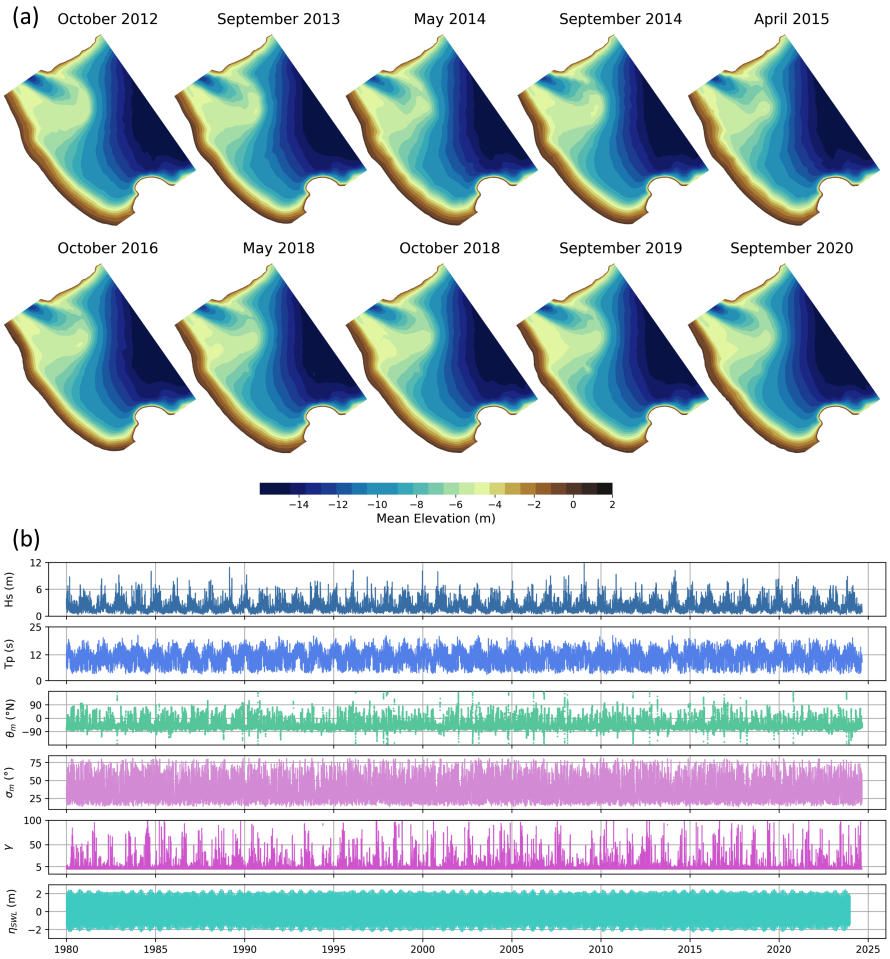

Figure 3.2: (a) The ten topobathymetries used in the presented work, ordered chronologically from the earliest (October 2012) to the most recent (September 2020). (b) Time series of the aggregated parameters inferred from the offshore wave spectra hindcast, plus the still water levels.

3.3 Coupled metamodel

This section presents the HyWaThy coupled metamodel, with its workflow illustrated in Fig. 3.3. Using as inputs the nearshore topobathymetries and the offshore oceanic forcings (spectral wave hindcast and levels), the metamodel starts by applying statistical techniques to define the representative beach and sea state parameters. The resulting outputs, synthetic nearshore bathymetries and offshore sea states, are then used as inputs to propagate waves in two stages. First, the offshore spectra are propagated with an offshore metamodel to four boundary points of the nearshore modeling domain. Second, these conditions, along with the synthetic nearshore bathymetries, serve as inputs for the nearshore hydrodynamic numerical model. The resulting simulations conform a pre-run library of cases that enables the efficient reconstruction of nearshore hydrodynamics through statistical interpolation. The outputs from the coupled metamodel are thus the nearshore spatial maps of H_s and θ_m, which are subsequently validated against numerical results.

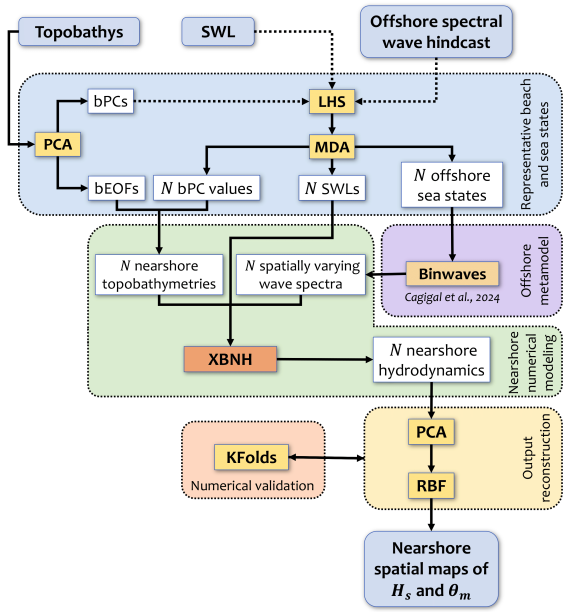

Figure 3.3: Flow chart of the proposed coupled metamodel.

3.3.1 Representative beach and sea state parameters

To determine the representative sea states for the study site, the first step consists of analyzing the 45-year offshore wave spectra time series from the hindcast. The aggregated wave parameters are calculated for each time using the wavespectra python package (https://github.com/wavespectra), being the variables of interest the significant wave height (H_s), the peak wave period (T_p), the mean wave direction (θ_m), the wave spreading (σ) and the JONSWAP peak enhancement factor (γ), as well as the still water level (η_{SWL}, referred to the same vertical datum as the topobathymetry, Mean Sea Level at Alicante (Spain)). The (γ) parameter has been obtained by fitting it to a potential equation as in Cagigal et al. (2021). For each one of them, a range of values is defined based on the limits defined by themselves in the hindcast dataset (Fig. 3.2b).

Given the predominance of unimodal sea states in the North-East Atlantic (Espejo et al., 2014), using (T_p) as a representative parameter is considered to be appropriate, given that it represents the primary concentration of energy within the spectrum. Nonetheless, if the metamodel were to be applied in a study site with a local wave climate characterized by mixed seas, using spectral partitions instead of aggregated parameters would be more pertinent (see Section 3.4 for further discussion).

Regarding the definition of the representative beach states for La Salvé beach, PCA is performed to the available Digital Elevation Models (DEMs) to identify dominant variability patterns in the seabed. PCA is an extremely useful statistical method capable of identifying the underlying patterns within noisy datasets, by re-projecting the original data on a new space, reducing the multidimensionality of the data while explaining the maximum variance of the sample data. The eigenvectors of the data covariance matrix (Empirical Orthogonal Functions, EOFs) define the vectors (axes) of the new space, while the Principal Components (PCs) are the projections of the original data over the new axes. EOFs are typically ordered by the amount of variance they explain (Explained Variance, EV), with the goal being to retain a reduced set of PCs that account for the desired level of variance. To explore the main modes of variability while reducing the noise in the data, an explained variance of 80% has been chosen, which is represented by 4 EOFs-PCs (Fig. 3.4). Hence, each topobathymetry

can be built as a linear combination of EOFs and PCs (hereafter bEOFs and bPCs, respectively) using the following equation:

$$z(x;t) = \overline{z}(x) + \sum_{i=1}^{B} bEOF_i(x) \cdot bPC_i(t) \tag{3.1}$$

where $\overline{z}(x, y)$ is the mean topobathymetry, and B is the number of bEOFs-bPCs that are needed to reach the desired EV.

In this work, the EOFs obtained by applying PCA to the bathymetries show certain spatial patterns possibly related to the above-mentioned interaction of waves, tides and river discharges (Section 3.2.1). In bEOF 1, silting is observed at the river mouth. A similar pattern appears in bEOF 2, with a slight eastward drift of the shoal that leads to depositions at its southern side and the river mouth. However, the beach face patterns differ significantly between these bEOFs. bEOF 1 reflects a sediment exchange between the beach face and the southern part of the bay, while bEOF 2 suggests a slight rotation of the spit. bEOF 4 most clearly captures the longshore bar movement, with intense red and blue hues along the beach. Meanwhile, bEOF 3 primarily highlights variations at the river mouth. The ranges of their associated PCs values are shown in Table 3.1), along with the hydrodynamic offshore parameters and their range of values.

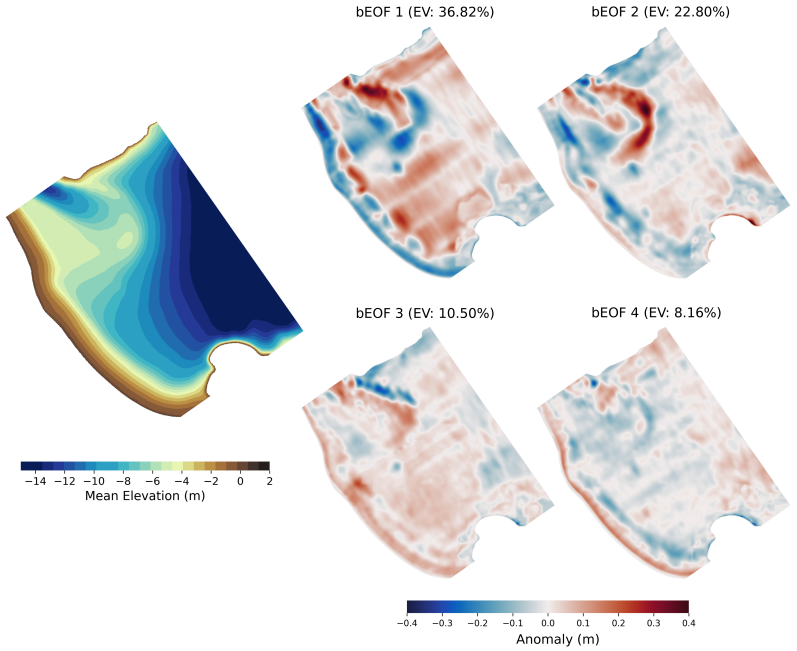

Figure 3.4: On the left side, mean topobathymetry from the field surveys from CEDEX. On the right side, first four bEOFs of the PCA applied to the same topobathymetries.

Parameter	Symbol	Ranges
Offshore significant wave height	H_s	[1, 9] m
Peak wave period	T_p	[8, 20] s
Offshore mean wave direction	θ_m	[-70, 70] º
Wave directional spreading	σ	[15, 40] º
JONSWAP peak enhancement factor	γ	[1, 5.5]
Still water level	SWL	[-2.1,2.9] m
Topobathymetry first principal component	$bPC1$	[-1.2, 2]
Topobathymetry second principal component	$bPC2$	[-1.3, 2.1]
Topobathymetry third principal component	$bPC3$	[-1.2, 2.5]
Topobathymetry fourth principal component	$bPC4$	[-1.5, 1.8]

Table 3.1: Upper and lower boundary values used for each variable.

To evenly cover the N_d=10 dimensional space, a set of 10000 sample points has been obtained using the LHS method (McKay et al., 1979), as in previous works (Parker et al., 2019; Ricondo et al., 2024b) or Section 2.3.1. To ensure the generation of realistic synthetic bathymetries within the multivariate space defined by the bPC values, a convex-hull algorithm (Barber et al., 1996) has been applied to the dataset across bPC1, bPC2, bPC3 and bPC4 dimensions.

Once the multidimensional parameter space is populated with M combinations, the MDA is used to select a subset of representative conditions to train the metamodel, denoted as $\{H_{S,j}, T_{P,j}, \theta_{m,j}, \sigma_j, \gamma_j, \eta_{SWL,j}, bPC_{1,j}, bPC_{2,j}, bPC_{3,j}, bPC_{4,j}\}; j = 1, ..., N$, where $N = 850$. The MDA, originally described by Kennard and Stone (1969) and later adapted by Camus et al. (2011a) for the study of multivariate wave climates, has been widely used in several state-of-the-art metamodels in recent years (Gainza et al., 2018; Espejo et al., 2023; Ricondo et al., 2024b). The number of cases, N, must be optimized for each specific location based on the coastal geomorphology, wave climate, and number of variables. This is achieved by evaluating the metamodel performance as N increases using the k-fold algorithm (see Section 3.3.5). The LHS dataset (M, 10000 samples) and the selected MDA subset ($N = 850$ representative cases), are presented in Fig. 3.5.

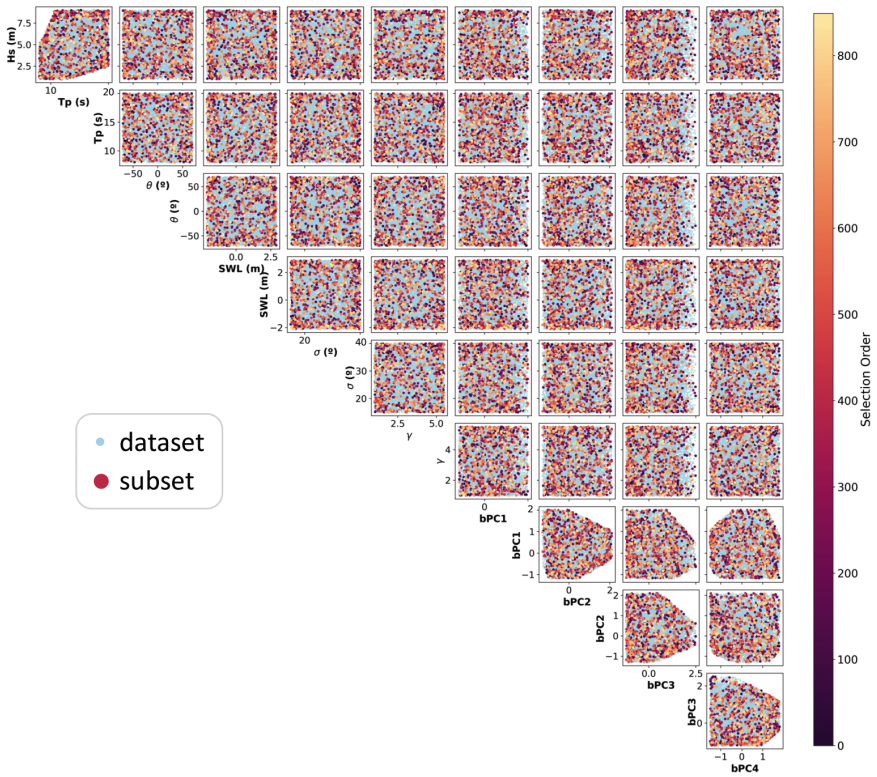

Figure 3.5: MDA-selected training cases (orange/red data points) covering the LHS-created synthetic dataset (light blue data points).

3.3.2 Offshore metamodel: BinWaves

The selection of $N = 850$ offshore wave parameters is used to force BinWaves (Cagigal et al., 2024). To do so, wave spectra are inferred from wave aggregated parameters using the wavespectra python package (https://github.com/wavespectra). BinWaves is a hybrid additive methodology that serves to efficiently propagate the full directional wave spectra to nearshore locations, based on the hypothesis that as waves propagate in deep waters the non-linear interactions can be neglected. This method disaggregates the full directional wave spectra into discrete frequency and direction energy "bins", and propagates with SWAN (Booij et al., 1999) monochromatic wave

systems to create a pre-run library of propagation coefficients. With these coefficients, any directional wave spectra representing the wave energy in the boundary can be reconstructed in the domain by rescaling and superposing the energy bins. In this work, it is used to propagate the offshore spectra to four points in the 15 m isobath, along the nearshore mesh offshore boundary (Fig. 3.1). Propagating waves to multiple nearshore points captures the spatial variability of the forcing more effectively, leading to a more accurate representation of the local wave climate. The number of target points is user-defined and does not increase computational cost after the precomputed library of propagation coefficients is generated for each location.

3.3.3 Nearshore numerical modeling: XBeach Non-Hydrostatic

The two-layer Non-Hydrostatic version of the XBeach (XBNH) model (P. Smit et al., 2013; Roelvink et al., 2018; de Ridder et al., 2021) is used to perform surf zone hydrodynamic simulations. This version uses a phase-resolving approach for infragravity and incident-band waves using a non-hydrostatic pressure correction term for the non-linear shallow water equations (P. Smit et al., 2010). The extension of XBNH to allow for two layers, similar to the multi-layer version of SWASH model (Zijlema et al., 2011), is based on the assumption of a constant non-hydrostatic pressure distribution in the lower layer, which significantly improves dispersive behaviour without increasing computational cost. Besides, the shoaling of waves in relatively deep water is better captured. The 1-layer notably underestimates wave heights when waves shoal from $kh = 2$ to shallow water, whereas the 2-layer model closely aligns with results from linear wave theory. XBNH fully resolves individual wave motions, accurately modeling nearshore processes such as runup, shoaling, refraction, and diffraction over complex bathymetries. It also explicitly resolves infragravity waves and wave-induced currents (McCall et al., 2010), allowing for more precise predictions of wave runup, swash, and overtopping (Lashley et al., 2018; Quataert et al., 2020; de Beer et al., 2021).

The spatially-varying spectral conditions obtained with BinWaves in the XBNH offshore boundary are used as forcing for the $N = 850$ simulations. The mesh, a structured rectangular grid orientated 55$^{\text{o}}$N, featuring a 5-metre resolution in both cross-shore and alongshore directions, extends from west of the tidal inlet to east

of the port. The lateral boundaries are set far enough from the Santoña Bay to reduce numerical noise, and the outputs are subsequently cropped to the bay for result processing. The short-wave friction coefficient (f_w) is assigned a constant value of 0.03 throughout the domain, in accordance with literature values for sandy bottoms (Storlazzi et al., 2017) and the guidelines provided in the model documentation.

The outputs from the XBNH simulations are obtained following a 600-second warm-up period, over a subsequent 1800-s time span. This duration is set based on the numerical stability of the simulations given the forcings and the geometry of the study site. Therefore, the output is the 1800-s mean H_s and θ_m obtained as a 2-D spatial distribution along La Salvé beach with spatial resolution of 5 m.

The XBNH simulations were run on a Rocky Linux 8 cluster (x86-64) with up to 5 nodes, each with 48 cores (2.10 GHz Intel Xeon Gold 5318Y) and 512 GB of RAM. The $N = 850$ cases were simulated with a maximum of 250 cases running simultaneously, completing in 2 days and 18 hours.

3.3.4 Output reconstruction

Once the N-selected ocean and beach input parameters and their N-transformed nearshore outputs are obtained, the underlying spatial relationship between input and output can be estimated with the Radial Basis Functions interpolation technique (RBFs; Franke, 1982). It is a non-linear interpolation technique based on a weighted sum of radially symmetric basis functions. Given its accuracy interpolating large sets of scattered data in high-dimensional spaces, as occurs with MDA-selected cases (Camus et al., 2011b), this technique has been used in previous metamodels with good results (Ricondo et al., 2024b; Zornoza-Aguado et al., 2024; amongst others). Since this process must be performed one by one for all N-selected ocean and beach input parameters, the computational cost increases significantly. Thus, a reduction of the dimensionality of the dataset while preserving the spatial patterns is carried out through the PCA technique.

Consequently, PCA is performed to study the metamodel outputs from N subset (nearshore spatial fields of mean H_s and θ_m) with two purposes. On one hand, as

in Section 3.3.1, it allows to obtain the dominant spatial modes (EOFs) and their physical relationships with each N subset case (which has a correspondent component weight (PCs)). On the other hand, as it reduces the multidimensionality of the data, it enhances the efficiency of the metamodel by reducing the input data for the reconstruction. Besides, the combination of the PCs with the EOFs represent the variance over the mean values, allowing a fast visual verification of the whole N simulations performance by identifying whether the results are consistent or not.

For each combination of SWL and synthetic bathymetries in the 850 cases, the sea domain is defined, and the shared cells across all cases are used as a mask. This approach also prevents PCA from capturing the intertidal zone, where breaking wave patterns could contaminate the outputs and mislead the analysis. The nearshore output for each set of input parameters in N can be obtained as a linear combination of EOFs and PCs applying the same principle as in Eq. 3.1, where in this case the variable t, corresponding to the date of acquisition of the topobathymetries, is every combination of the input parameters inside the subset N, and $\overline{z}(x)$ is the mean spatial field of the output variables of the N cases, $\overline{z}(x)$. For H_s, the algorithm identifies 17 main EOFs-PCs that explain the 99.5% of the data variance; while for θ_m, an EV of 98% is explained with the first 34 EOFs-PCs. For illustration purposes, the first 3 EOFs-PCs of the nearshore spatial fields of H_s are shown in Fig. 3.6. As no patterns in the first 3 PCs have been found in the scatter plots of bPCs, only wave parameter scatter plots are depicted in Fig. 3.6. In these scatter plots, some interesting patterns suggesting a physical relationship between the PCs and the local wave climate can be noticed. The first EOF-PC (Fig. 3.6b) describes the nearshore spatial distribution of H_s according to the offshore H_s-T_p relationship, as well as the low incidence of short-period waves coming from the NW sector: because of their lower wavelength, they do not refract-diffract in the Santoña Bay and therefore low values of H_s are found nearshore. In EOF-PC2 (Fig. 3.6c), the influence of SWL on nearshore H_s can be noticed: waves coming from the NE sector during high tides cause larger waves in the northern part of the beach, while large waves, independently of their provenience, break in the shoal and in the bar during low tides. Fig. 3.6d, representing EOF-PC3, represent the influence of the mean wave direction on nearshore H_s, as NE swells penetrate in the center part of the beach, breaking in the beach and in the bar, and strong NW swells increase H_s in the shoal.

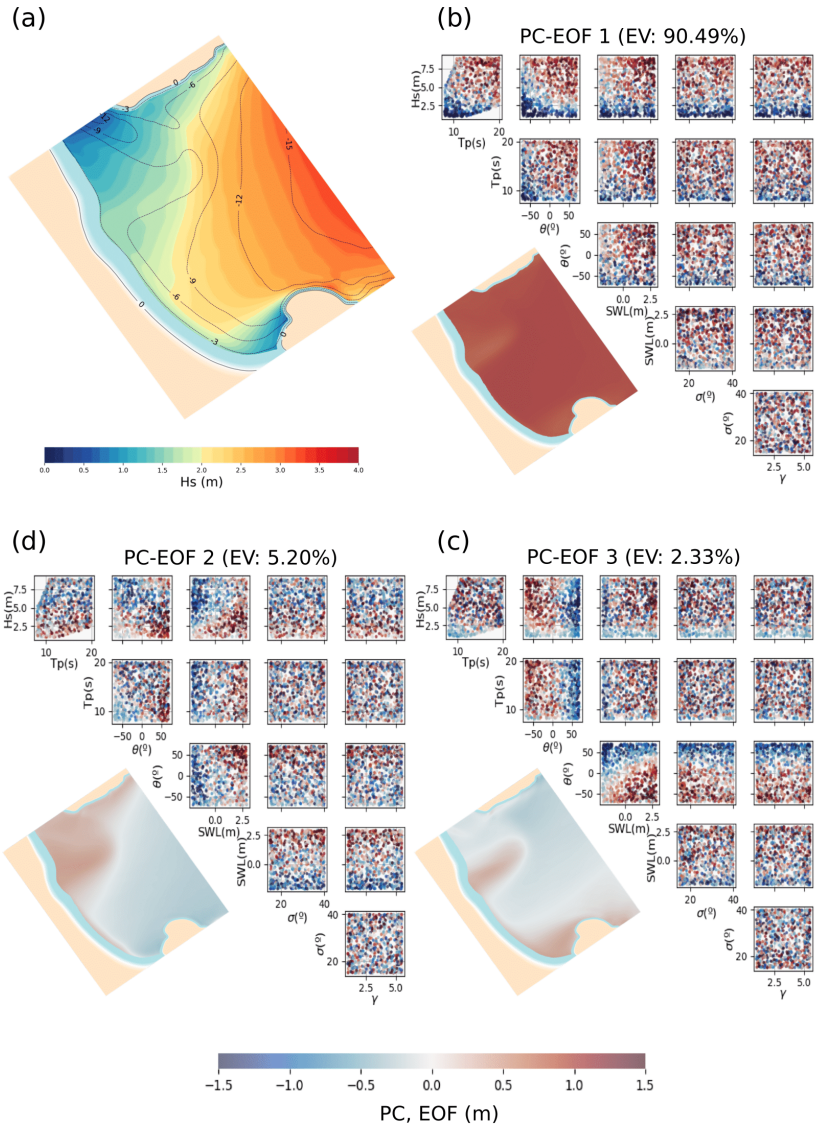

Figure 3.6: (a) Mean H_s spatial field of the 850 MDA-selected cases. (b), (c), and (d) represent the EOFs and scatter plots of the MDA subset wave parameters, colored according to the correspondent component weight, for H_s.

RBFs are then used to interpolate a surface to each PC of the identified set of PCs with the desired EV. This surface follows the general expression:

$$\widetilde{PC}(\mathbf{V}) = p(\mathbf{V}) + \sum_{i=1}^{N} a_i \Phi(||\, V - \, V_i||) \tag{3.2}$$

where $\mathbf{V}$ represents the vector of $N = 850$ cases $\{H_s, T_p, \theta_m, \sigma, \gamma, \eta_{SWL}, bPC_1, bPC_2, bPC_3, bPC_4\}$, $\widetilde{PC}(\mathbf{V})$ is the approximated surface for each PC obtained using the RBFs, $p(\mathbf{V})$ is a linear polynomial with coefficients $b = \{b_0, b_1, \ldots, b_{N_d}\}$, N_d is the dimension of the input forcing parameters (in this work, $N_d = 10$), $||\bullet||$ is the Euclidean norm, and Φ is a Gaussian function. Coefficients $a_i = [a_1, \ldots, a_N]$ and $b = [b_0, \ldots, b_{N_d}]$ are calculated for the selected PCs. Therefore, the estimated spatial field of the response function is:

$$y(x; \mathbf{V}) \approx \overline{y}(x) + \sum_{i=1}^{B} EOF_i(x) \cdot \widetilde{PC}_i(\mathbf{V}) \tag{3.3}$$

where $\overline{y}(x)$ is the mean spatial field along the $N = 850$ cases, and B is the number of PCs with the desired EV. The calculation of the coefficients a and b allows to interpolate inside the multivariate space defined by the user in Section 3.3.1, retrieving the PC values of outputs of unmodeled input combinations of parameters.

3.3.5 Numerical validation

A k-fold cross-validation ($k = 5$) on the different trained interpolation surfaces is carried out with a double objective: evaluate the mathematical model skill and detect potential overfitting or underfitting. This technique randomly rearranges and divides the dataset into k groups (or folds) and uses each group as a validation set only once, while the remaining groups ($k - 1$ folds) serve to train the model. This minimizes the influence of variability in a single random fold, providing a more reliable estimate of the model performance. The disparity between the predicted and modelled values is then quantified using the RMSE for each group. Starting with an initial guess of 1000 MDA-selected cases (which were required to be simulated), k-fold cross-validation is

applied to a varying number of N cases by reducing the number of samples until 100. Using mean and standard deviation of RMSE as performance metrics, the optimal N value is reached when increasing the number of cases no longer leads to a significant reduction in error. In this work, that occurred for $N = 850$ cases (mean RMSE for $H_s = 0.20m$; mean RMSE for $\theta_m = 1.75°$, Fig. 3.7a).

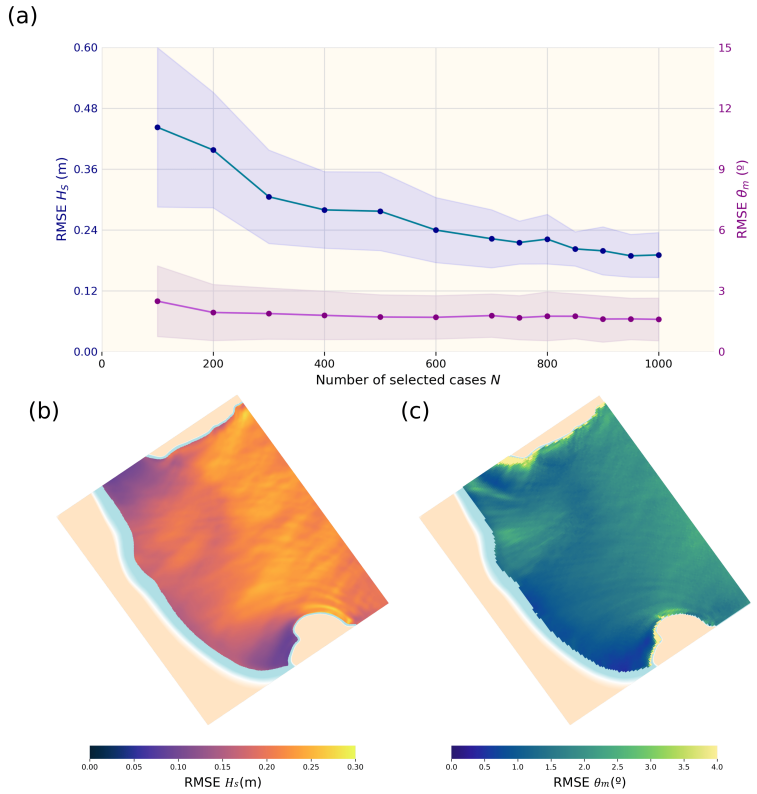

Figure 3.7: (a) K-fold cross validation on H_s and θ_m as a function of the number of cases used to build the metamodel. For each variable, the dots indicate the mean RMSE values along the domain, while the error bands are the standard deviation of the k-folds. Below, the RMSE spatial maps for H_s (b) and θ_m (c), for the selected $N = 850$ cases.

The orders of magnitude of the RMSE of the reconstructed H_s and θ_m (Fig. 3.7b and 3.7c respectively) are considered acceptable, with larger values in the highly reflec-

tive boundaries (i.e. the cliffs of Mount Buciero and the Port) mostly due to numerical instabilities that take place in such zones. On the other hand, the nearshore zone shows low errors for both variables, thus confirming the potential of HyWaThy as a reliable tool to downscale hydrodynamics from offshore to nearshore, and its good performance including the changing topobathymetries.

3.4 Results and discussion

Once the site-specific library of cases is computed, hydrodynamic conditions can be reconstructed in seconds, significantly reducing computational time and effort for realistic downscaling. To illustrate this, Fig. 3.8 compares a full dynamic XBNH simulation with the reconstructed output from HyWaThy. The reconstruction achieves a substantial reduction in computational cost—several orders of magnitude—while preserving much of the accuracy of the dynamic model.

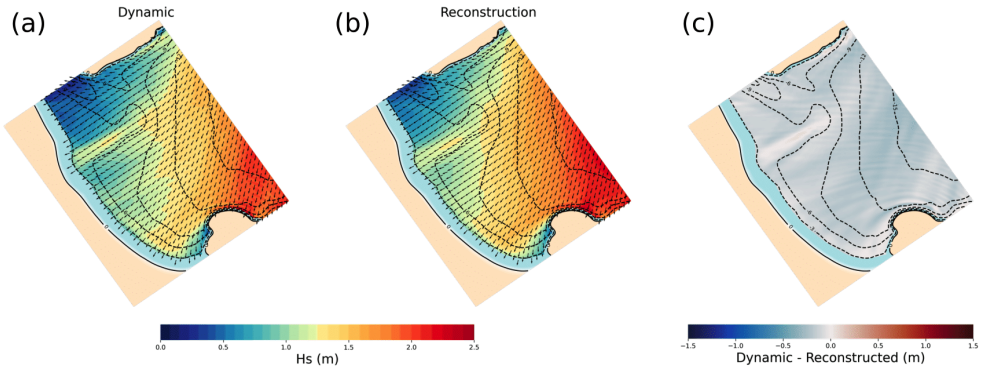

Figure 3.8: Performance of the coupled metamodel: (a) H_s and θ_m from a dynamic simulation of a sea state from April 24th 2012: $H_{S,0} = 4.72\,\text{m}$, $T_p = 12.3\,\text{s}$, $\theta_m = 304°$, $\sigma = 28°$, $\gamma = 0.3$, SWL $= -1.16\,\text{m}$, $bPC_1 = 1.65$, $bPC_2 = -0.44$, $bPC_3 = 0.63$, $bPC_4 = -0.08$, compared with (b) reconstructed H_s and θ_m with the proposed coupled metamodel. (c) shows the absolute difference in H_s between the dynamic simulation and the reconstruction.

In addition, the influence of the topobathymetric configuration on the spatial fields of H_s is shown in Fig. 3.9c, where the same offshore forcing (Fig. 3.9b) is used over

three bathymetries obtained by combining three different values of bPC1, bPC2, bPC3 and bPC4 (Fig. 3.9a). As pointed out in Section 3.2.1, the shoal plays a key role in La Salvé nearshore hydrodynamics, as it shifts the concentration of wave energy towards North or South depending on its configuration.

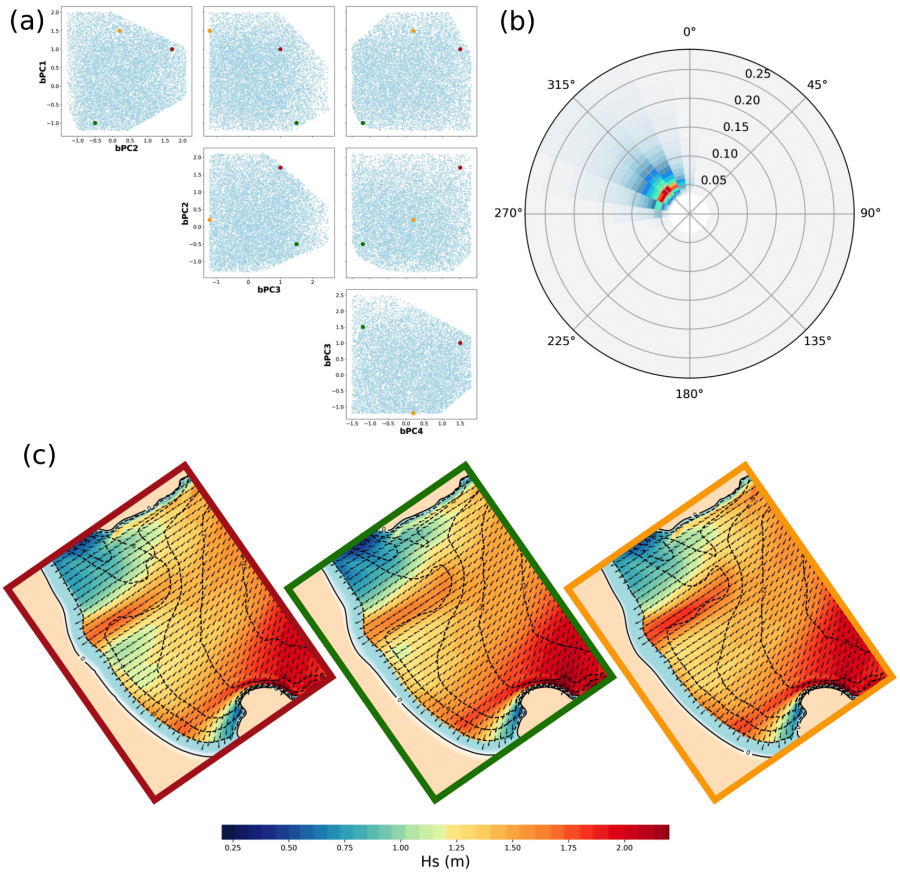

Figure 3.9: Reconstruction of the same sea state over different bathymetric configurations. (a) Representation of the bPC values corresponding to each bathymetry generated over the bPCs space. (b) Offshore wave spectra used as forcing (SWL is set as +1 m). (c) Reconstructed spatial distributions of H_s and θ_m over the different bathymetric configurations obtained by combining the bPC values in (a).

A key aspect of the presented metamodel is the availability of bathymetric data. Each PCA mode consists of spatial and temporal components, which describe characteristic spatial patterns and their associated chronology. Therefore, a large and consistently sampled dataset enhances the exploration of beach state variations at the study site, given that these PCA modes represent physical patterns of bathymetric change and the chronology described by the temporal eigenfunctions should be related to the local nearshore conditions (Miller & Dean, 2007b). The exploration of these modes would allow to create more realistic bathymetries taking into account all the natural modes of oscillation of a determined beach (e.g. winter-summer erosion and accretion patterns, beach rotations, bar migration, longitudinal patterns related to seiche waves, etc.).

Further works in a long-term observed site (see Vitousek et al. (2023) for an extense review), combined with state-of-the-art methods to infer bathymetry from remotely sensed coastal observations (Caballero and Stumpf, 2021; Viaña-Borja et al., 2023; Salameh et al., 2024; Viaña-Borja et al., 2025; Frugier et al., 2025; an overview can be found in Leder et al. (2023)) can help address the need for continuous monitoring required for such an extensive database. In this regard, several authors (Harris et al., 2011; Short and Jackson, 2013; Vitousek et al., 2023; amongst others) pointed out satellite imagery as the most realistic and promising way forward in providing useful data for studies of nearshore morphodynamics. As the performance of the presented coupled metamodel improves with larger datasets, incorporating these state-of-the-art methods to infer bathymetries would significantly enlarge the input nearshore data. This would not only enhance its performance, but expand its applicability from a specific, heavily surveyed study site to anywhere around the world with complementary field data to support satellite imagery.

As explained in Section 3.3.1, the bPCs-bEOFs obtained can be correlated with the local nearshore conditions. This reciprocal relationship allows to set an operational framework with the metamodel, where bPC values can be expressed as a function of the beach morphodynamic state, represented by the weighted mean dimensionless fall velocity ($\overline{\Omega}$, Splinter et al., 2014). Thus, the metamodel can operate in two modes. First, given a sea state, $\overline{\Omega}$ can be inferred (through an average beach slope), enabling the instantaneous generation of the corresponding topobathymetry. Second, if a topo-

bathymetry is also available, the bPC values can be extracted, and the metamodel would be ready to be used. So the metamodel would be useful for users with a sea state, independently of them having a topobathymetry or not. This dual functionality ensures the metamodel's versatility, allowing users to obtain reliable predictions from a given sea state, regardless of whether a topobathymetry is available.

Regarding the oceanic inputs of this metamodel, aggregated bulk parameters $\{H_s, T_p, \theta_m, \sigma, \gamma\}$ were used as parameters to generate the set of cases. Wave multimodality could be considered in the generation of the cases (as Ricondo et al. (2024b) proposed), introducing wave partitions (H_s, T_p, θ_p, σ_p and γ would be calculated for each individual wave system), thus increasing the complexity and applicability of the metamodel to multimodal environments.

3.5 Summary and conclusions

The work in this Chapter aims to extend the applicability of the hybrid method described in Chapter 2 for estimating nearshore hydrodynamics. Bathymetric changes have been included in the numerical modeling by exploring PCA as a tool to describe the physical interaction between waves, tides and sand. Additionally, XBNH has been forced with spectral conditions to fully capture nearshore hydrodynamics at the short-wave scale. The LHS method has been used to explore a wide range of parameter combinations for sea-beach conditions, while the MDA algorithm has been applied to select a reduced but representative sample of those conditions. Wave parameters from this subset have been used to reconstruct the offshore wave spectra, which are propagated to four points of the XBeach offshore boundary using BinWaves. The resulting spatially-varying spectra then force XBNH, with the seabed updated according to the bathymetry PC values from the subset. To reduce dimensionality and therefore facilitate RBF interpolation, PCA is applied to the XBNH outputs, H_s and θ_m. RBFs are fitted between sea-beach conditions and PCs to predict nearshore hydrodynamics for unmodeled conditions by interpolating these values. Finally, a k-fold cross-validation is performed over the new hybrid method as a numerical validation, and a comparison of reconstructed and modeled H_s and θ_m) spatial fields is also presented.

The coupled metamodel HyWaThy demonstrates high performance and computa-

tional efficiency while accounting for variability in nearshore forcing conditions and diverse topobathymetric configurations—an area currently underrepresented in existing downscaling approaches. Furthermore, the incorporation of XBNH into the metamodeling framework constitutes a novel contribution to nearshore hydrodynamic modeling. However, a validation of this methodology in a more-surveyed study site is necessary (i.e. instrumental data such as buoys and/or sensors) as well as an increase in input topobathymetries through satellite derived bathymetries, given that the PCA better captures the natural oscillation modes of the beach with larger datasets.

HyWaThy has potential as a tool for coastal management, given that it is able to reconstruct the nearshore hydrodynamics in a matter of seconds taking into account the evolution of the batymetry over time. It can serve to aid the coastal science community to tackle hot topics such as coastal erosion or coastal flooding through the use of Early Warning Systems. Its use could also be expanded to reconstruct other variables of interest, such as wave-induced currents (longshore currents, rip currents), which are critical in beach safety and water sports forecasts.

Chapter 4

High-resolution nearshore wave climate

4.1 Introduction

Many coastal applications rely on rapid, long-term historical records of oceanographic parameters in nearshore areas, as well as on the associated statistical analyses required to characterize the local wave climate. Such information is fundamental for understanding long-term coastal dynamics, planning adaptation measures, and designing infrastructure resilient to extreme events. However, obtaining high-resolution time series of nearshore hydrodynamic conditions is often constrained by limited data availability and high computational demands.

While several hindcast databases provide long-term wave datasets in deep waters (Pérez et al., 2017; Smith et al., 2020; Hersbach et al., 2020, amongst others), extended time series in nearshore areas are often unavailable (DeLeo et al., 2022). In such cases, nearshore wave analysis can be approached in two main ways: by first analyzing the offshore time series and then propagating selected conditions to shallow waters, or by downscaling the entire offshore dataset to the nearshore and performing the

analysis directly on the resulting nearshore data. In the latter, the use of hybrid methods enables a significant decrease in computational cost while preserving the representativeness of the original data (Camus et al., 2011b).

In Chapter 3, the proposed HyWaThy metamodel demonstrated an efficient, high-fidelity hybrid reconstruction of surf zone hydrodynamics, explicitly accounting for seabed variability, at a fraction of the computational cost required by dynamical simulations. Its low computational cost positions it as a strong alternative for coastal management applications such as early warning systems (e.g. Harley et al., 2016; Gaztelumendi et al., 2016; Stokes et al., 2021; Garzon et al., 2023), where timely forecasts are critical for decision-making. Beyond its operational potential, HyWaThy's high-resolution outputs enable comprehensive wave climate analyses throughout the nearshore domain. These analyses are essential for a wide range of applications, including the design of coastal structures (Puertos del Estado, 2009), the definition of operational thresholds for port activities (Puertos del Estado, 2009; EurOtop, 2018), beach erosion studies (Masselink & Heteren, 2014; Harley et al., 2017), assessments of habitat vulnerability to hydrodynamic stressors (Vozzo et al., 2021; Bertelli et al., 2023), and the design of nature-based solutions for coastal protection (Narayan et al., 2016). By bridging the gap between computational efficiency and physical detail, HyWaThy offers a valuable framework for advancing both research and practice in coastal engineering and risk management.

Therefore, this Chapter will focus on the application of the HyWaThy metamodel in La Salvé beach as a tool to downscale offshore wave spectra time series. First, section 4.2 presents the data used for the reconstruction of the last 85 years (1940-2024) of waves in the study area, which are analyzed and described in Section 4.3. Then, some practical uses of these data are described, such as the definition of the depth of closure in the study site (Section 4.3.1), the analysis of wave climate (Section 4.3.2), the interannual variability of the local wave climate with existing climate indices and tailor-made indices (Section 4.3.3) and the effects of the variation of the bathymetry to the extreme values of H_s (Section 4.3.4). The conclusions are covered in 4.4.

4.2 Data

The aggregated wave parameters needed as input for HyWaThy were retrieved from the global database of ERA5 (Hersbach et al., 2023; available in https://eart hdatahub.destine.eu/collections/era5/datasets/reanalysis-era5-single-levels-ocean). This dataset represents the longest open-source reanalysis available for the Cantabrian sea, with hourly ocean-wave fields from 1940 until the last closed month and updated monthly in a regular grid of 0.5 degrees. Regarding the bPC values, they were set to zero, thus representing the mean bathymetry, except in Section 4.3.4, where an analysis of the effects of the bathymetry on wave climate is performed.

4.3 Hindcast reconstruction

The hindcast reconstruction (more than 744.000 hours, Fig. 4.1) for the study site is completed in approximately 30 minutes using a single core of the computational cluster described in Section 3.3.3. The output consists of 85 years (1940-2024) hourly spatial maps of H_s at a 20-meter resolution across La Salvé beach (a trade-off between data handling efficiency and spatial accuracy determines the spatial resolution). These high-resolution outputs enable a range of coastal analyses, including the assessment of inter- and intra-annual variability (Section 4.3.1), the estimation of key beach system parameters such as the depth of closure (Section 4.3.2), the exploration of relationships between local wave climate and large-scale climate indices (Section 4.3.3), and the analysis of wave climate extremes at the local scale (Section 4.3.4). The fine spatial resolution of the results allows these analyses to fully account for nearshore physical processes influenced by seabed morphology, thanks to the phase-resolving capabilities of the XBeach Non-Hydrostatic (XBNH) model (de Ridder et al., 2021) inside the HyWaThy metamodel.

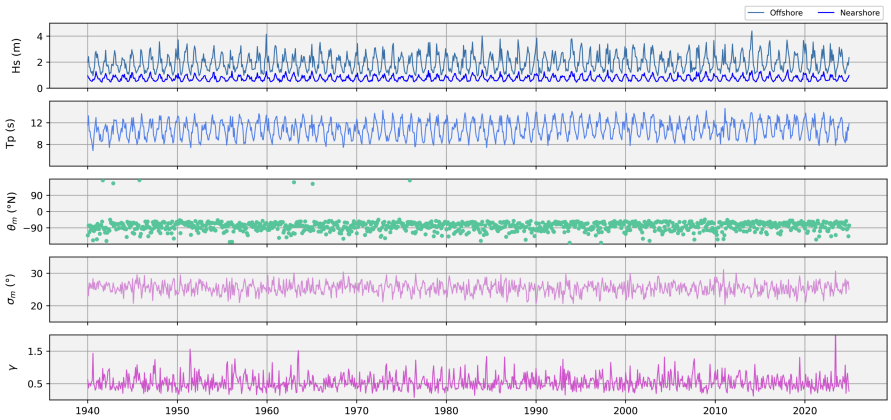

Figure 4.1: Monthly mean wave parameters from the period 1940-2024. In the upper plot, offshore H_s is represented along with nearshore H_s, obtained in the XBNH domain edge ($z \approx 15m$).

4.3.1 Depth of closure definition

As described in the literature (Hallermeier, 1980; Birkemeier, 1985), the term *depth of closure*, hereafter DoC, refers to a conceptual boundary used to distinguish between two zones of differing morphodynamic activity along the beach profile over short- to medium-term time scales (typically 1–10 years). The upper shoreface is considered the area where measurable changes in the beach profile are commonly observed, whereas the lower shoreface extends seaward from the limit of these significant changes to the wave base, where morphological variability is generally negligible (or within the uncertainty limits), despite potential bed agitation during high-energy wave events. The interface between these two zones defines the morphological depth of closure (DoC). Hence, DoC represents a morphodynamic boundary separating a landward, morphodynamically active region, from a seaward region that is generally considered morphodynamically non-active (Hallermeier, 1978; Nicholls et al., 1998). It is important to note that the definition of 'significant change' is ambiguous and depends on the time scale of consideration and the methods of morphological change detection (Valiente et al., 2019).

The challenge that the traditional methods to quantify DoC posed (comparison of large, multi-annual profiles to detect the point beyond which no significant changes on the profile are detected, generally related to bed-level change larger than the detection limit (Valiente et al., 2019)) motivated the development of indirect methods of prediction based on wave hydrodynamics and sediment characteristics affecting the shoreface. Examples of such indirect methods include wave-based formulations (Hallermeier, 1978, 1980; Birkemeier, 1985), with the latter proposing an expression for DoC of the form:

$$h^* = 1.75 H_{s_{12}} - 57.9 \frac{H_{s_{12}}^2}{g T_{p_{12}}^2} \tag{4.1}$$

where h^* is the predicted depth of closure over t years referenced to Mean Low Water, $H_{s_{12}}$ is the significant wave height seaward of the breaker zone that is exceeded for 12 hours per year, $T_{p_{12}}$ is the wave period associated with $H_{s_{12}}$ and g is the acceleration of gravity.

In this Section, a series of alongshore DoC points (herein, DoC array) is defined to perform a spatial analysis in La Salvé beach. For that, the nearshore wave hindcast is used to obtain the spatial variability of $H_{s_{12}}$ and $T_{p_{12}}$, given that these two variables are needed for the definition of h^*. For that, the intersection of the surface obtained from Eq. 4.1 with the mean topobathymetry is computed (Fig. 4.2)

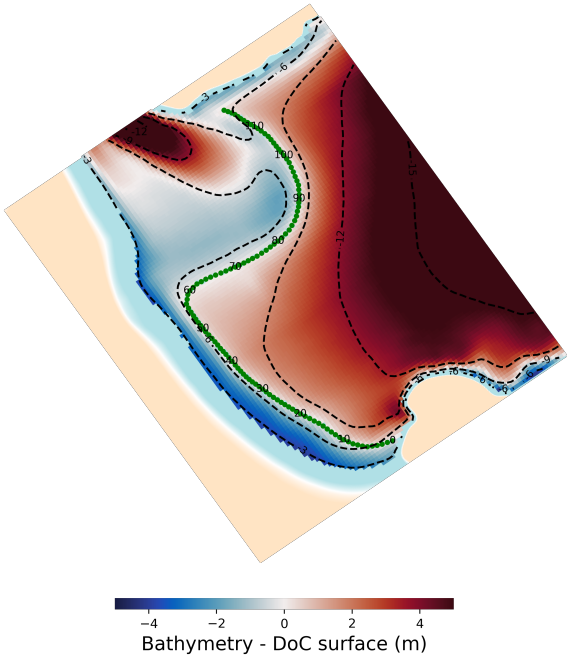

Figure 4.2: Difference between the surface defined with Birkemeier (1985) and the mean topobathymetry. The green dots represent the intersection of both surfaces, that is, the DoC array, numbered from 0 to 120 according to their index number.

The availability of wave data along the DoC array enables a wide range of analyses based on the assumption of non-breaking wave conditions in the nearshore zone. Under this hypothesis, it is possible to isolate the influence of hydrodynamic forcing from the complex surf zone processes, allowing for a clearer interpretation of how offshore wave conditions propagate and transform as they approach the shoreline. This facilitates the assessment of wave climate variability along the DoC array, including long-term trends and responses to regional or large-scale climatic drivers.

Moreover, the high-resolution spatial coverage provided by the DoC array allows for a detailed examination of spatial variability in wave parameters such as significant wave height, wave direction, and energy flux. This spatial detail is critical for identifying alongshore gradients and detecting local anomalies or patterns that may be linked to

geomorphological features or sediment transport pathways. Temporal variations can also be explored to understand how these spatial patterns evolve under different forcing conditions, including seasonal changes and extreme events. Ultimately, such analyses contribute to a more comprehensive understanding of nearshore dynamics and support improved coastal management and planning strategies.

4.3.2 Wave climate analysis

Once the H_s data along the DoC array have been reconstructed for the 85-year period, a spatio-temporal analysis of the wave climate can be conducted. Fig. 4.3 presents the monthly averages, calculated by calendar month, of the daily maximum H_s values along the DoC array, illustrating the spatio-temporal variability of the maximum H_s over the full 85-year dataset.

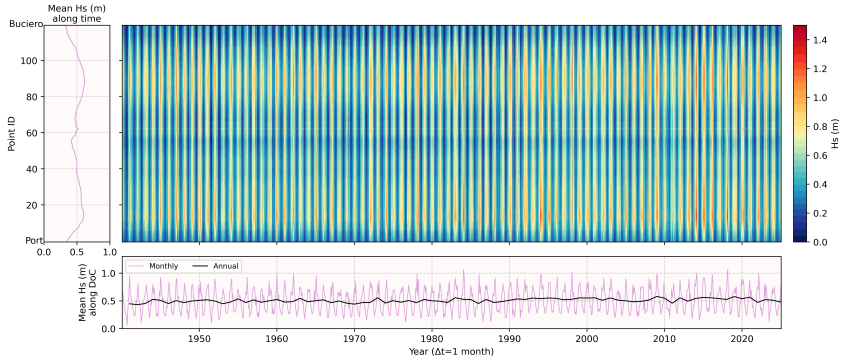

Figure 4.3: In the main plot, monthly average (by calendar month) of the daily maxima of H_s along the 85 years of data, averaged along the DoC array. To the left, average along time of H_s for each point of the DoC array. Below, average along each point of the DoC array for each time.

Fig. 4.3 clearly exhibit a pronounced seasonal pattern, characterized by energetic wave conditions during winter months and calmer conditions in summer. Differences in H_s are around 1 meter between summer and winter months, while T_p also decreases around 4 seconds and θ_m remains generally the same, shifting a bit towards East during

summer. The monthly mean values along the DoC array (shown below the main plot) further reveal an inter-annual variation in the average maximum H_s, showing oscillations with varying amplitude throughout the years. From a spatial perspective (as shown to the left of the main plot), larger maximum H_s values are concentrated near the Port (point IDs 15-25, see Fig. 4.2) and in the tidal ebb (point IDs 90 to 110). In addition, several extreme winter storms documented by the local press are also captured in the time series (in the main plot), including notable events like the ones from April 1994, March 2008 and March 2014 (adressed in Chapter 2). The latter occurred during a particularly energetic season clearly identifiable by the broader band of reddish tones in Fig. 4.3 main plot. The extreme events from that winter are also visible in Fig. 4.1, with a peak in the monthly means of H_s.

This analysis provides a foundation for identifying both spatial and temporal patterns in nearshore wave behavior over the 85-year period. By examining variations in wave height across different locations along the DoC array and tracking how these patterns evolve over time, it becomes possible to uncover recurring trends, anomalies, and long-term changes in the local wave climate. These insights are particularly valuable for understanding the dynamics of surf zone processes and their potential drivers.

Moreover, the identified patterns can be further explored in relation to large-scale climate indices, which are known to influence wave conditions across the North Atlantic region. Establishing such correlations allows for a better understanding of the influence of atmospheric variability on local wave climates, which in turn can enhance predictive capabilities.

4.3.3 Interannual variability

When characterizing the nearshore wave climate, many applications require a clear understanding of its variability (e.g., selection of ship routing, coastal flooding risk, nearshore hydrodynamics). On wave-dominated coastlines, nearshore processes are primarily driven by bulk wave parameters, which are themselves influenced by atmospheric circulation patterns. The anomalies can persist for several consecutive years, reflecting an important part of the interannual and inter-decadal climate variability (Castelle et al., 2018).

The long-distance interactions between different regions of the ocean and atmosphere, occurring across various time scales, are known as teleconnections. These patterns are typically identified by applying Principal Component Analysis (PCA) to Sea Level Pressure (SLP) anomaly fields, which produces independent modes of variability that correspond to established teleconnection indices.

As a result, the variability of H_s over the North Atlantic has been related to different regional climate patterns at different time scales (e.g. seasonality, Menéndez et al., 2009; Izaguirre et al., 2011; Godoi et al., 2016; and inter-annual variability, Méndez et al., 2006; Izaguirre et al., 2011; Godoi et al., 2016; Castelle et al., 2017; Morales-Márquez et al., 2020). Once the seasonal signal of extreme wave climate is captured, deviations from the average climatology are generally associated with changes in the atmospheric zonal circulation over the extratropical Northern Hemisphere. These patterns, which constitute the primary meteorological forcing behind extreme wave conditions in the North Atlantic, can also be characterized using SLP fields and gradients (Izaguirre et al., 2010; Camus et al., 2014b; Rueda et al., 2019). At longer temporal scales, atmospheric anomalies associated with major climate indices (such as the North Atlantic Oscillation (NAO), Eastern Atlantic (EA) pattern, or El Niño Southern Oscillation (ENSO) in the Pacific Ocean) have also been shown to influence both nearshore wave dynamics and beach morphology (Izaguirre et al., 2010; Barnard et al., 2015; Castelle et al., 2017; Montaño et al., 2021a; Almar et al., 2023).

To further explore the relationship between the interannual variability of extreme wave climate and large-scale atmospheric pressure patterns over the North Atlantic, the interannual variability of H_s along the DoC array is studied. Firstly, Section 4.3.3.1 presents a correlation analysis between the monthly mean H_s signal and different existing European regional climate patterns through Pearson correlation coefficients. In Section 4.3.3.2, the same methodology is applied using *ad hoc* climate indices specifically tailored to the study site.

4.3.3.1 Using existing indices

One of the most prominent teleconnection patterns influencing the North Atlantic basin year-round is the North Atlantic Oscillation (NAO, Barnston and Livezey, 1987;

Enfield et al., 2001). The NAO is characterized by a north–south dipole of sea-level pressure anomalies between the Icelandic Low and the Azores High (Hurrell, 1995), modulating the tracks and intensity of storms crossing the North Atlantic from the eastern seaboard of North America to Europe. These atmospheric changes have a well-established influence on wave climate variability across the basin.

A second major mode of low-frequency variability in the region is the Eastern Atlantic pattern (EA, Barnston and Livezey, 1987). It appears as a leading mode in all months and is structurally similar to the NAO, also exhibiting a north–south dipole of pressure anomalies. However, its anomaly centers are typically displaced southeastward relative to those of the NAO, suggesting a degree of interdependence between the two modes. The EA influences storm tracks and intensity, and along with the NAO, has been shown to significantly affect mean wave height anomalies across the North Atlantic (Woolf et al., 2003; Martínez-Asensio et al., 2016; Gleeson et al., 2019).

The Arctic Oscillation (AO, Thompson and Wallace, 1998, 2000, 2001) represents another important mode of atmospheric variability, particularly in the Northern Hemisphere. It is defined by opposing pressure anomalies between the Arctic and the mid-latitudes. A positive phase of the AO is associated with a stronger polar vortex and more zonal (west-to-east) flow, which tends to confine cold air masses to the polar regions. Conversely, a negative AO phase weakens the polar vortex, allowing cold Arctic air to penetrate further south. These shifts influence storm paths and wave generation processes in the North Atlantic.

The Atlantic Multidecadal Oscillation (AMO) is a long-term oscillation in North Atlantic sea surface temperatures (SSTs), operating on a time scale of approximately 60–80 years (Kerr, 2000; Sutton & Hodson, 2005; Ruiz-Barradas et al., 2013). Positive AMO phases are associated with warmer SSTs in the North Atlantic, which influence atmospheric pressure patterns and moisture transport. These changes can modulate the frequency and intensity of mid-latitude storms, thereby impacting wave climate over multidecadal time scales. Although its influence on short-term variability is less direct than that of the NAO or EA, the AMO plays a key role in long-term coastal and wave climate trends.

Finally, the Scandinavian Pattern (SCA) is characterized by a primary circulation anomaly centered over Scandinavia and extending into large portions of the Arctic Ocean (Barnston & Livezey, 1987). It is a dominant mode of low-frequency variability throughout most of the year, with the exception of June and July. The SCA influences the positioning of the jet stream and storm tracks over Europe and the North Atlantic, thereby affecting wave generation and propagation in the region.

Climate indices from further regions have been analyzed, such as ENSO, Pacific North American Index (PNA) or the Solar Flux, but are not presented due to the low significance they have for the local wave climate. The standardized time series of these teleconnection patterns for the 1940-2025 period were obtained from https://psl.noaa.gov/data/climateindices/list/.

Therefore, this Section explores the correlation between the zones of the DoC array and the abovementioned teleconnection patterns. To do so, the Pearson correlation coefficients between month-to-month H_s anomalies and each climate indice is computed along the DoC array (Fig. 4.4).

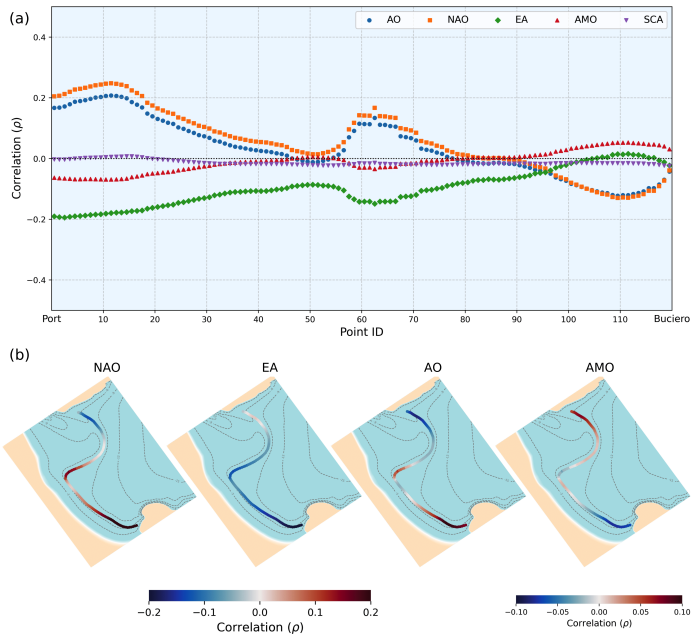

Figure 4.4: (a) Correlations between H_s monthly maxima along the DoC array and the five selected climate indices. (b) Spatial distribution of each array of correlations, for each teleconnection pattern. The bathymetry displayed is the mean bathymetry.

As illustrated in Fig. 4.4, the spatial distribution of H_s at the southern end of La Salvé beach is primarily influenced by a positive correlation with the NAO and AO indices, and a negative correlation with the EA pattern. Moving northward along the beach, the strength of both correlations generally decreases. However, just before the shoal (point IDs between 60 and 70), the influence of the NAO and AO becomes more pronounced again, with positive correlations re-emerging. At the northern end of the beach, a shift in the correlation patterns is observed, where the NAO and AO exhibit negative correlations, while the AMO shows a weakly positive relationship.

To further examine the spatial variability, Fig. 4.5 presents the spatial anomalies of monthly averaged H_s in the last 50 years in relation with the NAO index. Overall, a weak correspondence is observed between these H_s anomalies and the NAO during

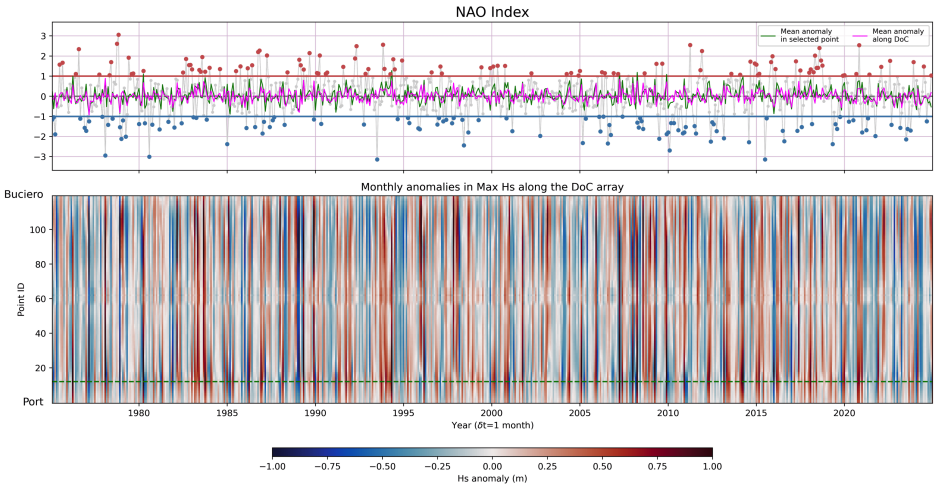

Figure 4.5: Monthly anomalies (by calendar month) for the last 50 years of daily maximum H_s along the DoC array, compared with the NAO signal. Below, the point with the largest correlation is selected, and the anomaly is plotted in green in the upper plot, along with the mean anomaly along DoC array.

the available dates. The point with the strongest correlation is displayed in the upper plot along with the mean of the DoC array, showing some interdependence between larger anomalies an extreme positive values of the NAO (some peaks such as one in 1980, or the early 2000s, can be noticed).

However, as will be explained in the follwoing Section, a stronger correlation emerges when comparing the anomalies in extreme wave conditions with the principal components obtained from a PCA of standardized SLP anomalies over the North Atlantic region, given that those anomalies characterize the meteorological forcing of extreme wave climate in the Cantabrian Sea.

4.3.3.2 Using *ad hoc* indices

To obtain a site-specific teleconnection pattern, PCA is applied to monthly SLP anomalies across the North Atlantic, cropped with ESTELA (Pérez et al., 2014). ESTELA is a method to identify and quantify the source areas and propagation pathways

of wave energy that influence the wave climate at a specific coastal or offshore location. This approach accounts for the geographic configuration of the North coast of Spain, and the potential dissipation of wave energy as it travels from distant wind-generating regions to La Salvé beach, and has been applied in previous works such as Cagigal et al. (2020) and Camus et al. (2014a). Giving as output spatial maps with spatial resolution of 1^{o}x1^{o}, it combines geographic and physical criteria using global wave hindcast data, and defines the propagation pathways for any location by following four steps: excluding areas blocked by land using great circle paths; reconstructing the full directional wave spectrum; estimating the wave energy flux traveling toward the target point; and calculating net energy generation and dissipation areas using a polar grid centered at the target point.

Once the ESTELA method is applied for La Salvé beach, PCA is applied to the cropped, month-to-month standardized SLP anomalies over the North Atlantic, thus obtaining their main oscillation modes (or patterns). In Fig. 4.6a, the cropped area and the first 9 EOFs, explaining 85% of the variance, can be identified. As observed, the first 6 patterns account for most of the variability, capturing the most significant fluctuations in the SLP anomalies. Therefore, the white areas in the maps typically correspond to the transition zones between high- and low-pressure systems, which are often associated with strong wind activity. For instance, EOF2 suggests the presence of northwesterly winds over the Newfoundland and Labrador region. Moreover, the areas with intense color indicate either anticyclonic or storm systems, depending on the sign of the correspondent PC. For example, EOF3 and EOF6 represent these high- or low-pressure systems just over the Cantabrian Sea, while EOF4 and EOF5 reflect similar dynamics over the western North Atlantic.

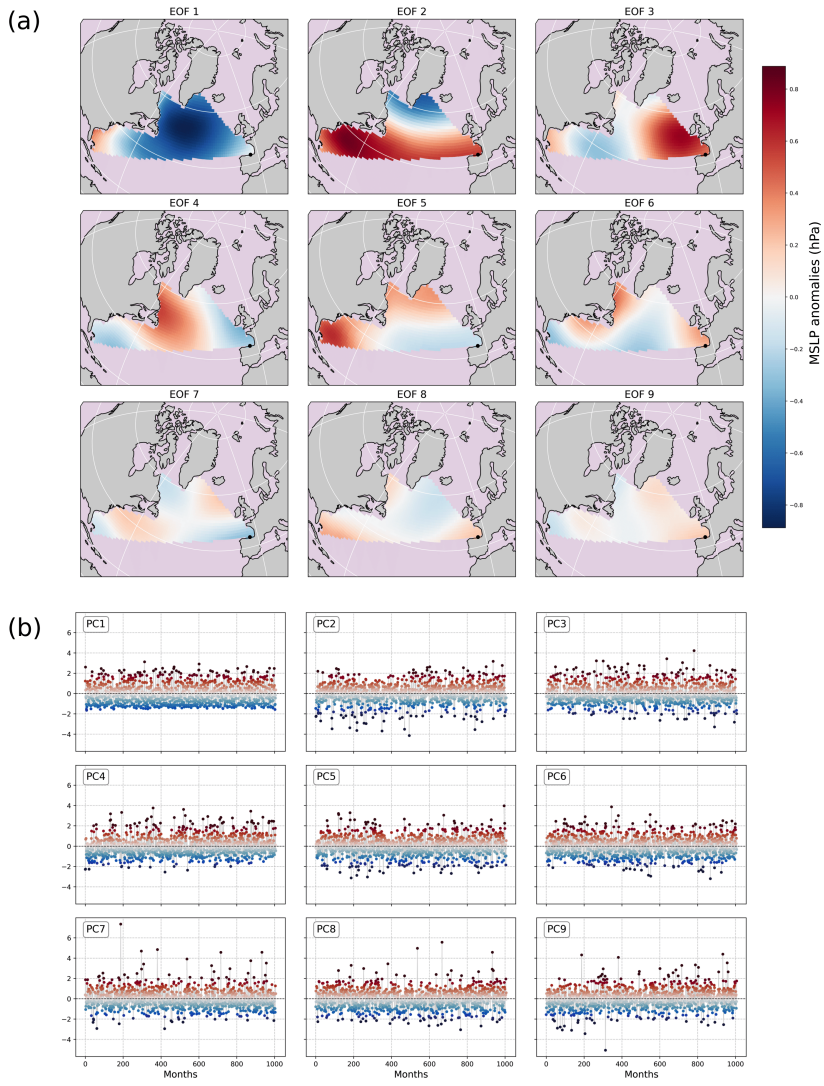

Figure 4.6: (a) EOFs of the SLP anomalies of the North Atlantic, cropped with the ESTELA for Laredo (location indicated with a black dot). (b) First 9 PCs of the SLP anomalies of the North Atlantic, cropped with the ESTELA for Laredo.

The PCs shown in Fig. 4.6b can therefore be used as custom *ad hoc* indices tailored

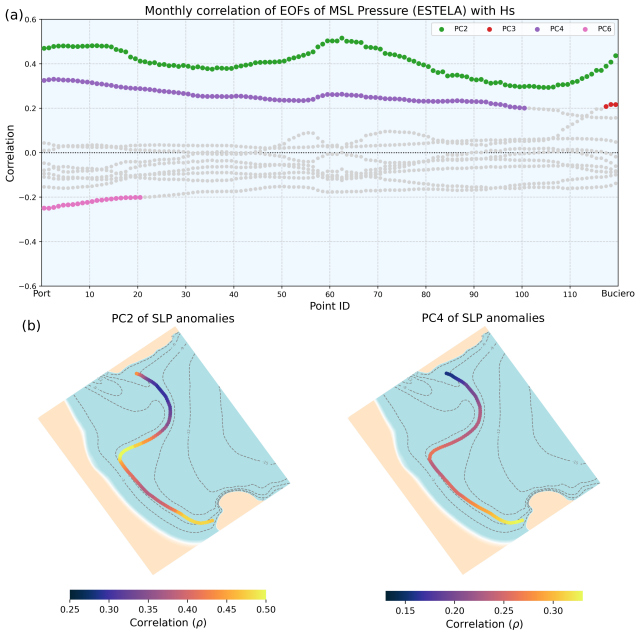

Figure 4.7: (a) Correlations between H_s monthly maxima along the DoC array and the first 9 PCs of SLP anomalies. PCs whose correlations are below 0.2 are not colored. (b) Spatial distribution of each array of correlations, for the two most correlated PCs (PC2 and PC4). The bathymetry displayed is the mean bathymetry.

to the study site, given that they describe the signals of one of the main atmospheric circulation patterns that drive wave generation in the Cantabrian Sea. Thus, the spatial correlation between the first 9 PCs and the monthly maxima of H_s obtained along the DoC array is studied (Fig. 4.7).

Larger correlations can be noticed compared with the ones obtained with the existing indices for the North Atlantic (Fig. 4.4). PC2 has a major positive correlation for the nearshore wave climate, having influence in the southern end and in the tidal ebb. PC4 also is correlated positively with Hs, but its influence decreases while going up north. On the other hand, PC6 shows negative correlations near the port. Attending to the spatial patterns described in Fig. 4.6a, PC2 corresponds to northwesterly winds blowing over the Newfoundland and Labrador region, one of the main drivers of swells

arriving to the Cantabrian Sea. PC4 and PC6, in turn, relate with different location of storms over the North Atlantic basin.

As in the previous section, the spatial variability is analyzed for a defined time span (for illustration purposes, the last 50 years, Fig. 4.8). A correlation between the H_s monthly anomalies and PC2 can be spatially explored. Again, the point with the strongest correlation is displayed in the upper plot along with the mean of the DoC array, showing more interdependence than previously with the NAO. Larger anomalies are more related to extreme positive values of the PC2, such as the peaks in 1980, 1994, or 2005. Some of the peaks detected in Section 4.3.3.1 also appear in PC2, likely because the *ad hoc* index is a refined or site-specific adaptation of broader large-scale patterns that are groundes in established indices such as the NAO.

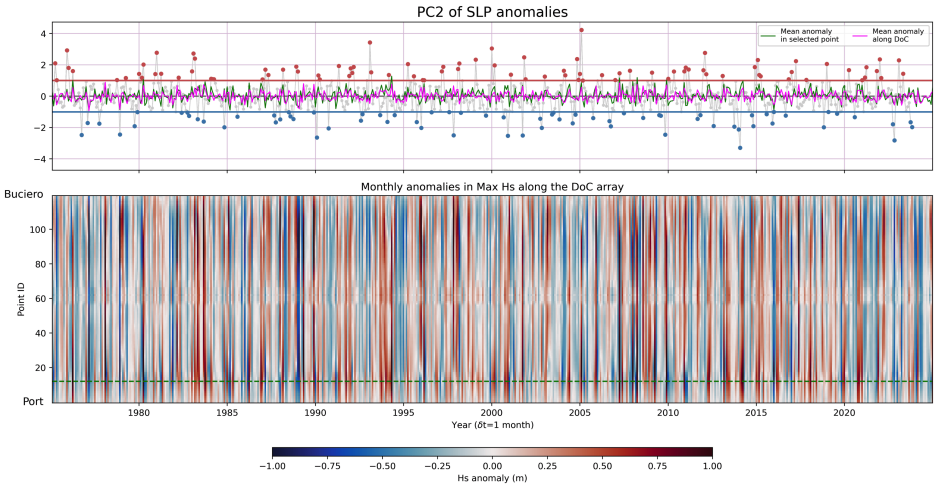

Figure 4.8: Monthly anomalies for the last 50 years of maximum H_s along the DoC array, compared with the PC2 of the SLP anomalies signal. Below, the point with the largest correlation is selected, and the anomaly is plotted in green in the upper plot, along with the mean anomaly along DoC array.

4.3.4 Bathymetry effects on extreme long-term distribution of significant wave height

Understanding extreme wave climate is crucial, as changes in extremes can have far more severe consequences for coastal communities and ecosystems compared to changes in average climate. Proper characterization of the extreme wave climate is essential for the design, operation, and resilience of coastal infrastructure, and serves as the foundation for most coastal risk assessments (e.g. flooding, erosion, or saltwater intrusions).

Traditionally, coastal zone analyses are conducted in specific locations defined by a latitude and a longitude, where H_s time series are obtained, usually through dynamic downscaling. Subsequent statistical analyses are then applied to these point-based datasets. Among these, a widely used approach to study extreme wave climate involves estimating return levels for H_s over defined return periods. This is typically done by fitting a series of annual or seasonal maxima to the Generalized Extreme Value (GEV) distribution. Based on classical extreme value theory, the GEV distribution describes the statistical behavior of the maxima series of a variable, generally representing stochastic natural process. This makes it widely applicable across geophysical and environmental sciences. By fitting the GEV distribution to observed wave maxima, the magnitude of extreme wave events associated with various return periods (e.g., 50-year or 100-year events) can be estimated. These estimates are fundamental for risk-informed decision-making in coastal planning, infrastructure design, and the development of adaptive strategies under changing climate conditions.

The application of the HyWaThy metamodel significantly enhances the efficiency of this classical framework. Rather than producing a single-point time series, HyWaThy generates high-resolution, spatially distributed reconstructions of H_s, enabling comprehensive analyses across the entire study domain. With only one metamodel run, any point within the modeled area can be queried for extreme value assessment, thus reducing computational effort while increasing analytical flexibility and spatial coverage. To illustrate this, Fig. 4.9 shows the spatial maps of different H_s statistics commonly used in coastal engineering, such as the mean significant wave height (H_s), the 1% exceedence wave height ($H_{s_{99\%}}$), as well as the corresponding significant wave

heights related to the 50- and 100-year return period ($H_{s_{T=50}}$ and $H_{s_{T=100}}$, respectively). To obtain these statistics, the 85-year hourly hindcast is reconstructed with HyWaThy over the mean bathymetry.

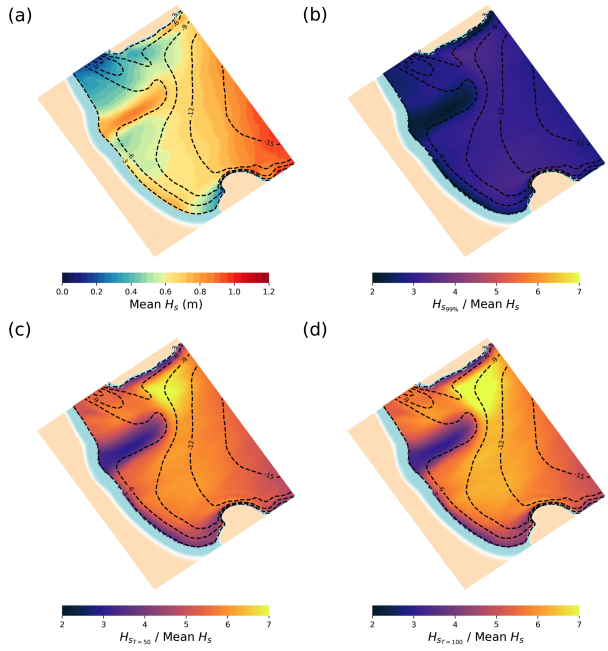

Figure 4.9: Using mean bathymetry: (a) spatial map of mean H_s, (b) spatial map of $H_{s_{99\%}}$, (c) spatial map of H_s correspondent to the 50-year return period and (d)spatial map of H_s correspondent to the 100-year return period. (b), (c) and (d) represent the variables in non-dimensional form (normalized by H_s) to better illustrate their variation relative to the mean H_s.

Fig. 4.9 illustrates how the most significant variations between the extreme distributions of H_s along La Salvé beach are concentrated in two key areas: the tidal ebb delta and the southern end of the beach. Additionally, noticeable differences emerge depending on the statistical indicator used to characterize wave extremes. For instance, the dimensionless $H_{s_{99\%}}$ shown in Fig. 4.9b only reaches values up to three to four times greater than the mean H_s in the aforementioned areas. In contrast, the wave heights associated with 50- and 100-year return periods (Figures 4.9c and 4.9d,

respectively) exhibit even more pronounced differences, with peaks ranging from six to seven times the mean H_s. Moreover, although the general spatial distribution remains similar across the different statistics, discrepancies begin to appear as the analysis shifts toward the upper tail of the extreme value distribution.

On the other hand, the role of seabed morphology in shaping the local wave climate is thoroughly examined by employing the three bathymetric configurations previously introduced in Section 3.4, whose associated bathymetric principal component (bPC) values are detailed in Table 4.1. Each of these bathymetries represents a different configurations of the beach bottom, capturing different phases of La Salvé beach variability. By inputting them into the HyWaThy metamodel, an 85-year hindcast of hourly H_s is propagated across the study domain, yielding high-resolution spatial maps for each bathymetric scenario.

This approach enables a direct comparison of the influence of seabed variability on the transformation of wave energy in the nearshore zone. Through this reconstruction, spatial differences in wave height fields can be analyzed and attributed to specific morphological features, such as the tidal ebb or nearshore bars, pointing out how seabed evolution modulates wave refraction, shoaling, and breaking processes. The resulting spatial datasets also provide a robust basis for further applications, such as identifying areas of persistent high wave energy, assessing exposure to extreme events under different seabed conditions, and supporting erosion or flooding risk modeling.

	Bathymetry 1	**Bathymetry 2**	**Bathymetry 3**
bPC1	1	-1	1.5
bPC2	1.7	-0.5	0.2
bPC3	1	1.5	-1.2
bPC4	1.5	-1.2	0.2

Table 4.1: Bathymetry principal components (bPCs) for each selected bathymetry.

Fig. 4.10 presents a comparison of nearshore mean H_s spatial maps for each of the three bathymetries, using the mean bathymetry as a reference. Notable differences are observed, with variations reaching up to 0.4 meters in certain areas, emphasizing

the critical role that bathymetric configuration plays in determining nearshore H_s values. Moreover, distinct spatial patterns emerge among the three cases, particularly in the vicinity of the tidal ebb delta, south of Mount Buciero, and near the Port. These variations reflect differences in wave energy transformation processes—such as refraction, shoaling, and diffraction—driven by seabed morphology. These processes are accurately resolved thanks to the non-hydrostatic mode of the XBeach model (P. Smit et al., 2013; Roelvink et al., 2018; de Ridder et al., 2021) used in the HyWaThy metamodel.

Fig. 4.10 presents a comparative analysis of nearshore mean H_s spatial distributions derived from simulations using the three distinct bathymetric configurations from Table 4.1, with the mean bathymetry serving as the reference case. The comparison reveals notable discrepancies in H_s spatial patterns across different regions of the domain. These discrepancies underscore the fundamental influence of seabed morphology on the modulation of nearshore wave dynamics. In particular, distinct spatial patterns emerge among the three bathymetries, highlighting sensitive areas such as the tidal ebb delta, the southern end of La Salvé beach, and the vicinity of the Port.

These localized differences can be attributed to variations in wave energy transformation processes that are directly influenced by seabed features. The use of the XBNH model, which resolves short-wave group dynamics and depth-induced wave breaking at high spatial resolution, allows the HyWaThy metamodel to capture these complex interactions with high fidelity. This capacity to resolve bathymetry-driven spatial heterogeneities in H_s distribution is particularly relevant for coastal engineering applications.

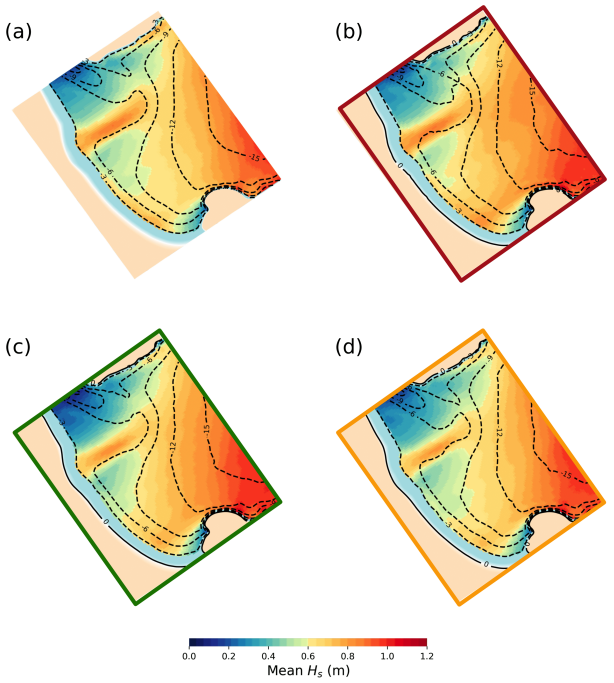

Figure 4.10: Mean H_s spatial maps for (a) mean bathymetry, (b) bathymetry 1, (c) bathymetry 2 and (d) bathymetry 3.

The analysis presented in this Chapter demonstrates the potential of the metamodel to support various coastal engineering applications, such as the design and operation of coastal infrastructure, given that they often rely on estimates associated with statistics of H_s, as outlined in widely used guidelines such as Puertos del Estado, 2009; EurOtop, 2018. Additionally, incorporating bathymetric changes enables the consideration of physical processes that influence H_s alongshore variability, providing a valuable input for a range of coastal applications, including erosion and flood risk assessment.

4.4 Summary and conclusions

In this Chapter, several applications of the HyWaThy coupled metamodel, previously described in Chapter 3, are explored to estimate nearshore hydrodynamics. An 85-year hourly hindcast of H_s was reconstructed in approximately 30 minutes, using a spatial resolution of 20 meters. The spatio-temporal resolution of the outputs was determined based on expert judgment, as long as it remains within the limits of the available data.

Using these high-resolution outputs, a range of coastal engineering anaylses has been performed. First, a two-dimensional definition of the depth of closure (DoC) has been developed by computing H_s statistics and estimating the DoC array. Next, wave climate variability along this array has been examined to identify temporal and spatial patterns, including the alongshore effects of historical storm events and the seasonality signal.

Building on this spatio-temporal dataset, correlations between local wave conditions and both large-scale climate indices dominant in the North Atlantic (e.g., NAO, EA, AO) and custom *ad hoc* indices tailored to the study site have been analyzed. These relationships help quantify the influence of atmospheric variability on the hydrodynamics within La Salvé beach, offering valuable insights for applications such as erosion monitoring, coastal risk assessment, and beach safety planning.

Finally, high-resolution spatial maps of different statistics of H_s are reconstructed in the domain, pointing out the potential of HyWaThy as an alternative for generating large nearshore wave time series. Furthermore, the influence of bathymetric variability on wave conditions has been evaluated by comparing the mean H_s maps derived from three different bathymetries, revealing how local seabed changes can affect the intensity and spatial distribution of waves along the beach.

The rapid, high-resolution outputs provided by the HyWaThy metamodel make it a valuable alternative to traditional downscaling approaches, particularly considering that bathymetric changes can be included in the analyses.

Chapter 5

Summary and future research

5.1 Summary and conclusions

In this thesis, different approaches have been explored and developed towards enhanced surf zone hydrodynamics predictions. The main focus of this research is based on the use of high-resolution, high-fidelity hybrid metamodels to study surf zone hydrodynamic variables, such as TWL components and waves, and their physical relationship with the seabed morphology. The combination of machine learning methods (such as LHS, MDA, PCA and RBF) with numerical models allows to produce fast and accurate estimates of nearshore wave climate, that can be used for several applications in coastal engineering and coastal management. All tools and methodologies developed in this study have been implemented in Python and are fully reproducible through user-friendly Jupyter notebooks. While the analysis has been conducted in La Salvé beach (Spain), the proposed approaches are generalizable and can be applied to other regions globally.

The first aim was to characterize the surf zone waves (H_s) and wave-induced TWL components (η_{setup} and η_{IG}). This was accomplished by using the oceanic parameters from open-data, offshore wave hindcast to define synthetic events that cover the past, present and future plausible sea states in the region, as well as field data of the

bathymetry. Then, by implementing a hybrid methodology that is able to couple a metamodel (Ricondo et al., 2023), XBeach in *surfbeat* mode (Roelvink et al., 2009; Roelvink et al., 2010), data-mining techniques and statistical tools, nearshore variables (H_s, η_{setup} and η_{IG}) on the timescale of wave groups can be efficiently obtained with no need of extensive computational resources. The statistical validation demonstrates the skill of the proposed hybrid metamodel for an application in the Cantabrian Sea.

Next, to perform a high-fidelity downscaling of surf-zone hydrodynamics, two key aspects were considered crucial: the inclusion of bathymetric change over time and modeling at a spatial scale that can describe physical phenomena that are relevant in the surf zone (e.g. refraction, diffraction, breaking and shoaling). Thus, the second contribution of this thesis was focused on the enhancement of the hybrid metamodel previously described, so that it is able to account for the variability of the bathymetry in the nearshore zone and the reciprocal relationship it has with wave propagation. The proposed HyWaThy coupled metamodel is based on a combination of an additive offshore wave model (BinWaves, Cagigal et al., 2024) and a non-hydrostatic hydrodynamic model (XBeach in *non-hydrostatic* mode, de Ridder et al., 2021), along with a previous analysis (PCA) to represent the natural oscillation modes of the beach bathymetry. The results show that HyWaThy is able to accurately predict nearshore wave climate in La Salvé beach, with a good agreement between modeled and observed values, and is ready to be used in other study sites.

Finally, the third objective was to generate a high-resolution nearshore wave climate for La Salvé beach using the HyWaThy metamodel. An 85-year hourly hindcast of H_s was reconstructed in approximately 30 minutes at a spatial resolution of 20 meters. This downscaled nearshore wave climate allowed to perform diverse coastal engineering analyses aimed at improving the understanding of the Santoña Bay wave dynamics. First, a two-dimensional characterization of the depth of closure was conducted. Based on the resulting locations, the spatio-temporal variability of wave conditions along the depth of closure was studied, along with its correlation with large-scale climate indices. Lastly, high-resolution spatial maps of different statistics of H_s were reconstructed across the domain, pointing out the potential of HyWaThy as an effective alternative for generating large nearshore wave time series. Furthermore, the influence of bathymetric variability on wave conditions has been evaluated by comparing the mean H_s

maps derived from three different bathymetries.

In summary, the results support the conclusion that hybrid approaches, which combine high-fidelity numerical models with statistical techniques, provide a cost-effective alternative for rapidly estimating high-resolution surf zone hydrodynamics. The HyWaThy coupled metamodel shows strong potential as a coastal management tool, as it is able to address pressing challenges in coastal science, such as erosion and flooding, especially when integrated into Early Warning Systems.

5.2 Future research

The presented methodologies assumed specific hypotheses and were developed within the constraints of site-specific limitations. These factors open lines of future research to be explored, in order to establish a more robust and generalizable framework, widening the range of coastal regions where the proposed metamodels can be applied. The following points describe the key research needs and the potential directions for future efforts:

- Introduction of wave multimodality in the oceanic forcings. This would imply more variables in the generation of the multivariate, synthetic cases (and therefore a need for a greater number of pre-run cases), but would allow to apply these metamodels in areas affected by multimodal directional spectra.

- Incorporation of state-of-the-art methods to infer bathymetries from satellite data. Populating the topobathymetric input data is the main need of the HyWaThy coupled metamodel, as it would not only enhance its performance (by capturing a broader range of oscillation modes), but also extend its applicability beyond a specific, heavily surveyed study site to anywhere around the world, provided that supporting *in situ* data are available to calibrate and validate satellite-derived information.

- Inclusion of the intertidal zone in the study domain. To prevent biases produced by wave breaking patterns under varying SWLs, the intertidal zone has been

excluded from the outputs of the PCA applied to the H_s spatial fields. However, further investigation into methods to incorporate this zone may be valuable, as it still hosts relevant physical processes during high tides.

- If long-term, high-fidelity topobathymetric data is available, correlate it with the local nearshore conditions. This would allow to set an operational framework with the HyWaThy metamodel, in which any user could infer a topobathymetry from any given sea state, or infer the bPC values from any given topobathymetry. Additionally, considering that La Salvé beach morphodynamic state remains predominantly dissipative over time, future works could involve relocating the study to a more morphodynamically dynamic beach.

- Expansion of the variables to model. The HyWaThy metamodel could be extended to reconstruct other relevant variables, such as wave-induced currents (longshore currents, rip currents), which play a critical role in beach safety and forecasting for recreational water activities.

- Calibrate and validate the metamodel using instrumental data. It is essential to ensure a reliable performance of the metamodel, as the XBeach model has been run using some default setup parameters or values derived from existing literature (e.g., friction coefficients). Although the numerical validation has demonstrated satisfactory results, validation against *in-situ* measurements is necessary to definitively confirm the accuracy and robustness of the metamodel.

Bibliography

Afentoulis, V., Papadimitriou, A., Belibassakis, K., & Tsoukala, V. (2022). A coupled model for sediment transport dynamics and prediction of seabed morphology with application to 1dh/2dh coastal engineering problems. *Oceanologia*, *64*, 514–534. https://doi.org/10.1016/J.OCEANO.2022.03.007

Agulles, M., & Jordà, G. (2022). Flooding of sandy beaches in a changing climate and the potential of nature based solution for impact mitigation. *EGU22*. https://doi.org/10.5194/EGUSPHERE-EGU22-4959

Alegría-Arzaburu, A. R., Garcia-Walther, J., Serratos, L. O., Vega, J. V., & Senner, N. R. (2025). The impact of beachface morphology on habitat suitability and breeding success of least terns and snowy plovers. *Estuaries and Coasts 2025 48:5*, *48*, 1–15. https://doi.org/10.1007/S12237-025-01574-5

Almar, R., Boucharel, J., Graffin, M., Abessolo, G. O., Thoumyre, G., Papa, F., Ranasinghe, R., Montano, J., Bergsma, E. W., Baba, M. W., & Jin, F. F. (2023). Influence of el niño on the variability of global shoreline position. *Nature Communications 2023 14:1*, *14*, 1–13. https://doi.org/10.1038/s41467-023-38742-9

Anderson, D. L., Ruggiero, P., Mendez, F. J., Barnard, P. L., Erikson, L. H., O'Neill, A. C., Merrifield, M., Rueda, A., Cagigal, L., & Marra, J. (2021). Projecting climate dependent coastal flood risk with a hybrid statistical dynamical model. *Earth's Future*, *9*, e2021EF002285. https://doi.org/10.1029/2021EF002285

Aubrey, D. (1978). *Statistical and dynamical prediction of changes in natural sand and beaches*. University of California.

Barber, C. B., Dobkin, D. P., & Huhdanpaa, H. (1996). The quickhull algorithm for convex hulls. *ACM Transactions on Mathematical Software (TOMS)*, *22*, 469–483. https://doi.org/10.1145/235815.235821

Barboza, F. R., & Defeo, O. (2015). Global diversity patterns in sandy beach macrofauna: A biogeographic analysis. *Scientific Reports 2015 5:1*, *5*, 1–9. https://doi.org/10.1038/srep14515

Barnard, P. L., Short, A. D., Harley, M. D., Splinter, K. D., Vitousek, S., Turner, I. L., Allan, J., Banno, M., Bryan, K. R., Doria, A., Hansen, J. E., Kato, S.,

Kuriyama, Y., Randall-Goodwin, E., Ruggiero, P., Walker, I. J., & Heathfield, D. K. (2015). Coastal vulnerability across the pacific dominated by el niño/southern oscillation. *Nature Geoscience 2015 8:10*, *8*, 801–807. https://doi.org/10.1038/ngeo2539

Barnston, A. G., & Livezey, R. E. (1987). Classification, seasonality and persistence of low-frequency atmospheric circulation patterns. *Monthly Weather Review*, *115*, 1083–1126. https://doi.org/10.1175/1520-0493(1987)115⟨1083:CSAPOL⟩2.0.CO;2

Battjes, J. (1974). Surf similarity. *Coastal Engineering Proceedings*, *1*, 26. https://doi.org/10.9753/icce.v14.26

Bellotti, G., Franco, L., & Cecioni, C. (2021). Regional downscaling of copernicus era5 wave data for coastal engineering activities and operational coastal services. *Water 2021, Vol. 13, Page 859*, *13*, 859. https://doi.org/10.3390/W13060859

Bertelli, C. M., Bennett, W. G., Karunarathna, H., Reeve, D. E., Unsworth, R. K., & Bull, J. C. (2023). High-resolution wave data for improving marine habitat suitability models. *Frontiers in Marine Science*, *9*, 1004829. https://doi.org/10.3389/FMARS.2022.1004829/BIBTEX

Bertin, X., de Bakker, A., van Dongeren, A., Coco, G., André, G., Ardhuin, F., Bonneton, P., Bouchette, F., Castelle, B., Crawford, W. C., Davidson, M., Deen, M., Dodet, G., Guérin, T., Inch, K., Leckler, F., McCall, R., Muller, H., Olabarrieta, M., ... Tissier, M. (2018). Infragravity waves: From driving mechanisms to impacts. *Earth-Science Reviews*, *177*, 774–799. https://doi.org/10.1016/J.EARSCIREV.2018.01.002

Bingölbali, B., Akpınar, A., Jafali, H., & Vledder, G. P. V. (2019). Downscaling of wave climate in the western black sea. *Ocean Engineering*, *172*, 31–45. https://doi.org/10.1016/J.OCEANENG.2018.11.042

Birkemeier, W. A. (1985). Field data on seaward limit of profile change. *Journal of Waterway, Port, Coastal, and Ocean Engineering*, *111*, 598–602. https://doi.org/10.1061/(ASCE)0733-950X(1985)111:3(598)

Booij, N., Ris, R. C., & Holthuijsen, L. H. (1999). A third-generation wave model for coastal regions: 1. model description and validation. *Journal of Geophysical Research: Oceans*, *104*, 7649–7666. https://doi.org/10.1029/98JC02622

Bramante, J. F., Ashton, A. D., Storlazzi, C. D., Cheriton, O. M., & Donnelly, J. P. (2020). Sea level rise will drive divergent sediment transport patterns on fore reefs and reef flats, potentially causing erosion on atoll islands. *Journal of Geophysical Research: Earth Surface*, *125*, e2019JF005446. https://doi.org/10.1029/2019JF005446

Bujan, N., Cox, R., & Masselink, G. (2019). From fine sand to boulders: Examining the relationship between beach-face slope and sediment size. *Marine Geology*, *417*, 106012. https://doi.org/10.1016/J.MARGEO.2019.106012

Caballero, I., & Stumpf, R. P. (2021). On the use of sentinel-2 satellites and lidar surveys for the change detection of shallow bathymetry: The case study of north carolina inlets. *Coastal Engineering*, *169*, 103936. https://doi.org/10.1016/J.COASTALENG.2021.103936

Cagigal, L., Méndez, F. J., Ricondo, A., Gutiérrez-Barceló, D., Bosserelle, C., & Hoeke, R. (2024). Binwaves: An additive hybrid method to downscale directional wave spectra to nearshore areas. *Ocean Modelling*, *189*, 102346. https://doi.org/10.1016/J.OCEMOD.2024.102346

Cagigal, L., Rueda, A., Anderson, D., Ruggiero, P., Merrifield, M. A., Montaño, J., Coco, G., & Méndez, F. J. (2020). A multivariate, stochastic, climate-based wave emulator for shoreline change modelling. *Ocean Modelling*, *154*, 101695. https://doi.org/10.1016/J.OCEMOD.2020.101695

Cagigal, L., Rueda, A., Ricondo, A., Pérez, J., Ripoll, N., Coco, G., & Méndez, F. J. (2021). Climate-based emulator of distant swell trains and local seas approaching a pacific atoll. *Journal of Geophysical Research: Oceans*, *126*, e2020JC016919. https://doi.org/10.1029/2020JC016919

Camus, P., Mendez, F. J., & Medina, R. (2011b). A hybrid efficient method to downscale wave climate to coastal areas. *Coastal Engineering*, *58*, 851–862. https://doi.org/10.1016/J.COASTALENG.2011.05.007

Camus, P., Mendez, F. J., Medina, R., & Cofiño, A. S. (2011a). Analysis of clustering and selection algorithms for the study of multivariate wave climate. *Coastal Engineering*, *58*, 453–462. https://doi.org/10.1016/J.COASTALENG.2011.02.003

Camus, P., Méndez, F. J., Losada, I. J., Menéndez, M., Espejo, A., Pérez, J., Rueda, A., & Guanche, Y. (2014a). A method for finding the optimal predictor indices for local wave climate conditions. *Ocean Dynamics*, *64*, 1025–1038. https://doi.org/10.1007/S10236-014-0737-2/FIGURES/12

Camus, P., Menéndez, M., Méndez, F. J., Izaguirre, C., Espejo, A., Cánovas, V., Pérez, J., Rueda, A., Losada, I. J., & Medina, R. (2014b). A weather-type statistical downscaling framework for ocean wave climate. *Journal of Geophysical Research: Oceans*, *119*, 7389–7405. https://doi.org/10.1002/2014JC010141

Caruso, M. F., & Marani, M. (2022). Extreme-coastal-water-level estimation and projection: A comparison of statistical methods. *Natural Hazards and Earth System Sciences*, *22*, 1109–1128. https://doi.org/10.5194/NHESS-22-1109-2022

Castelle, B., Dodet, G., Masselink, G., & Scott, T. (2017). A new climate index controlling winter wave activity along the atlantic coast of europe: The west europe pressure anomaly. *Geophysical Research Letters*, *44*, 1384–1392. https://doi.org/10.1002/2016GL072379

Castelle, B., Dodet, G., Masselink, G., & Scott, T. (2018). Increased winter-mean wave height, variability, and periodicity in the northeast atlantic over 1949–2017.

Geophysical Research Letters, *45*, 3586–3596. https://doi.org/10.1002/2017GL076884

Castelle, B., Marieu, V., Bujan, S., Splinter, K. D., Robinet, A., Sénéchal, N., & Ferreira, S. (2015). Impact of the winter 2013–2014 series of severe western europe storms on a double-barred sandy coast: Beach and dune erosion and megacusp embayments. *Geomorphology*, *238*, 135–148. https://doi.org/10.1016/J.GEOMORPH.2015.03.006

Castelle, B., & Masselink, G. (2023). Morphodynamics of wave-dominated beaches. *Cambridge Prisms: Coastal Futures*, *1*, e1. https://doi.org/10.1017/CFT.2022.2

Cheriton, O. M., Storlazzi, C. D., & Rosenberger, K. J. (2016). Observations of wave transformation over a fringing coral reef and the importance of low-frequency waves and offshore water levels to runup, overwash, and coastal flooding. *Journal of Geophysical Research: Oceans*, *121*, 3121–3140. https://doi.org/10.1002/2015JC011231

Christiaanse, J. C., Antolínez, J. A., Marshall, C. D., Figlus, J., Dellapenna, T. M., & Reniers, A. J. (2025). Beach groundwater response to ocean processes and rain on a mild-sloping barrier island: Implications for sea turtle nest flooding. *Coastal Engineering*, *201*, 104795. https://doi.org/10.1016/J.COASTALENG.2025.104795

Clemente, M. F., D'Ambrosio, V., & Focareta, M. (2022). The proposal of the coastriskbysea: Coastal zones risk assessment for built environment by extreme sea level, based on the new copernicus coastal zones data. *International Journal of Disaster Risk Reduction*, *75*, 102947. https://doi.org/10.1016/J.IJDRR.2022.102947

Cohn, N., Brodie, K. L., Johnson, B., & Palmsten, M. L. (2021). Hotspot dune erosion on an intermediate beach. *Coastal Engineering*, *170*, 103998. https://doi.org/10.1016/J.COASTALENG.2021.103998

Costanza, R., de Groot, R., Sutton, P., van der Ploeg, S., Anderson, S. J., Kubiszewski, I., Farber, S., & Turner, R. K. (2014). Changes in the global value of ecosystem services. *Global Environmental Change*, *26*, 152–158. https://doi.org/10.1016/J.GLOENVCHA.2014.04.002

Dada, O. A., Almar, R., Morand, P., Bergsma, E. W., Angnuureng, D. B., & Minderhoud, P. S. (2023). Future socioeconomic development along the west african coast forms a larger hazard than sea level rise. *Communications Earth & Environment 2023 4:1*, *4*, 1–12. https://doi.org/10.1038/s43247-023-00807-4

Dalrymple, R. A., & Thompson, W. W. (1976). Study of equilibrium beach profiles. *Coastal Engineering Proceedings*, *1*, 74. https://doi.org/10.9753/icce.v15.74

de Beer, A. F., McCall, R. T., Long, J. W., Tissier, M. F., & Reniers, A. J. (2021). Simulating wave runup on an intermediate–reflective beach using a wave-resolving

and a wave-averaged version of xbeach. *Coastal Engineering*, *163*, 103788. https://doi.org/10.1016/J.COASTALENG.2020.103788

de Ridder, M. P., Smit, P. B., van Dongeren, A. R., McCall, R. T., Nederhoff, K., & Reniers, A. J. (2021). Efficient two-layer non-hydrostatic wave model with accurate dispersive behaviour. *Coastal Engineering*, *164*, 103808. https://doi.org/10.1016/J.COASTALENG.2020.103808

Dean, R. (1973). Heuristic models of sand transport in the surf zone. *Proceedings of the First Australian Conference on Coastal Engineering*, 208–214.

Dean, R. G., & Bender, C. J. (2006). Static wave setup with emphasis on damping effects by vegetation and bottom friction. *Coastal Engineering*, *53*, 149–156. https://doi.org/10.1016/J.COASTALENG.2005.10.005

DeLeo, F., Enríquez, A. R., Orfila, A., & Besio, G. (2022). Uncertainty assessment of significant wave height return levels downscaling for coastal application. *Applied Ocean Research*, *127*, 103303. https://doi.org/10.1016/J.APOR.2022.103303

Didier, D., Bandet, M., Bernatchez, P., & Dumont, D. (2019). Modelling coastal flood propagation under sea level rise: A case study in maria, eastern canada. *Geosciences 2019, Vol. 9, Page 76*, *9*, 76. https://doi.org/10.3390/GEOSCIENCES9020076

Dodet, G., Bertin, X., Bruneau, N., Fortunato, A. B., Nahon, A., & Roland, A. (2013). Wave-current interactions in a wave-dominated tidal inlet. *Journal of Geophysical Research: Oceans*, *118*, 1587–1605. https://doi.org/10.1002/JGRC.20146

Dongeren, A. V., Veeramony, J., Ormondt, M. V., Nederhoff, K., & Penko, A. (2023, April). Forecasting hurricane impacts on coasts using coastal storm modeling system (cosmos). https://doi.org/10.1142/9789811275135_0242

Durrant, T., Greenslade, D., Hemer, M., & Trenham, C. (2014). *A global wave hindcast focussed on the central and south pacific* (tech. rep.). CAWCR Technical Report 070. http://www.cawcr.gov.au/technical-reports/CTR_070.pdf

Enfield, D. B., Mestas-Nuñez, A. M., & Trimble, P. J. (2001). The atlantic multidecadal oscillation and its relation to rainfall and river flows in the continental u.s. *Geophysical Research Letters*, *28*, 2077–2080. https://doi.org/10.1029/2000GL012745

Espejo, A., Camus, P., Losada, I. J., & Méndez, F. J. (2014). Spectral ocean wave climate variability based on atmospheric circulation patterns. *Journal of Physical Oceanography*, *44*, 2139–2152. https://doi.org/10.1175/JPO-D-13-0276.1

Espejo, A., Wandres, M., Damlamian, H., Divesh, A., Giblin, J., Aucan, J., Eria, M., & Toorua, U. (2023). Efficient coastal inundation early-warning system for low-lying atolls, dealing with lagoon and ocean side inundation in tarawa, kiribati. *Weather and Climate Extremes*, *42*, 100615. https://doi.org/10.1016/J.WACE.2023.100615

European Environment Agency. (2021). Eea indicators: Climate change adaptation. extreme sea levels and coastal flooding. https://www.eea.europa.eu/ims/extreme-sea-levels-and-coastal-flooding

European Environment Agency. (2022). Economic losses and fatalities from weather- and climate-related events in europe. https://www.eea.europa.eu/publications/economic-losses-and-fatalities-from

EurOtop. (2018). *Manual on wave overtopping of sea defences and related structures. an overtopping manueal largely based on european research, but for worldwide application* (J. van der Meer, N. Allsop, T. Bruce, A. Kortenhaus, T. Pullen, H. Schüttrumpf, P. Troch, & B. Zanuttigh, Eds.). https://www.overtopping-manual.com/assets/downloads/EurOtop_II_2018_Final_version.pdf

Fernández-Montblanc, T., Duo, E., & Ciavola, P. (2020). Dune reconstruction and revegetation as a potential measure to decrease coastal erosion and flooding under extreme storm conditions. *Ocean & Coastal Management*, *188*, 105075. https://doi.org/10.1016/J.OCECOAMAN.2019.105075

Ferreira, A. M., Fortes, C. J., Reis, M. T., & Garzon, J. L. (2020). Análise de eventos de risco através de modelação numérica xbeach. caso de estudo - costa da caparica. *Revista Recursos Hídricos*, *41*, 51–63. https://doi.org/10.5894/RH41N2-CTI4

Floods Directive. (2007). Directive 2007/60/ec of 26 november 2007 on the assessment and management of flood risks. https://environment.ec.europa.eu/topics/water/floods_en

Franke, R. (1982). Scattered data interpolation: Tests of some methods. *Mathematics of Computation*, *38*, 181–200. https://doi.org/10.1090/S0025-5718-1982-0637296-4

Frugier, S., Almar, R., Bergsma, E., & Granjou, A. (2025). Sbi: A sandbar extraction spectral index for multi-spectral satellite optical imagery. *Coastal Engineering*, *200*, 104752. https://doi.org/10.1016/J.COASTALENG.2025.104752

Gainza, J., Rueda, A., Camus, P., Tomás, A., Méndez, F. J., Sano, M., & Tomlinson, R. (2018). A meta-modelling approach for estimating long-term wave run-up and total water level on beaches. *Journal of Coastal Research*, *34*, 475–489. https://doi.org/10.2112/JCOASTRES-D-16-00198.1

Gallien, T. W. (2016). Validated coastal flood modeling at imperial beach, california: Comparing total water level, empirical and numerical overtopping methodologies. *Coastal Engineering*, *111*, 95–104. https://doi.org/10.1016/J.COASTALENG.2016.01.014

Gallien, T. W., O'Reilly, W. C., Flick, R. E., & Guza, R. T. (2015). Geometric properties of anthropogenic flood control berms on southern california beaches. *Ocean & Coastal Management*, *105*, 35–47. https://doi.org/10.1016/J.OCECOAMAN.2014.12.014

Garrote, J., Díaz-Álvarez, A., Nganhane, H. V., & Heydt, G. G. (2018). The severe 2013–14 winter storms in the historical evolution of cantabrian (northern spain) beach-dune systems. *Geosciences 2018, Vol. 8, Page 459*, *8*, 459. https://doi.org/10.3390/GEOSCIENCES8120459

Garzon, J. L., Ferreira, Zózimo, A. C., Fortes, C. J., Ferreira, A. M., Pinheiro, L. V., & Reis, M. T. (2023). Development of a bayesian networks-based early warning system for wave-induced flooding. *International Journal of Disaster Risk Reduction*, *96*, 103931. https://doi.org/10.1016/J.IJDRR.2023.103931

Garzón, J., Ferreira, O., Ferreira, A., & Fortes, C. (2022). Wave-induced flooding risk assessment for the development of early warning systems. *Proceedings of the 39th IAHR World Congress*, 19–24. https://doi.org/https://doi.org/10.3850/IAHR-39WC2521716X20221411

Gaztelumendi, S., Egaña, J., Liria, P., Gonzalez, M., Aranda, J. A., & Anitua, P. (2016). The new euskalmet coastal–maritime warning system. *Advances in Science and Research*, *13*, 91–96. https://doi.org/10.5194/ASR-13-91-2016

Glavovic, B., Dawson, R., Chow, W., Garschagen, M., Haasnoot, M., Singh, C., & Thomas, A. (2022). Cross-chapter paper 2: Cities and settlements by the sea. In H.-O. Pörtner, D. Roberts, M. Tignor, E. Poloczanska, K. Mintenbeck, A. Alegría, M. Craig, S. Langsdorf, S. Löschke, V. Möller, A. Okem, & B. Rama (Eds.), *Climate change 2022: Impacts, adaptation and vulnerability. contribution of working group ii to the sixth assessment report of the intergovernmental panel on climate change* (pp. 2163–2194). Cambridge University Press. https://doi.org/10.1017/9781009325844.019

Gleeson, E., Clancy, C., Zubiate, L., Janjić, J., Gallagher, S., & Dias, F. (2019). Teleconnections and extreme ocean states in the northeast atlantic ocean. *Advances in Science and Research*, *16*, 11–29. https://doi.org/10.5194/ASR-16-11-2019

Godoi, V. A., Bryan, K. R., & Gorman, R. M. (2016). Regional influence of climate patterns on the wave climate of the southwestern pacific: The new zealand region. *Journal of Geophysical Research: Oceans*, *121*, 4056–4076. https://doi.org/10.1002/2015JC011572

Gomes, M. P., Pinho, J. L., do Carmo, J. S. A., & Santos, L. (2015). Hazard assessment of storm events for the battery, new york. *Ocean & Coastal Management*, *118*, 22–31. https://doi.org/10.1016/J.OCECOAMAN.2015.11.006

Gracia, A., Rangel-Buitrago, N., Oakley, J. A., & Williams, A. T. (2018). Use of ecosystems in coastal erosion management. *Ocean & Coastal Management*, *156*, 277–289. https://doi.org/10.1016/J.OCECOAMAN.2017.07.009

Haigh, I. D., Wadey, M. P., Wahl, T., Ozsoy, O., Nicholls, R. J., Brown, J. M., Horsburgh, K., & Gouldby, B. (2016). Spatial and temporal analysis of extreme sea level and storm surge events around the coastline of the uk. *Scientific Data 2016 3:1*, *3*, 1–14. https://doi.org/10.1038/sdata.2016.107

Haigh, I. D., Wijeratne, E. M., MacPherson, L. R., Pattiaratchi, C. B., Mason, M. S., Crompton, R. P., & George, S. (2014). Estimating present day extreme water level exceedance probabilities around the coastline of australia: Tides, extra-tropical storm surges and mean sea level. *Climate Dynamics*, *42*, 121–138. https://doi.org/10.1007/S00382-012-1652-1/FIGURES/10

Hallermeier, R. J. (1978). Uses for a calculated limit depth to beach erosion. *Coastal Engineering 1978*, 1493–1512. https://doi.org/10.1061/9780872621909.090

Hallermeier, R. J. (1980). A profile zonation for seasonal sand beaches from wave climate. *Coastal Engineering*, *4*, 253–277. https://doi.org/10.1016/0378-3839(80)90022-8

Harley, M. D., Valentini, A., Armaroli, C., Perini, L., Calabrese, L., & Ciavola, P. (2016). Can an early-warning system help minimize the impacts of coastal storms? a case study of the 2012 halloween storm, northern italy. *Natural Hazards and Earth System Sciences*, *16*, 209–222. https://doi.org/10.5194/NHESS-16-209-2016

Harley, M. D., Turner, I. L., Kinsela, M. A., Middleton, J. H., Mumford, P. J., Splinter, K. D., Phillips, M. S., Simmons, J. A., Hanslow, D. J., & Short, A. D. (2017). Extreme coastal erosion enhanced by anomalous extratropical storm wave direction. *Scientific Reports 2017 7:1*, *7*, 1–9. https://doi.org/10.1038/s41598-017-05792-1

Harris, L., Nel, R., & Schoeman, D. (2011). Mapping beach morphodynamics remotely: A novel application tested on south african sandy shores. *Estuarine, Coastal and Shelf Science*, *92*, 78–89. https://doi.org/10.1016/J.ECSS.2010.12.013

Henderson, S. M., & Bowen, A. J. (2002). Observations of surf beat forcing and dissipation. *Journal of Geophysical Research: Oceans*, *107*, 14–1. https://doi.org/10.1029/2000JC000498

Hersbach, H., Bell, B., Berrisford, P., Biavati, G., Horányi, A., Sabater, J. M., Nicolas, J., Peubey, C., Radu, R., Rozum, I., Schepers, D., Simmons, A., Soci, C., Dee, D., & Thépaut, J.-N. (2023). Era5 hourly data on single levels from 1940 to present. https://doi.org/10.24381/cds.adbb2d47

Hersbach, H., Bell, B., Berrisford, P., Hirahara, S., Horányi, A., Muñoz-Sabater, J., Nicolas, J., Peubey, C., Radu, R., Schepers, D., Simmons, A., Soci, C., Abdalla, S., Abellan, X., Balsamo, G., Bechtold, P., Biavati, G., Bidlot, J., Bonavita, M., ... Thépaut, J. N. (2020). The era5 global reanalysis. *Quarterly Journal of the Royal Meteorological Society*, *146*, 1999–2049. https://doi.org/10.1002/QJ.3803

Hoeke, R. K., McInnes, K. L., Kruger, J. C., McNaught, R. J., Hunter, J. R., & Smithers, S. G. (2013). Widespread inundation of pacific islands triggered by distant-source wind-waves. *Global and Planetary Change*, *108*, 128–138. https://doi.org/10.1016/J.GLOPLACHA.2013.06.006

Holthuijsen, L. H., Booij, N., & Herbers, T. H. (1989). A prediction model for stationary, short-crested waves in shallow water with ambient currents. *Coastal Engineering*, *13*, 23–54. https://doi.org/10.1016/0378-3839(89)90031-8

Holthuijsen, L. (2007). *Waves in oceanic and coastal waters*. Cambridge University Press. https://doi.org/https://doi.org/10.1017/CBO9780511618536

Hurrell, J. W. (1995). Decadal trends in the north atlantic oscillation: Regional temperatures and precipitation. *Science*, *269*, 676–679. https://doi.org/10.1126/SCIENCE.269.5224.676

Integrated Marine Observing System (IMOS). (2019). *33 years of globally calibrated wave height and wind speed data based on altimeter observations* (tech. rep.). https://doi.org/https://doi.org/10.26198/5c77588b32cc1

IPCC. (2023). *Climate change 2022 – impacts, adaptation and vulnerability: Working group ii contribution to the sixth assessment report of the intergovernmental panel on climate change*. Cambridge University Press. https://doi.org/10.1017/9781009325844

Izaguirre, C., Mendez, F. J., Menendez, M., Luceño, A., & Losada, I. J. (2010). Extreme wave climate variability in southern europe using satellite data. *Journal of Geophysical Research: Oceans*, *115*, 4009. https://doi.org/10.1029/2009JC005802

Izaguirre, C., Méndez, F. J., Menéndez, M., & Losada, I. J. (2011). Global extreme wave height variability based on satellite data. *Geophysical Research Letters*, *38*. https://doi.org/10.1029/2011GL047302

Jackson, D., Beyers, J. H., Lynch, K., Cooper, J. A., Baas, A. C., & Delgado-Fernandez, I. (2011). Investigation of three-dimensional wind flow behaviour over coastal dune morphology under offshore winds using computational fluid dynamics (cfd) and ultrasonic anemometry. *Earth Surface Processes and Landforms*, *36*, 1113–1124. https://doi.org/10.1002/ESP.2139

Jackson, D., & Short, A. (2020). *Sandy beach morphodynamics* (1st). Elsevier. https://doi.org/10.1016/C2018-0-02420-2

Kennard, R. W., & Stone, L. A. (1969). Computer aided design of experiments. *Technometrics*, *11*, 137–148. https://doi.org/10.1080/00401706.1969.10490666

Kerr, R. A. (2000). A north atlantic climate pacemaker for the centuries. *Science*, *288*, 1984–1986. https://doi.org/10.1126/SCIENCE.288.5473.1984

Klovan, J. (1966). The use of factor analysis in determining depositional environments from grain size distributions. *Journal of Sedimentary Petrology*, *36*, 115–125. https://doi.org/https://doi.org/10.1306/74D7141A-2B21-11D7-8648000102C1865D

Lashley, C. H., Roelvink, D., van Dongeren, A., Buckley, M. L., & Lowe, R. J. (2018). Nonhydrostatic and surfbeat model predictions of extreme wave run-up in fringing reef environments. *Coastal Engineering*, *137*, 11–27. https://doi.org/10.1016/J.COASTALENG.2018.03.007

Leaman, C. K., Harley, M. D., Splinter, K. D., Thran, M. C., Kinsela, M. A., & Turner, I. L. (2021). A storm hazard matrix combining coastal flooding and beach erosion. *Coastal Engineering*, *170*, 104001. https://doi.org/10.1016/J.COASTALENG.2021.104001

Leder, T. D., Baučić, M., Leder, N., & Gilić, F. (2023). Optical satellite-derived bathymetry: An overview and wos and scopus bibliometric analysis. *Remote Sensing 2023, Vol. 15, Page 1294*, *15*, 1294. https://doi.org/10.3390/RS15051294

Lemke, L., & Miller, J. K. (2020). Evaluation of storms through the lens of erosion potential along the new jersey, usa coast. *Coastal Engineering*, *158*, 103699. https://doi.org/10.1016/J.COASTALENG.2020.103699

Lemos, G., Menendez, M., Semedo, A., Miranda, P. M., & Hemer, M. (2021). On the decreases in north atlantic significant wave heights from climate projections. *Climate Dynamics*, *57*, 2301–2324. https://doi.org/10.1007/S00382-021-05807-8/TABLES/7

Li, Y., & Pan, D. (2024). Empirical orthogonal function analysis on long-term profile evolution of tidal flats along a curved coast in the qiantang river estuary, china. *Journal of Marine Science and Engineering 2024, Vol. 12, Page 1089*, *12*, 1089. https://doi.org/10.3390/JMSE12071089

Liang, G., & Seymour, J. (1991). Complex principal component analysis of wave-like sand motions. *Proceedings of the Coastal Sediments '91 Conference*, 2175–2186.

Liu, J. T., & Zarillo, G. A. (1989). Distribution of grain sizes across a transgressive shoreface. *Marine Geology*, *87*, 121–136. https://doi.org/10.1016/0025-3227(89)90057-1

Losada, M. A., Medina, R., Vidal, C., & Losada, I. J. (1993). Temporal and spatial cross-shore distributions of sediment at "el puntal" spit, santander, spain. *Proceedings of the Coastal Engineering Conference*, *2*, 2251–2264. https://doi.org/10.1061/9780872629332.172

Losada, M., Medina, C., Vidal, C., & Roldán, A. (1990). Historical evolution and morphological analysis of el puntal spit, santander (spain). *Journal of Coastal Research*, *7*, 711–722.

Luijendijk, A., Hagenaars, G., Ranasinghe, R., Baart, F., Donchyts, G., & Aarninkhof, S. (2018). The state of the world's beaches. *Scientific Reports 2018 8:1*, *8*, 1–11. https://doi.org/10.1038/s41598-018-24630-6

Mancini, G., Briganti, R., Mccall, R., Dodd, N., & Zhu, F. (2021). Numerical modelling of intra-wave sediment transport on sandy beaches using a non-hydrostatic, wave-resolving model. *Ocean Dynamics*, *71*, 1–20. https://doi.org/10.1007/s10236-020-01416-x

Marra, J., Sweet, W., Leuliette, E., Kruk, M., Genz, A., Storlazzi, C., Ruggiero, P., Leung, M., Anderson, D. L., Merrifield, M., Becker, J., Robertson, I., Widlansky,

M. J., Thompson, P. R., Mendez, F., Rueda, A., Antolinez, J. A., Cagigal, L., Menendez, M., ... Chiesa, C. (2023). *Advancing best practices for the analysis of the vulnerability of military installations in the pacific basin to coastal flooding under a changing climate – rc-2644* (tech. rep.). U.S. Department of Defense Strategic Environmental Research and Development Program.

Martínez-Asensio, A., Tsimplis, M. N., Marcos, M., Feng, X., Gomis, D., Jordà, G., & Josey, S. A. (2016). Response of the north atlantic wave climate to atmospheric modes of variability. *International Journal of Climatology*, *36*, 1210–1225. https://doi.org/10.1002/JOC.4415

Masselink, G., Castelle, B., Scott, T., Dodet, G., Suanez, S., Jackson, D., & Floc'H, F. (2016). Extreme wave activity during 2013/2014 winter and morphological impacts along the atlantic coast of europe. *Geophysical Research Letters*, *43*, 2135–2143. https://doi.org/10.1002/2015GL067492

Masselink, G., & Heteren, S. V. (2014). Response of wave-dominated and mixed-energy barriers to storms. *Marine Geology*, *352*, 321–347. https://doi.org/10.1016/J.MARGEO.2013.11.004

Masselink, G., & Lazarus, E. D. (2019). Defining coastal resilience. *Water 2019, Vol. 11, Page 2587*, *11*, 2587. https://doi.org/10.3390/W11122587

Maul, G., & Duedall, I. (2019). Demography of coastal populations. In C. Finkl & C. Makowski (Eds.), *Encyclopedia of coastal science. encyclopedia of earth sciences series*. Springer, Cham. https://doi.org/https://doi.org/10.1007/978-3-319-93806-6_115

Mazzaretto, O. M., Menéndez, M., & Lobeto, H. (2022). A global evaluation of the jonswap spectra suitability on coastal areas. *Ocean Engineering*, *266*, 112756. https://doi.org/10.1016/J.OCEANENG.2022.112756

McCall, R. T., de Vries, J. S. V. T., Plant, N. G., Dongeren, A. R. V., Roelvink, J. A., Thompson, D. M., & Reniers, A. J. (2010). Two-dimensional time dependent hurricane overwash and erosion modeling at santa rosa island. *Coastal Engineering*, *57*, 668–683. https://doi.org/10.1016/J.COASTALENG.2010.02.006

McKay, M. D., Beckman, R. J., & Conover, W. J. (1979). A comparison of three methods for selecting values of input variables in the analysis of output from a computer code. *Technometrics*, *21*, 239. https://doi.org/10.2307/1268522

Medina, R., Losada, I., Losada, M., & Vidal, C. (1995). Variabilidad de los perfiles de playa: Forma y distribución granulométrica. *Ingeniería del Agua*, *2*, 133–142.

Medina, R., Losada, M. A., Losada, I. J., & Vidal, C. (1994). Temporal and spatial relationship between sediment grain size and beach profile. *Marine Geology*, *118*, 195–206. https://doi.org/10.1016/0025-3227(94)90083-3

Méndez, F. J., Menéndez, M., Luceño, A., & Losada, I. J. (2006). Estimation of the long-term variability of extreme significant wave height using a time-dependent peak over threshold (pot) model. *Journal of Geophysical Research: Oceans*, *111*, 7024. https://doi.org/10.1029/2005JC003344

Menéndez, M., Méndez, F. J., Izaguirre, C., Luceño, A., & Losada, I. J. (2009). The influence of seasonality on estimating return values of significant wave height. *Coastal Engineering*, *56*, 211–219. https://doi.org/10.1016/J.COASTALENG.2008.07.004

Merkens, J. L., Reimann, L., Hinkel, J., & Vafeidis, A. T. (2016). Gridded population projections for the coastal zone under the shared socioeconomic pathways. *Global and Planetary Change*, *145*, 57–66. https://doi.org/10.1016/J.GLOPLACHA.2016.08.009

Merrifield, M. A., Johnson, M., Guza, R. T., Fiedler, J. W., Young, A. P., Henderson, C. S., Lange, A. M., O'Reilly, W. C., Ludka, B. C., Okihiro, M., Gallien, T., Pappas, K., Engeman, L., Behrens, J., & Terrill, E. (2021). An early warning system for wave-driven coastal flooding at imperial beach, ca. *Natural Hazards*, *108*, 2591–2612. https://doi.org/10.1007/S11069-021-04790-X/FIGURES/12

Miller, J. K., & Dean, R. G. (2007a). Shoreline variability via empirical orthogonal function analysis: Part i temporal and spatial characteristics. *Coastal Engineering*, *54*, 111–131. https://doi.org/10.1016/J.COASTALENG.2006.08.013

Miller, J. K., & Dean, R. G. (2007b). Shoreline variability via empirical orthogonal function analysis: Part ii relationship to nearshore conditions. *Coastal Engineering*, *54*, 133–150. https://doi.org/10.1016/J.COASTALENG.2006.08.014

Montaño, J., Coco, G., Cagigal, L., Mendez, F., Rueda, A., Bryan, K. R., & Harley, M. D. (2021a). A multiscale approach to shoreline prediction. *Geophysical Research Letters*, *48*, e2020GL090587. https://doi.org/10.1029/2020GL090587

Montaño, J., Coco, G., Chataigner, T., Yates, M., Dantec, N. L., Suanez, S., Cagigal, L., Floc'h, F., & Townend, I. (2021b). Time-scales of a dune-beach system and implications for shoreline modeling. *Journal of Geophysical Research: Earth Surface*, *126*, e2021JF006169. https://doi.org/10.1029/2021JF006169

Moraes, R. P., Reguero, B. G., Mazarrasa, I., Ricker, M., & Juanes, J. A. (2022). Nature-based solutions in coastal and estuarine areas of europe. *Frontiers in Environmental Science*, *10*, 829526. https://doi.org/10.3389/FENVS.2022.829526/BIBTEX

Morales-Márquez, V., Orfila, A., Simarro, G., & Marcos, M. (2020). Extreme waves and climatic patterns of variability in the eastern north atlantic and mediterranean basins. *Ocean Science*, *16*, 1385–1398. https://doi.org/10.5194/OS-16-1385-2020

Narayan, S., Beck, M. W., Reguero, B. G., Losada, I. J., Wesenbeeck, B. V., Pontee, N., Sanchirico, J. N., Ingram, J. C., Lange, G. M., & Burks-Copes, K. A. (2016). The effectiveness, costs and coastal protection benefits of natural and nature-based defences. *PLOS ONE*, *11*, e0154735. https://doi.org/10.1371/JOURNAL.PONE.0154735

Nazari, R., Vasiliadis, H., Karimi, M., Fahad, M. G. R., Simon, S., Zhang, T., Sun, Q., & Peters, R. (2022). Hydrodynamic study of the impact of extreme flooding

events on wastewater treatment plants considering total water level. *Natural Hazards Review*, *23*, 04021056. https://doi.org/10.1061/(ASCE)NH.1527-6996.0000531/ASSET/1118198B-11D0-49CD-9DEA-003CA9AFDFE7/ASSETS/IMAGES/LARGE/FIGURE7.JPG

Nederhoff, K., Saleh, R., Tehranirad, B., Herdman, L., Erikson, L., Barnard, P. L., & van der Wegen, M. (2021). Drivers of extreme water levels in a large, urban, high-energy coastal estuary – a case study of the san francisco bay. *Coastal Engineering*, *170*, 103984. https://doi.org/10.1016/J.COASTALENG.2021.103984

Nicholls, R. J., Larson, M., Capobianco, M., & Birkemeier, W. A. (1998). Depth of closure: Improving understanding and prediction. *Proceedings of the Coastal Engineering Conference*, *3*, 2888–2901. https://doi.org/10.1061/9780784404119.219

Nielsen, P. (1992, July). *Coastal bottom boundary layers and sediment transport* (Vol. 4). WORLD SCIENTIFIC. https://doi.org/10.1142/1269

Oppenheimer, M., Glavovic, B., Hinkel, J., van de Wal, R., Magnan, A., Abd-Elgawad, A., Cai, R., Cifuentes-Jara, M., DeConto, R., Ghosh, T., Hay, J., Isla, F., Marzeion, B., Meyssignac, B., & Sebesvari, Z. (2022). Sea level rise and implications for low-lying islands, coasts and communities. In H.-O. Pörtner, D. Roberts, V. Masson-Delmotte, P. Zhai, M. Tignor, E. Poloczanska, K. Mintenbeck, A. Alegría, M. Nicolai, A. Okem, J. Petzold, B. Rama, & N. Weyer (Eds.), *Ipcc special report on the ocean and cryosphere in a changing climate*. Cambridge: Cambridge University Press. https://www.ipcc.ch/site/assets/uploads/sites/3/2019/11/08_SROCC_Ch04_FINAL.pdf

Orlando, L., Ortega, L., & Defeo, O. (2019). Multi-decadal variability in sandy beach area and the role of climate forcing. *Estuarine, Coastal and Shelf Science*, *218*, 197–203. https://doi.org/10.1016/J.ECSS.2018.12.015

Pallares, E., Lopez, J., Espino, M., & Sánchez-Arcilla, A. (2017). Comparison between nested grids and unstructured grids for a high-resolution wave forecasting system in the western mediterranean sea. *Journal of Operational Oceanography*, *10*, 45–58. https://doi.org/10.1080/1755876X.2016.1260389

Parker, K., Erikson, L., Thomas, J., Nederhoff, K., Barnard, P., & Muis, S. (2023). Relative contributions of water-level components to extreme water levels along the us southeast atlantic coast from a regional-scale water-level hindcast. *Natural Hazards*, *117*, 2219–2248. https://doi.org/10.1007/S11069-023-05939-6

Parker, K., Ruggiero, P., Serafin, K. A., & Hill, D. F. (2019). Emulation as an approach for rapid estuarine modeling. *Coastal Engineering*, *150*, 79–93. https://doi.org/10.1016/J.COASTALENG.2019.03.004

Payo, A., Favis-Mortlock, D., Dickson, M., Hall, J. W., Hurst, M. D., Walkden, M. J., Townend, I., Ives, M. C., Nicholls, R. J., & Ellis, M. A. (2017). Coastal modelling environment version 1.0: A framework for integrating landform-specific

component models in order to simulate decadal to centennial morphological changes on complex coasts. *Geoscientific Model Development*, *10*, 2715–2740. https://doi.org/10.5194/GMD-10-2715-2017

Pérez, J., Méndez, F. J., Menéndez, M., & Losada, I. J. (2014). Estela: A method for evaluating the source and travel time of the wave energy reaching a local area. *Ocean Dynamics*, *64*, 1181–1191. https://doi.org/10.1007/S10236-014-0740-7/FIGURES/9

Pérez, J., Menéndez, M., & Losada, I. J. (2017). Gow2: A global wave hindcast for coastal applications. *Coastal Engineering*, *124*, 1–11. https://doi.org/10.1016/J.COASTALENG.2017.03.005

Plant, N. G., & Stockdon, H. F. (2015). How well can wave runup be predicted? comment on laudier et al. (2011) and stockdon et al. (2006). *Coastal Engineering*, *102*, 44–48. https://doi.org/10.1016/J.COASTALENG.2015.05.001

Pörtner, H.-O., & et al. (2022). Technical summary. In H.-O. Pörtner & et al. (Eds.), *Climate change 2022: Impacts, adaptation and vulnerability. contribution of working group ii to the sixth assessment report of the intergovernmental panel on climate change.* (pp. 37–118). Cambridge University Press. https://doi.org/https://doi.org/10.1017/9781009325844.002

Puertos del Estado, M. d. T. y. M. S. (2009). *Rom 1.0-09 obras de abrigo (parte 1) bases y factores para el proyecto, agentes climáticos*. https://www.puertos.es/servicios/publicaciones/recomendaciones-para-obras-maritimas

Quataert, E., Storlazzi, C., van Dongeren, A., & McCall, R. (2020). The importance of explicitly modelling sea-swell waves for runup on reef-lined coasts. *Coastal Engineering*, *160*, 103704. https://doi.org/10.1016/J.COASTALENG.2020.103704

Ramakrishnan, R., Agrawal, R., Remya, P. G., NagaKumar, K. C. V., Demudu, G., Rajawat, A. S., Nair, B., & Rao, K. N. (2018). Modelling coastal erosion: A case study of yarada beach near visakhapatnam, east coast of india. *Ocean & Coastal Management*, *156*, 239–248. https://doi.org/10.1016/J.OCECOAMAN.2017.08.013

Reguero, B. G., Losada, I. J., & Méndez, F. J. (2019). A recent increase in global wave power as a consequence of oceanic warming. *Nature Communications 2019 10:1*, *10*, 1–14. https://doi.org/10.1038/s41467-018-08066-0

Reimann, L., Vafeidis, A. T., & Honsel, L. E. (2023). Population development as a driver of coastal risk: Current trends and future pathways. *Cambridge Prisms: Coastal Futures*, *1*, e14. https://doi.org/10.1017/CFT.2023.3

Ricondo, A., Cagigal, L., Pérez-Díaz, B., & Méndez, F. J. (2024a). Hyswash: A hybrid model for nearshore wave processes. *Ocean Engineering*, *291*, 116419. https://doi.org/10.1016/J.OCEANENG.2023.116419

Ricondo, A., Cagigal, L., Pérez-Díaz, B., & Méndez, F. J. (2024b). Introducing bimodal sea-states in a hybrid model for nearshore wave processes. *Coastal Engineering*, *192*, 104556. https://doi.org/10.1016/J.COASTALENG.2024.104556

Ricondo, A., Cagigal, L., Rueda, A., Hoeke, R., Storlazzi, C. D., & Méndez, F. J. (2023). Hywaves: Hybrid downscaling of multimodal wave spectra to nearshore areas. *Ocean Modelling*, *184*, 102210. https://doi.org/10.1016/J.OCEMOD.2023.102210

Rodriguez, A. R., Fiedler, J., Engeman, L., Vawter, A., Merrifield, M., Marra, J. J., & Boone, D. (2024). Coastal flood hazard workshop: Advancements in bridging scales and disciplines for future risk assessment. *Bulletin of the American Meteorological Society*, *105*, E1995–E2001. https://doi.org/10.1175/BAMS-D-24-0213.1

Roelvink, D., Reniers, A., van Dongeren, A., van Thiel De Vries, J., Lescinski, J., & McCall, R. (2010, June). *Xbeach model description and manual* (tech. rep.). Unesco-IHE Institute for Water Education, Deltares and Delft University of Technology. https://svn.oss.deltares.nl/repos/openearthtools/sandbox/DSD_2014/XBeachExecutable/xbeach_manual.pdf

Roelvink, D., McCall, R., Mehvar, S., Nederhoff, K., & Dastgheib, A. (2018). Improving predictions of swash dynamics in xbeach: The role of groupiness and incident-band runup. *Coastal Engineering*, *134*, 103–123. https://doi.org/10.1016/J.COASTALENG.2017.07.004

Roelvink, D., Reniers, A., van Dongeren, A., van Thiel de Vries, J., McCall, R., & Lescinski, J. (2009). Modelling storm impacts on beaches, dunes and barrier islands. *Coastal Engineering*, *56*, 1133–1152. https://doi.org/10.1016/J.COASTALENG.2009.08.006

Romano-Moreno, E., Diaz-Hernandez, G., Lara, J. L., Tomás, A., & Jaime, F. F. (2022). Wave downscaling strategies for practical wave agitation studies in harbours. *Coastal Engineering*, *175*, 104140. https://doi.org/10.1016/J.COASTALENG.2022.104140

Rueda, A., Cagigal, L., Pearson, S., Antolínez, J. A., Storlazzi, C., van Dongeren, A., Camus, P., & Mendez, F. J. (2019). Hycreww: A hybrid coral reef wave and water level metamodel. *Computers & Geosciences*, *127*, 85–90. https://doi.org/10.1016/J.CAGEO.2019.03.004

Ruiz-Barradas, A., Nigam, S., & Kavvada, A. (2013). The atlantic multidecadal oscillation in twentieth century climate simulations: Uneven progress from cmip3 to cmip5. *Climate Dynamics*, *41*, 3301–3315. https://doi.org/10.1007/S00382-013-1810-0/FIGURES/6

Salameh, E., Desroches, D., Deloffre, J., Fjørtoft, R., Mendoza, E. T., Turki, I., Froideval, L., Levaillant, R., Déchamps, S., Picot, N., Laignel, B., & Frappart, F. (2024). Evaluating swot's interferometric capabilities for mapping intertidal

topography. *Remote Sensing of Environment*, *314*, 114401. https://doi.org/10.1016/J.RSE.2024.114401

Sallenger, A. (2000). Storm impact scale for barrier islands. *Journal of Coastal Research*, *16*, 890–895.

Schlacher, T. A., Jones, A. R., Dugan, J. E., Weston, M. A., Harris, L., Schoeman, D. S., Hubbard, D. M., Scapini, F., Nel, R., Lastra, M., McLachlan, A., & Peterson, C. H. (2014). Open-coast sandy beaches and coastal dunes. *Coastal Conservation*, 37–94. https://doi.org/10.1017/CBO9781139137089.004

Serafin, K. A., & Ruggiero, P. (2014). Simulating extreme total water levels using a time-dependent, extreme value approach. *Journal of Geophysical Research: Oceans*, *119*, 6305–6329. https://doi.org/10.1002/2014JC010093

Serafin, K. A., Ruggiero, P., & Stockdon, H. F. (2017). The relative contribution of waves, tides, and nontidal residuals to extreme total water levels on u.s. west coast sandy beaches. *Geophysical Research Letters*, *44*, 1839–1847. https://doi.org/10.1002/2016GL071020

Short, A. D., & Jackson, D. W. (2013). Beach morphodynamics. *Treatise on Geomorphology*, *10*, 106–129. https://doi.org/10.1016/B978-0-12-374739-6.00275-X

Smit, P. B., Janssen, T. T., & Herbers, T. H. (2015). Stochastic modeling of inhomogeneous ocean waves. *Ocean Modelling*, *96*, 26–35. https://doi.org/10.1016/J.OCEMOD.2015.06.009

Smit, P., Stelling, G., Roelvink, D., de Vries, J. V. T., McCall, R., Dongeren, A. V., Zwinkels, C., & Jacobs, R. (2010). *Xbeach: Non-hydrostatic model: Validation, verification and model description* (tech. rep.). Delft University of Technology.

Smit, P., Zijlema, M., & Stelling, G. (2013). Depth-induced wave breaking in a non-hydrostatic, near-shore wave model. *Coastal Engineering*, *76*, 1–16. https://doi.org/10.1016/J.COASTALENG.2013.01.008

Smith, G. A., Hemer, M., Greenslade, D., Trenham, C., Zieger, S., & Durrant, T. (2020). Global wave hindcast with australian and pacific island focus: From past to present. *Geoscience Data Journal*, *8*, 24–33. https://doi.org/10.1002/GDJ3.104

Splinter, K. D., Davidson, M. A., Barnard, P., Castelle, B., Oltman-Shay, J., Turner, I. L., Davidson, M. A., Barnard, P., Castelle, B., & Oltman-Shay, J. (2014). A generalized equilibrium model for predicting daily to interannual shoreline response. *Journal of Geophysical Research: Earth Surface*, *119*, 1936–1958. https://doi.org/10.1002/2014JF003106

Stockdon, H. F., Holman, R. A., Howd, P. A., & Sallenger, A. H. (2006). Empirical parameterization of setup, swash, and runup. *Coastal Engineering*, *53*, 573–588. https://doi.org/10.1016/J.COASTALENG.2005.12.005

Stockdon, H. F., Sallenger, A. H., Holman, R. A., & Howd, P. A. (2007). A simple model for the spatially-variable coastal response to hurricanes. *Marine Geology*, *238*, 1–20. https://doi.org/10.1016/J.MARGEO.2006.11.004

Stokes, K., Poate, T., Masselink, G., King, E., Saulter, A., & Ely, N. (2021). Forecasting coastal overtopping at engineered and naturally defended coastlines. *Coastal Engineering*, *164*, 103827. https://doi.org/10.1016/J.COASTALENG.2020.103827

Storlazzi, C. D., Gingerich, S., Swarzenski, P., Cheriton, O., Voss, C., Oberle, F., Logan, J., Rosenberger, K., Fregoso, T., Rosa, S., Johnson, A., Erikson, L., Field, D., Piniak, G., Malhotra, A., Finkbeiner, M., van Dongeren, A., Quataert, E., van Rooijen, A., ... Zhang, C. (2017). The impact of sea-level rise and climate change on department of defense installations on atolls in the pacific ocean (rc-2334): U.s. geological survey administrative report for the u.s. department of defense strategic environmental research and development program. https://serdp-estcp.mil/projects/details/95efb057-4dc7-4874-b8c7-a2dca867445a

Storlazzi, C. D., Reguero, B. G., L, C. G., Alkins, K. C., Lowrie, C., Nederhoff, K. M., Erikson, L. H., O'neill, A. C., & Beck, M. W. (2024). *Forecasting storm-induced coastal flooding for 21st century sea-level rise scenarios in the hawaiian, mariana, and american samoan islands* (tech. rep.). U.S. Geological Survey. US Geological Survey. https://doi.org/10.3133/DR1184

Sutton, R. T., & Hodson, D. L. (2005). Ocean science: Atlantic ocean forcing of north american and european summer climate. *Science*, *309*, 115–118. https://doi.org/10.1126/SCIENCE.1109496/SUPPL_FILE/SUTTON_SOM.PDF

Thompson, D. W., & Wallace, J. M. (1998). The arctic oscillation signature in the wintertime geopotential height and temperature fields. *Geophysical Research Letters*, *25*, 1297–1300. https://doi.org/10.1029/98GL00950

Thompson, D. W., & Wallace, J. M. (2000). Annular modes in the extratropical circulation. part i: Month-to-month variability. *Journal of Climate*, *13*, 1000–1016. https://doi.org/10.1175/1520-0442(2000)013⟨1000:AMITEC⟩2.0.CO;2

Thompson, D. W., & Wallace, J. M. (2001). Regional climate impacts of the northern hemisphere annular mode. *Science*, *293*, 85–89. https://doi.org/10.1126/SCIENCE.1058958/ASSET/968B3DBB-3CA5-4ED4-86F3-69F9269E152F/ASSETS/GRAPHIC/SE2519557004.JPEG

Tintoré, J., Medina, R., Gómez-Pujol, L., Orfila, A., & Vizoso, G. (2009). Integrated and interdisciplinary scientific approach to coastal management. *Ocean & Coastal Management*, *52*, 493–505. https://doi.org/10.1016/J.OCECOAMAN.2009.08.002

Toimil, A., Álvarez-Cuesta, M., & Losada, I. J. (2023). Neglecting the effect of long- and short-term erosion can lead to spurious coastal flood risk projections and maladaptation. *Coastal Engineering*, *179*, 104248. https://doi.org/10.1016/J.COASTALENG.2022.104248

Toimil, A., Losada, I., Álvarez-Cuesta, M., & Cozannet, G. L. (2024). The flood protection benefits provided by beaches. *EGU24*. https://doi.org/10.5194/EGUSPHERE-EGU24-8709

Tolman, H. (1991). A third-generation model for wind waves on slowly varying, unsteady, and inhomogeneous depths and currents. *Journal of Physical Oceanography*, *21*, 782–797. https://doi.org/https://doi.org/10.1175/1520-0485(1991)021⟨0782:ATGMFW⟩2.0.CO;2

Toth, L. T., Storlazzi, C. D., Kuffner, I. B., Quataert, E., Reyns, J., McCall, R., Stathakopoulos, A., Hillis-Starr, Z., Holloway, N. H., Ewen, K. A., Pollock, C. G., Code, T., & Aronson, R. B. (2023). The potential for coral reef restoration to mitigate coastal flooding as sea levels rise. *Nature Communications 2023 14:1*, *14*, 1–13. https://doi.org/10.1038/s41467-023-37858-2

Turner, I. L., Leaman, C. K., Harley, M. D., Thran, M. C., David, D. R., Splinter, K. D., Matheen, N., Hansen, J. E., Cuttler, M. V., Greenslade, D. J., Zieger, S., & Lowe, R. J. (2024). A framework for national-scale coastal storm hazards early warning. *Coastal Engineering*, *192*, 104571. https://doi.org/10.1016/J.COASTALENG.2024.104571

UN. (2023). *Early warnings for all: Executive action plan 2023-2027* (tech. rep.). United Nations. https://www.un.org/en/climatechange/early-warnings-for-all

Valiente, N. G., Masselink, G., Scott, T., Conley, D., & McCarroll, R. J. (2019). Role of waves and tides on depth of closure and potential for headland bypassing. *Marine Geology*, *407*, 60–75. https://doi.org/10.1016/J.MARGEO.2018.10.009

van Vloten, S. O., Cagigal, L., Rueda, A., Ripoll, N., & Méndez, F. J. (2022). Hytcwaves: A hybrid model for downscaling tropical cyclone induced extreme waves climate. *Ocean Modelling*, *178*, 102100. https://doi.org/10.1016/J.OCEMOD.2022.102100

Varing, A., Filipot, J. F., Delpey, M., Guitton, G., Collard, F., Platzer, P., Roeber, V., & Morichon, D. (2021). Spatial distribution of wave energy over complex coastal bathymetries: Development of methodologies for comparing modeled wave fields with satellite observations. *Coastal Engineering*, *169*, 103793. https://doi.org/10.1016/J.COASTALENG.2020.103793

Viaña-Borja, S. P., González-Villanueva, R., Alejo, I., Stumpf, R. P., Navarro, G., & Caballero, I. (2025). Satellite-derived bathymetry using sentinel-2 in mesotidal coasts. *Coastal Engineering*, *195*, 104644. https://doi.org/10.1016/J.COASTALENG.2024.104644

Viaña-Borja, S. P., Fernández-Mora, A., Stumpf, R. P., Navarro, G., & Caballero, I. (2023). Semi-automated bathymetry using sentinel-2 for coastal monitoring in the western mediterranean. *International Journal of Applied Earth Observation and Geoinformation*, *120*, 103328. https://doi.org/10.1016/J.JAG.2023.103328

Vitousek, S., Barnard, P. L., Fletcher, C. H., Frazer, N., Erikson, L., & Storlazzi, C. D. (2017). Doubling of coastal flooding frequency within decades due to sea-level

rise. *Scientific Reports 2017 7:1*, *7*, 1–9. https://doi.org/10.1038/s41598-017-01362-7

Vitousek, S., Buscombe, D., Vos, K., Barnard, P. L., Ritchie, A. C., & Warrick, J. A. (2023). The future of coastal monitoring through satellite remote sensing. *Cambridge Prisms: Coastal Futures*, *1*, e10. https://doi.org/10.1017/CFT.2022.4

Vousdoukas, M. I., Mentaschi, L., Voukouvalas, E., Verlaan, M., Jevrejeva, S., Jackson, L. P., & Feyen, L. (2018). Global probabilistic projections of extreme sea levels show intensification of coastal flood hazard. *Nature Communications 2018 9:1*, *9*, 1–12. https://doi.org/10.1038/s41467-018-04692-w

Vousdoukas, M. I., Voukouvalas, E., Mentaschi, L., Dottori, F., Giardino, A., Bouziotas, D., Bianchi, A., Salamon, P., & Feyen, L. (2016). Developments in large-scale coastal flood hazard mapping. *Natural Hazards and Earth System Sciences*, *16*, 1841–1853. https://doi.org/10.5194/NHESS-16-1841-2016

Vozzo, M. L., Cumbo, V. R., Crosswell, J. R., & Bishop, M. J. (2021). Wave energy alters biodiversity by shaping intraspecific traits of a habitat-forming species. *Oikos*, *130*, 52–65. https://doi.org/10.1111/OIK.07590

Vuik, V., Jonkman, S. N., Borsje, B. W., & Suzuki, T. (2016). Nature-based flood protection: The efficiency of vegetated foreshores for reducing wave loads on coastal dikes. *Coastal Engineering*, *116*, 42–56. https://doi.org/10.1016/J.COASTALENG.2016.06.001

Wandres, M., Aucan, J., Espejo, A., Jackson, N., N'Yeurt, A. D. R., & Damlamian, H. (2020). Distant-source swells cause coastal inundation on fiji's coral coast. *Frontiers in Marine Science*, *7*, 539966. https://doi.org/10.3389/FMARS.2020.00546/BIBTEX

Winant, C. D., Inman, D. L., & Nordstrom, C. E. (1975). Description of seasonal beach changes using empirical eigenfunctions. *Journal of Geophysical Research*, *80*, 1979–1986. https://doi.org/10.1029/JC080I015P01979

WMO. (2022). *Guidelines on implementation of a coastal inundation forecast-early warning system* (Vol. 1293). World Meteorological Organization.

Wölfl, A. C., Snaith, H., Amirebrahimi, S., Devey, C. W., Dorschel, B., Ferrini, V., Huvenne, V. A., Jakobsson, M., Jencks, J., Johnston, G., Lamarche, G., Mayer, L., Millar, D., Pedersen, T. H., Picard, K., Reitz, A., Schmitt, T., Visbeck, M., Weatherall, P., & Wigley, R. (2019). Seafloor mapping - the challenge of a truly global ocean bathymetry. *Frontiers in Marine Science*, *6*, 434383. https://doi.org/10.3389/FMARS.2019.00283/BIBTEX

Woolf, D. K., Cotton, P. D., & Challenor, P. G. (2003). Measurements of the offshore wave climate around the british isles by satellite altimeter. *Philosophical Transactions of the Royal Society of London. Series A: Mathematical, Physical and Engineering Sciences*, *361*, 27–31. https://doi.org/10.1098/RSTA.2002.1103

Wright, L. D., & Short, A. D. (1984). Morphodynamic variability of surf zones and beaches: A synthesis. *Marine Geology*, *56*, 93–118. https://doi.org/10.1016/0025-3227(84)90008-2

Zijlema, M., Stelling, G., & Smit, P. (2011). Swash: An operational public domain code for simulating wave fields and rapidly varied flows in coastal waters. *Coastal Engineering*, *58*, 992–1012. https://doi.org/10.1016/J.COASTALENG.2011.05.015

Zornoza-Aguado, M., Pérez-Díaz, B., Cagigal, L., Castanedo, S., & Méndez, F. J. (2024). An efficient metamodel to downscale total water level in open beaches. *Estuarine, Coastal and Shelf Science*, *299*, 108705. https://doi.org/10.1016/J.ECSS.2024.108705